Institut des géosciences de l'environnement

Grenoble, 24/03/2020

Reference: gmd-2019-272

Dear Editor,

We have revised our manuscript entitled “Representation of the Denmark Strait Overflow in a z-coordinate eddying configuration of the NEMO (v3.6) ocean model: Resolution and parameter impacts” by Pedro Colombo and co-Authors that we submitted as an Article to GMD.

We carefully considered all remarks of the three reviewers and prepared a response for each of them.

So we are pleased to submit the revised paper and the response to the review.

With our best regards,

Pedro Colombo

Institut des Géosciences de l'Environnement, Grenoble

Institut des Géosciences de l'Environnement
Université Grenoble Alpes
CS 40700
38058 Grenoble cedex 9

www.ige-grenoble.fr

Unité Mixte de Recherche
CNRS / IRD / UGA / G-INP
UMR 5001 / UR 252

Geophysical Model Development Discussion gmd-2019-272-RC1

Representation of the Denmark Strait Overflow in a z-coordinate eddying configuration of the NEMO (v3.6) ocean model: Resolution and parameter impacts" by Pedro Colombo et al.

Response to the Reviewer 1

We greatly appreciate comments which helped to largely improve the clarity of our manuscript. In the following, we provide our responses in a point-by-point manner. In our responses below, we use the following legend:

- *Italic characters* for the Reviewers' comments.
- Blue color for our answers to the comments.
- *Blue color in italic* for the revised text, the specific changes being sometimes outlined in *magenta*.

Introduction

Reviewer's comment.
2-7 High salinity shelf water which is a source for Antarctic Bottom Water is an overflow too and could/should be mentioned here. Around Antarctica most models struggle to get the dense water from the shelf into the abyssal ocean without entraining too much surrounding water.
We agree, and we include explicitly this important process in the revised paper (Page 2, starting line 10). Note that this paragraph has also been modified to respond to the comments of reviewer 3.
"Overflows of importance because of their contribution to the general circulation are those associated with; the Denmark Strait and the Faroe Bank Channel where dense cold waters formed in the Arctic Ocean and the Nordic Seas flows into the North Atlantic (Girton and Standford (2003), Brearley et al. (2012), Hansen and Østerhus (2007)); the strait of Gibraltar where dense saline waters generated in the Mediterranean Sea overflow into the Atlantic Ocean (Baringer and Price (1997)); the strait of Bab-el-Manded where the highly saline Red Sea waters flow into the Gulf of Aden and the Indian ocean (Peters et al. (2005)),and the continental shelves of the polar oceans (Killworth, 1977, Baines and Condie, 1998), in particular around Antarctica where the high salinity shelf waters formed in Polynyas ventilate the Antarctic Bottom waters (Mathiot et al., , Purkey et al., 2018). More reference papers can be found in Legg et al. (2009), Magaldi et al. (2015), Mastropole et al. (2017)."

We added two references.
Mathiot, P., Jourdain, N.C., Barnier, B., Gallée, H., Molines, J.-M., Le Sommer, J., and Penduff, T., 2012: Sensitivity of coastal polynyas and high-salinity shelf water production in the Ross Sea, Antarctica, to the atmospheric forcing. Ocean Dynamics 62, 701–723 (2012). https://doi.org/10.1007/s10236-012-0531-y.

Purkey S.G., Smethie W. M. Jr., Gebbie, G., Gordon, A. L., Sonnerup, R. E., Warner M. J., and Bullister, J. L., 2018: A Synoptic View of the Ventilation and Circulation of Antarctic Bottom Water from Chlorofluorocarbons and Natural Tracers. Annu. Rev. Mar. Sci., 10:8.1–8.25. https://doi.org/10.1146/annurev-marine-121916-063414.

Methods

Reviewer's comment.
Figure 1. As far as I can tell, only section 29, 24, 20, 16 and Denmark Strait have been used. I do not see much value showing all the other sections. I suggest reducing them to the once which are being shown. I am aware that they are meant to show DSOW core.
Yes, the other sections are used in the study to calculate the path of the overflow. The integral calculations described in Appendix B are performed over the extent of these sections, integration across the section leading to the red spots which identify the path of the DSO in the control simulation.

We modified Fig. 1 which now includes only the 4 most relevant sections (see below).

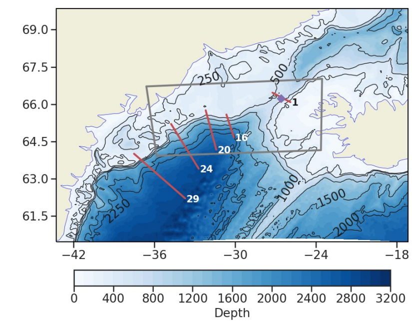

Figure 1. Regional model domain. In color the ocean depth. The 250, 500, 1000, 1500 and 2000 meter depth isobaths are contoured in black. The grey box indicates the region where the 2-way grid refinement (1/36° and 1/60°) is applied in some simulations. The location of the various sections used to monitor the model solution are shown by the red lines.

The other sections are shown in the Appendix B (Fig. B1) where the calculation of the path of the overflow is discussed. The path of the overflow is also shown for the Control and the 1/60°-150 Levels simulations in Fig. B1 (see below).

Figure and text in the Appendix B:

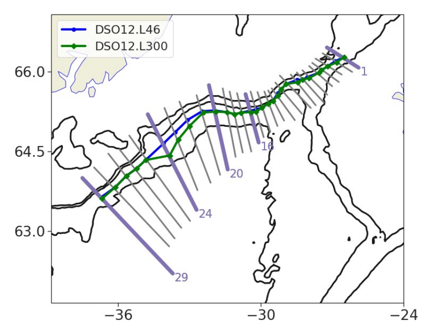

"Figure B1. Overflow path. Contours show the 500, 1000 and 2000 meter depth isobaths. The location of the various sections used to monitor the model solution are indicated by grey and purple lines. The blue/green dots indicate for each section the location of the center of the vein of the DSO in the Control simulation (blue, DSO12.L46) and in the 1/12° 300 levels simulation (green, DSO12.L300), the blue/green lines outline the path of the overflow in these simulations."

The text below has been added in the Appendix B (Page 30).
"The position of the center of the overflow has been calculated with equations B1 and B2 at each of the 29 sections shown in Figure B1, thus defining the mean path of the overflow in the simulations. This path is used to produce the results shown in Fig. 9 and in Fig.17."

Reviewer's comment.
Please see my comment how alternatively the DSOW could be tracked, which would not require individual sections.
Regarding the suggestion of an alternative way to track the DSOW with the minimum bottom temperature, it should work to define the path, but it may also face limitations especially in case of large salinity biases. Because our sensitivity tests are scanning a large range of parameters, we cannot exclude cases where the bottom temperature signature of the overflow may hardly be different (or even warmer) from that of the ambient fluid, in case for example, of entrainment of highly saline waters. We expect difficulties with such method in

simulations where the DSO is considerably unrealistic, which may happen when scanning a large set of parameters and resolutions. Our method based on the calculation of the center of mass and speed of the vein of fluid (Appendix B), which uses potential density and velocity, has the advantage to account for possible compensation in T/S biases and to provide, in addition to the location of the path, the depth of the core (not necessarily at the bottom) from which we can also approximate the thickness of the plume.

We decided to keep our method to calculate the path of the overflow (although we do not use the depth of the plume in the paper).

Reviewer's comment:
Figure 2. It is hard to compare those fields. I would suggest showing the mean from the global configuration and anomalies to the regional setup. In this case it becomes clearer where the differences are. Since both models use the same grid calculating anomalies should be easy.
We followed this recommendation and plotted the difference in current speed between global and control in subplots 2(c,d) instead of the current speed of Control, but the vectors are the currents of the Control. The vector field in these subplots is still the one from Control. We modified the figure legend and the text of the paper accordingly. At the moment the figures are built from the various subplots by Latex. We shall reduce spaces between subplots, as suggested in the next comment, in the final version of the paper.

The new figure legend is as follows:
"Figure 2. Surface (a) and bottom (b) mean currents (year 76) in the global ORCA12 simulation. Vectors/Colors indicate current direction/speed in $m.s^{-1}$. Surface (c) and bottom (d) mean currents (year 76) in the regional DSO12.L46 regional simulation. Vectors indicate direction and amplitude of the current. Colors indicate the current speed difference between the global and the regional simulation (in $m.s^{-1}$). Blue/red indicate that the current speed is greater/smaller in the Control/Regional simulation. Vectors at the bottom circulation are scaled by a factor of 7 compared to the surface for visibility reasons."

Change in the text (Page 8, starting line 5).
"*The large-scale circulation patterns is found to be very similar in both simulations, as illustrated with the surface and bottom currents shown in Fig. 2. The predominant currents such as the East Greenland Current (EGC), the Irminger Current (IC) and the DSO itself are very similar between the global and the regional model. This circulation scheme also compares well with that described from observations in Daniault et al. (2016) and from an ORCA12 model circulation simulation in Marzocchi et al. (2015).*"

Reviewer's comment:
All the subsequent figures have a lot of white spaces between the subplots. If there is any chance to move subplot labels into the figures that would allow to reduce the white spaces and improve the visibility/readability of the figures.
We agree, and all figures will be modified is a way similar to that applied to Figure 2 before the revised paper is submitted.

Reviewer's comment:
8-14. It appears that the DSOW has a seasonal cycle, which is not present in observations in the Denmark Strait (Jochumsen et al. 2012). Although this is not too critical for this study it shows that likely the formation regions of DSOW in the Nordic Seas are not captured correctly (Våge et al. 2013). That could explain why the transport variability is so low. The seasonal signal usually originates from the EGC and Fram Strait.
We agree that the seasonal cycle is not realistic and we now mention this in the revised paper (see below). What is important in this figure is that it demonstrates that the regional model is a reliable simulator of what the global model produces in that region, and therefore it is a "good result" that it reproduces this seasonal signal. The reviewer's remark led us to give a greater attention to this signal. Our investigation performed with the regional model, revealed that it is the barotropic circulation that is driving this seasonal signal (see the new Figure 3). We address this issue by showing and discussing the barotropic transport in Figure 3.

The low values of the transport std shown in Fig. 3 are also a consequence of the sampling used for the model outpouts which are 5-day means (the standard outpout of the global model simulations). Although the regional model outputs are daily means, we used 5-day means in this figure for the purpose of comparison with the global model. When daily means are used the std increases up to 0.7 Sv (more than double), but still remains below what is observed. We do not comment this in the paper, but we indicate in the figure legend that

Modified Figure 3:

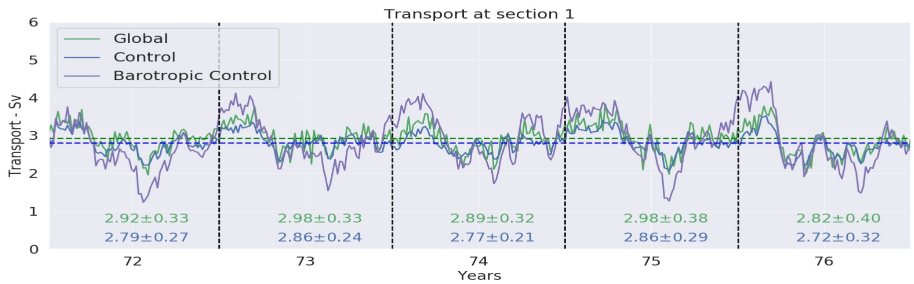

"Figure 3. Time evolution of the volume transport of waters of potential density greater than 27.80 kgm^{-3} at the sill section (Section 1 in Fig. 1) in the Control (blue line) and the Global (green line) simulations (the latter providing the open boundary conditions). Annual mean and std (in Sv) are indicated for every individual year of simulation. The depth-integrated (barotropic) transport is shown for the Control simulation (purple line). 5-day mean values are used to produce this figure."

Modified text (page 8, line 19):

"The standard deviation computed from 5-day outputs (~0.3 Sv in the control run, increasing to 0.7 Sv when calculated from daily values) is rather small when compared to the 1.6 Sv of Macrander et al. (2005). The modelled flow of dense waters presents a marked seasonal cycle which is not present in observations (Jochumsen et al. 2012). This signal is the signature of the large seasonality of the barotropic flow (Fig. 3) that constrains the whole water column."

Figure 4. I would swop (a) and (b) so you can avoid starting in line 8-16 with Figure 4b and later going back to Figure 4a.

This figure has been modified to include a plot showing the observations of Mastropole et al. (2017). The Figure legend and the text have been modified as follows in the revised version of the paper.

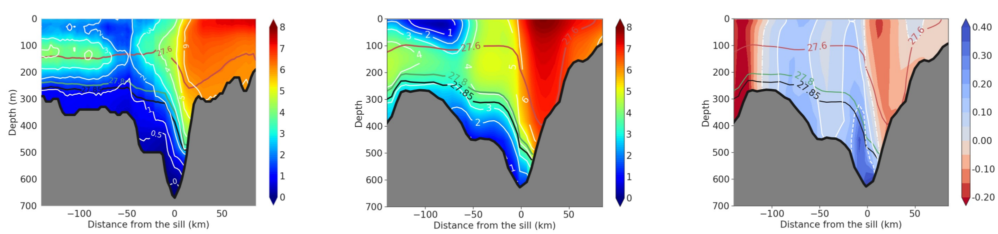

(a) Observations (b) DSO12.L46 (c) DSO12.L46

"Figure 4. Mean flow characteristics (annual mean of year 76) in the global simulation at the sill. Temperature (°C) in colours and white contours for (a) the observations (Mastropole et al., 2017) and (b) the control simulation (1/12° and 46 vertical levels). Potential density values (σ_0) are shown by the contour lines coloured in red (27:6), green (27:8) and black (27:85). (c) The velocity normal to the section in the control simulation (southward velocity in blue colour being negative). White lines indicate the 0 ms^{-1} contour (dotted line), the -0.1 ms^{-1} (full line) and the -0.2 ms^{-1} contour (dashed line). The model section being taken along the model coordinate, the topography is slightly different in the model."

The text now reads (8-24):

“Fig. 4 presents the characteristics of the mean flow across the sill. The model simulation is compared to the data of Mastropole et al. (2017) who processed over 110 shipboard hydrographic sections across Denmark Strait (representing over 1000 temperature and salinity profiles) to estimate the mean conditions of the flow at the sill. Compared with the compilation of observations of Mastropole et al. (2017) (Fig. 4a) the model simulation (Fig. 4b) shows a similar distribution of the isopycnals, specially the location of the 27.8 isopycnal. However, the observations exhibit waters denser than 28.0 in the deepest part of the sill which the model does not reproduce. Large flaws are noticed regarding the temperature of the deepest waters which are barely below 1°C when observations clearly show temperatures below 0°C (also seen in the observations presented in e.g. Jochumsen et al. (2012), Jochumsen et al. (2015), Zhurbas et al. (2016)). A bias toward greater salinity values (not shown) is also found in the control experiment which shows bottom salinity of 34.91 compared to 34.9 in the observations shown in Mastropole et al. (2017), but the resulting stratification in density shows patterns that are consistent with observations. The distribution of velocities (Fig. 4c) is also found realistic when compared with observations (i.e. the Fig. 2b of Jochumsen et al. (2012)) with a bottom intensified flow of dense waters (up to 0.4 ms^{-1}) in the deepest part of the sill. Although the present setup is designed to investigate model sensitivity in twin experiments and not for comparison with observations ends, the control run appears to provide a flow of dense waters at the sill that is stable over the 5 year period of integration and reproduces qualitatively the major patterns of the overflow “source waters” seen in the observations. Therefore, despite existing biases, the presence of a well identified dense overflow at the sill confirms the adequacy of the configuration for the sensitivity studies.”

*Figure 5-6 (*Fig. 6-7 in the revised paper*). Is there the chance to include observational values here (CTD casts) along some of these sections? That would help to illustrate how the solution should look like.*

As we say in the paper (section 2.2), the initial conditions of the simulations, which come from a long term (~90 years) global simulation, are significantly different from observations, as the flaws in the representation of the overflows (and other flaws) have modified the mass field (too warm and salty, as discussed). The main objectives of these figures is to compare the solution in twin sensitivity experiments.

To address this comment, we decided to add one figure (Figure 5 in the revised paper, see below), comparing the model solution to observations at a given section. This figure compares the model with observations collected during the ASOF project (Quadfasel, 2004) at the downstream-most section among those shown in the paper (i.e. section 29 in Fig. 1). We chose that section because it is a good illustration of the major flaws of the “end product” in the Control run (the plume is too warm, diluted, does not reach deep enough, and is hardly distinguishable from the ambient fluid). It complements Fig. 4 which shows the “source waters”. It also provides guidance regarding assessment of improvements which will be acknowledged if the plume is colder, or deeper, or separated from the ambient fluid by sharper gradients. We modified the text of the paper accordingly.

New Figure 5:

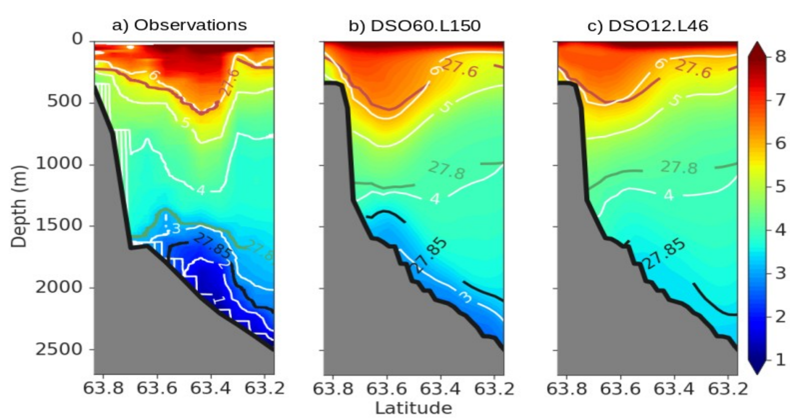

Figure 5: Potential Temperature (°C) at section 29 in (a) the observations (ASOF6-section, Quadfasel, 2004), (b) the 1/60°, 150 levels simulation (annual mean), and (c) the 1/12°, 46 level simulation (annual mean). Red/Green/Black full lines are isopycnals 27.6/27.8/27.85. White lines are isotherms by 1°C interval. For Fig. b), the section 29 is outside (~100 km downstream) the 1/60° AGRIF zoom, so the effective resolution is 1/12°.

But the water masses acquired their properties upstream within the 1/60° resolution zoom. Observation data were downloaded at: https://doi.pangaea.de/10.1594/PANGAEA.890362.

Text changes related to this Fig.5 (page 9, starting line 6):

"Finally, in order to assess improvements in the sensitivity tests, the major flaws of the control simulation must be described. If similarities with observations are found at the sill, the evolution of the DSO plume in the Irminger basin is shown to be unrealistic in the present setup of the control simulation, and presents the same flaws as in the global run. This is demonstrated by the analysis of the temperature and potential density profiles at the most downstream cross-section (section 29) where the model solution is compared to observations (Fig. 5), and at the other cross-sections along the path of the DSO in the Control simulation (the plots on the left hand side of Fig. 6 and 7). The evolution of the DSO plume as it flows southward along the East Greenland shelf break is represented by a well-marked bottom boundary current (e.g. the bottom currents in Fig. 2) carrying waters of greater density than the ambient waters. Far downstream the sill (section 29) the observations show a well-defined plume of cold water confined below the 27.8 isopycnal under 1500 m depth (Fig. 5a). The bottom temperature is still below 1°C. In the Control simulation (Fig. 5c), one can clearly identify the core of the DSO plume by the 27.85 isopycnal, so it is clear that the plume has been sinking to greater depth as it moved southward. This evolution is only qualitatively consistent with the observations at this section. The modelled plume is significantly warmer and exhibits a core temperature of 3.5° (against 2°C or less in the observations). The plume is also much wider than observed, exhibits much smaller temperature and salinity gradients separating the plume from the interior ocean, indicating a greater dilution with ambient waters. The plume is barely distinguishable from the ambient fluid below 2000m when it is still well marked at that depth in the observations. The sinking and dilution of the plume as it flows southward along the slope of the Greenland shelf is well illustrated in Fig. 6 and 7 (left hand panels) which display the potential temperature at the other sections. If the overflow waters are still well-marked at section 16 (Fig. 6a), it is barely distinguishable from the ambient water at section 29."

Maybe just adding density contours would/could already help.

Main isopycnals (27.6, 27.8 and 27.85) are present in every plot showing vertical sections.

9-1 It remains unclear where this statement is based on, as far as I can tell observations along these sections are not shown or provided.

This statement is based on the comparison with the ASOF sections shown in Quadfasel (2004). This remark suggests that this is not clearly formulated. We consider that the addition of the new Figure 5 and the changes in the text to account for it are clarifying this issue.

Reveiwer's comment:

I recommend a re-write of section 8-29 until the results section. The main point is not clear to me. Is it that in the control simulation the temperature in the DSOW layer are more diluted than in the other simulation? If so, this should go in the results section and would also help avoid talking about Figure 7 twice.

Section 2.3 has three parts that each have a specific purpose to set the paradigm of our study that is: what we shall learn from the regional model will be relevant for the global model, the model solution with the "standard" (i.e. used in most global simulations) parameterization and resolution produces a well-identified overflow so the regional model is relevant for this study, and major flaws in the representation of the overflow properties are identified so it will be possible to assess improvements.

The first part (Page 8 starting line 1) demonstrates that the Regional model reproduces faithfully the global model solution. It ends with: *"Therefore this regional model appears as a reliable simulator of what the global model produces in that region"*. This part is essential part of the paradigm of the study.

The second part (Page 8 starting line 15) describes the properties of the source waters (at the sill) and characterizes their flaws. This part is important because a reasonable degree of realism is needed at the sill for the study of the DSO. This part has been improved by adding tin Fig. 4 the observations by Mastropole et al. (2017). This part ends with the following statement: *"Therefore, despite existing biases, the presence of a well* *identified dense overflow at the sill confirms the adequacy of the configuration for the sensitivity studies".* It has been slightly modified to account for the additional plot showing observations.

The third part (Page 9 starting line 7) characterizes, in the control simulation, the flaws in the representation of the overflow along its path, i.e. at the 4 downstream sections for which there are observations from Quadfasel (2004). The main point of this section is to characterize the major flaws of the control experiment, and to demonstrate that they are not different from the flaws of the global model.

The reviewer's comment indicates that its objective of the third part was not made very clear in the text. We consider that the addition of the new Fig. 5 and the changes in the text relative to this part (see our comments about Fig. 5 above) are clarifying this issue especially since we introduce more clearly the objective, this part beginning with (Page 10 starting line 1):
"Finally, in order to assess improvements in the sensitivity tests, the major flaws of the control simulation must be qualified."

Results:

*Figure 7 (*Fig. 8 in the revised paper*). Is it necessary to show the "warm" >3.6 ◦ C waters? It distracts from the cold DSOW in the Irminger Sea and would allow to get a bit more structure in these plots. Have you tried using anomalies plots here, to make the point clear that with more vertical levels the bottom water gets eroded?*
Interesting comment. We modified the plots using a color palette that emphasizes waters below 4°C. Indeed we found that this change makes the figure more readable.

Reviewer's comment:
*Figure 7,10,11 (*8,11,12 in the revised paper*). I think it would help to overlay the DSOW path in these simulations.*
We did not overlay the DSO path on these figures because it tends to mask the details of the overflow properties, especially in their initial descent. We show the overflow path for two of our simulations in Fig. B1 in the Appendix and the reader can refer to this figure. The overflow path, as calculated in Appendix B, is used to make Figures 9.
Fig. 1B and the associated text have been shown above is the discussion of Fig. 1.

Reviewer's comment:
As the authors stated the DSOW is characterised by a temperature minimum, so the path in these simulations could be also defined by the zonal minimum in the regional for each latitude, an alternative way to what the authors use at present.
Regarding the calculation of the path of the overflow, we already answered this comment before, and we decided to keep our method to calculate the path of the overflow.

Reviewer's comment:
*22-14 I am not convinced that reducing the model bias in the source waters will help. Results in Figure 16 (*Fig. 17 in the revised paper*) show that even if modelled temperature would agree with observations, temperatures downstream would end up being warmer than the observations.*
We agree with the referee's analysis of Fig. 16 (Fig. 17 in the revised version). Nevertheless, there is no chance to obtain a realistic representation of the DSO if the source waters (i.e. the waters at the sill and the ambient waters) do not have the correct properties. Therefore, reducing the bias in the sources waters is a necessary condition, but will likely not be sufficient. We slightly modified the text to make this clearer (page 24 line 21):
"Improved initial and boundary conditions (i.e. correcting for the warm bias of 0.3°C at the sill and for the warm and salty bias of the entrained waters of the Irminger Current) should reduce this difference, but to a point which is difficult to estimate. Either way, the 1.5°C difference shown in Fig. 17 is a quite wide gap that such bias correction will likely not be sufficient to fill."

Technical corrections:
I could not spot any typos but hope a native speaker might help.

We did our best with our co-authors.

Geophysical Model Development Discussion gmd-2019-272-RC2

Representation of the Denmark Strait Overflow in a z-coordinate eddying configuration of the NEMO (v3.6) ocean model: Resolution and parameter impacts" by Pedro Colombo et al.

Response to the Reviewer 2

We greatly appreciate comments which helped to largely improve the clarity of our manuscript. In the following, we provide our responses in a point-by-point manner. In our responses below, we use the following legend:

- *Italic characters* for the Reviewers' comments.
- Blue color for our answers to the comments.
- *Blue color in italic* for the revised text, the specific changes being sometimes outlined in *magenta*.

The story, if summarized, is that one should be 'resolving' the topographic slope in the sense that the aspect ratio dz/dx of mesh cells is higher than the slope, and that vertical mesh resolution has to be sufficient to represent the plume (in this manuscript 150 layers provide several points (5-6) across the overflow plume in vertical direction).

Reviewer's comment 1.
My main problem with the manuscript in its current form is that this story is presented as something unexpected and not known. This starts from the abstract and is repeated several times in the text. However, at least as concern the dz/dx ratio, the limitation on this ratio is well known (and authors themselves mention several papers). The second aspect is also general enough to be surprising, of course, the overflow plume has to be resolved vertically, there is no hope on representing the overflow otherwise. The statements like "Contrary to expectations ..." are strange in this context, it is, in contrast, in agreement with expectations. The value of the manuscript is not in the fact that it finds something new and unexpected ("It is found that when the local slope of the grid is weaker than the slope of the topography the result is a more diluted vein" - Is not this known?), but in exploring and documenting precise limitations for the particular ocean circulation model, which will be appreciated by the NEMO community and very likely by other ocean modeling groups. I would recommend that the authors look critically at their statements and adjust the manuscript accordingly (the Abstract, introduction, conclusions in the first turn). I do not think the present form is acceptable.
We agree that based on the paradigm of convective entrainment expressed by Winton et al. (1998) in their figure 7, we could have expected the sensitivity that we observed. However, we were somewhat surprised by these results because we are working in a range of resolutions that correspond to those for which previous studies (e.g. Winton, 1998) suggest that the representation of the frictional sinking would be achieve with reasonable accuracy (Winton et al. (1998) state in the conclusion of their paper that: "*These conditions imply that resolution on the order of 30–50 m in the vertical and 3–5 km in the horizontal will be needed to represent frictional sinking with reasonable accuracy. This resolution is prohibitive for climate simulations*". With resolution of 5 km to 1 km (i.e. 1/12° to 1/60°) and a large number of vertical levels (150 to 300 levels of resolution of 30 m to 10 m in the depth range 600-1000 m, see Figure A1), we thought possible a behavior that would be dominated by the resolved frictional dynamics.

But finally, our study shows that the convective entrainment paradigm, driven by the EVD parameterization, remains dominant in setting the bottom temperature of the plume. Consequently, we agree to revise our statements regarding our "surprising" or "unexpected" results.

The changes made in the revised paper are listed below:

In the abstract (Page 1, lines 4-5): The text in magenta has been removed.
"~~Contrary to expectations,~~ In the given numerical set-up, the increase of the vertical resolution did not bring improvement at eddy-permitting resolution (1/12°)."

In the Results (Page 16, lines 7-8): The text in magenta has been removed.

"Finally, the representation of the DSO is even more degraded in the 300 level case, this resolution exhibiting the greatest dilution of the DSO waters among all resolutions. ~~which was not expected since it should allow for the best resolution of the bottom Ekman layer~~"

In the Conclusion (Page 24, line 31): The text in magenta has been removed/replaced from the original text. *"~~The first unexpected~~ A first result is that the representation of the overflow showed very little sensitivity to any parameter except the horizontal and vertical resolutions. A second result is that, ~~Contrary to expectations,~~ in the given numerical set-up, the increase of the vertical resolution did not bring any improvement when an eddy-permitting horizontal grid resolution of 1/12° (i.e. ~5km) is used."*

Reviewer's comment 2.
Even in higher resolution runs the bottom topography was kept from 1/12 degree case, and question arises as what will happen if the topography were adjusted according to the resolution. I would appreciate some discussion of the aspect of resolving the topography. For example, what would happen if 1/12 degree simulations were run on a smoother topography? This might add some useful insight.

When horizontal resolution is increased, the bottom topography is bi-linearly interpolated from the 1/12° grid onto the finer grid (1/36° or 1/60°). Therefore, topographic changes still occur at the scale of the finer grid, but the topographic slope remaining constant over a 1/12° blocks (because of the bi-linear interpolation). This is illustrated in Figure 13a,b for example where the original 1/12° (46 levels) and the interpolated on 150 levels topographies can be compared.

It is very difficult to answer the question without running new model simulations, especially when the bottom topography is realistic and partial steps are used. The study of Penduff et al. (2001) addressed this issue of topographic smoothing and concluded that in an absence of a correct parameterization of current-topography interactions, a certain amount of topographic smoothing have a beneficial impact on geopotential coordinate model solution. Based on these results, we suspect that using an un-smoothed topography in the higher resolution experiments would tend to degrade the results. However, the study of Penduff at al. (2001), focused on the large scale circulation of the South Atlantic (i.e. the Confluence of the Malvinas and Brazil currents, the Zapiola Anticyclone in the Argentinian Basin) did not look at overflows, and we are not confident enough on the generalization of their results to make any comments on that issue in the paper.

We rather not discuss this complex issue in the revised paper.

Penduff, Barnier, Kerbiriou and Verron, 2001: How topographic smoothing contributes to differences between the eddy flows simulated by sigma- and geopotential-coordinate models. J. Phys. Oceanogr., 32, 122-137.

Reviewer's comment 3.
The manuscript is well written, however it tends to overdefine and at too many places phrases could be more concise. Some editing would be good at this level, but it is up to authors.
We somewhat agree with this comment, and this is likely the reason why the paper is so long. When submitting our paper to GMD, we attempted to make it interesting to and understood by oceanographers, but also by scientists from different scientific fields, as they could bring different and original views to our problems and methods. For this reason, we may have over-defined the context, and few other modelling or methodological aspects of the study, in order to make the paper accessible to scientists of different fields.

We have been through the paper again and attempted to be more concise in our comment, but still keeping our objective of being understood by non-oceanographers.

Some small issues (not all)

Page 2 line 7 check citation style: Corrected
23 'at that resolution' – which one? Can be removed. Removed

Page 3 line 4 'yield to'???? The entire sentence can be written as:

The first complication arises from the the neglect of vertical acceleration in the hydrostatic approximation leading to misrepresentation ... (see 3 above). Corrected

line 30 remove , after (2009) Corrected

page 4 lines 8 and 12 'Despite' and then again 'despite' Corrected
29 'is presented in' – contains "is presented in" is widely used. No change.

page 5 line 24 citation style Corrected

page 6 line 4 citation style Corrected
Caption to Fig.2 an –> and; Surface (a,b) and bottom (c, d) current speed (year 75) in the global ORCA12 (a,c) and regional DSO12.L46 simulations. Only every fourth point is shown.… Corrected in the new legend, since the Figure has been slightly modified to answer comments of Reviewer 1.

page 11 lines 4,5 Following the convention for DSO12.L46, the simulations … Corrected

page 14 line 9 Is NEMO different from all others?
Although we know the general principle of other models (e.g. MIT, HYCOM, FESOM, ROMS), we do not know precisely enough the details of the implementation of their numerics and parameterizations to make pertinent comments of that issue. In the current NEMO framework, the option widely used is to treat the static instabilities with EVD. No change in the text.
line 24 your formula does not express the ratio. Corrected
line 28 250 km wide. Corrected
line 29 when? At time t=0 of the simulation. This is the general definition of initial conditions: the state of the fluid at the beginning of the simulation. To make sure that this is clear, the initial condition is described in one single sentence (page 16, line 35).
"Initial conditions are as follows: a blob of cold water is placed on the bottom of the shelf with a temperature of 10°C, the temperature of the ambient fluid in the rest of the domain being 15°C and the salinity being constant (35 g/kg) in the whole domain."

Page 18
line 1 over-resolving the slope vertically worsens the overflow representation Corrected
line 2 there exists or there is Corrected
line 7 Which rationale is meant?
We refer to the rationale of the paper, i.e. what is needed to improve or understanding of the sensitivity of the representation of the DSO in NEMO to the model parameters and resolution ….
But it is absolutely not necessary to recall the main paradigm of the study here. The text now is (Page 20, line 10):
"~~Continuing with our rationale,~~ We now evaluate the representation …"

page 20 line 13 acceleration? or speed-up (units are of velocity) Corrected, speed-up
line 14 5 - 6 points Corrected

Geophysical Model Development Discussion gmd-2019-272-RC3

Representation of the Denmark Strait Overflow in a z-coordinate eddying configuration of the NEMO (v3.6) ocean model: Resolution and parameter impacts" by Pedro Colombo et al.

Response to the Reviewer 3

We greatly appreciated this extensive and detailed review which raised interesting issues and helped to largely improve the clarity of our manuscript. In the following, we provide our responses in a point-by-point manner. In our responses below, we use the following legend:

- *Italic characters* for the Reviewers' comments.
- Blue color for our answers to the comments.
- *Blue color in italic* for the revised text, changes being sometimes outlined in *magenta*.

Reviewer's comment 1.
Absence of figures with observations. It is very hard to follow the text, when the authors refer to figures in the other papers. I found only one plot (Fig 16) to be very informative. Is it possible to plot similar figures from observations? I believe that most of the observed data are present in databases such as EN4.
We agree with the reviewer that referring to figures published in other papers does not make the reading easy. Following the recommendations, we added figures with observations.

Modification of Figure 4:
This figure now includes the section from Mastropole et al. (M2017) in the paper, such that our assessment of the properties of the overflow "source waters" that compares the model data with M2017 data (Section 2.3) does not require going back and forth between our figure and the figure shown in M2017. We obtained the observation data from R. Pickart group at WHOI. The Figure legend and the text have been modified as follows in the revised version of the paper.

New Figure 4:

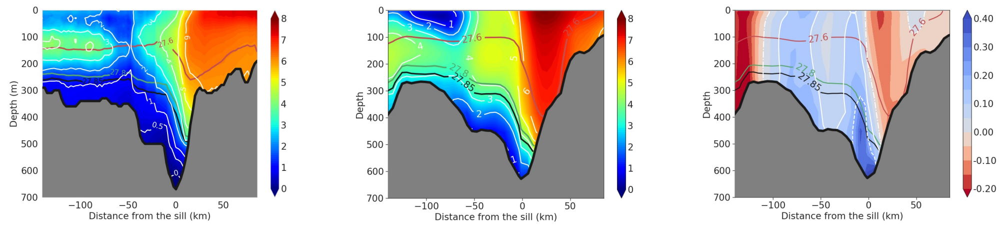

(a) Observations (b) DSO12.L46 (c) DSO12.L46

"Figure 4. Mean flow characteristics (annual mean of year 76) in the global simulation at the sill. Temperature (°C) in colours and white contours for (a) the observations (Mastropole et al., 2017) and (b) the control simulation (1/12° and 46 vertical levels). Potential density values (σ_0) are shown by the contour lines coloured in red (27:6), green (27:8) and black (27:85). (c) The velocity normal to the section in the control simulation (southward velocity in blue colour being negative). White lines indicate the 0 ms^{-1} contour (dotted line), the -0.1 ms^{-1} (full line) and the -0.2 ms^{-1} contour (dashed line). The model section being taken along the model coordinate, the topography is slightly different in the model."

The text now reads (page 8 starting line 24):
"Fig. 4 presents the characteristics of the mean flow across the sill. The model simulation is compared to the data of Mastropole et al. (2017) who processed over 110 shipboard hydrographic sections across Denmark Strait (representing over 1000 temperature and salinity profiles) to estimate the mean conditions of the flow at the sill (Fig. 4a). The model simulation (Fig. 4b) shows a similar distribution of the isopycnals, specially the location of the 27.8 isopycnal. However, the observations exhibit waters denser than 28.0 in the deepest part of the sill which the model does not reproduce. Large flaws are noticed regarding the temperature of the deepest waters which are barely below 1°C when observations clearly show temperatures below 0°C (also

seen in the observations presented in e.g. Jochumsen et al., 2012, Jochumsen et al., 2015, Zhurbas et al., 2016). A bias toward greater salinity values (not shown) is also found in the control experiment which shows bottom salinity of 34.91 compared to 34.9 in the observations shown in Mastropole et al. (2017), but the resulting stratification in density (Fig. 4b) shows patterns that are consistent with observations. The distribution of velocities (Fig. 4c) is also found realistic when compared with observations (i.e. the Fig. 2b of Jochumsen et al., 2012) with a bottom intensified flow of dense waters (up to 0.4 ms^{-1}) in the deepest part of the sill. Although the present setup is designed to investigate model sensitivity in twin experiments and not for comparison with observations ends, the control run appears to provide a flow of dense waters at the sill that is stable over the 5 year period of integration and reproduces qualitatively the major patterns of the overflow "source waters" seen in the observations. Therefore, despite existing biases, the presence of a well identified dense overflow at the sill confirms the adequacy of the configuration for the sensitivity studies."

Additional Figure (New Figure 5):

We added a new figure comparing the model with observations at the downstream-most section among those shown in the paper (i.e. section 29 in Fig. 1). We chose that section because :

- it is a good illustration of the major flaws of the "end product" in the Control run (the plume is too warm, diluted, does not reach deep enough, and is hardly distinguishale from the ambient fluid), and therefore it complements Fig 4 which shows the "source waters".
- It provides guidance regarding assessment of improvement: improvements will be akcnowledged if the plume is colder, or deeper, or separated from the ambient fluid by sharper gradients.

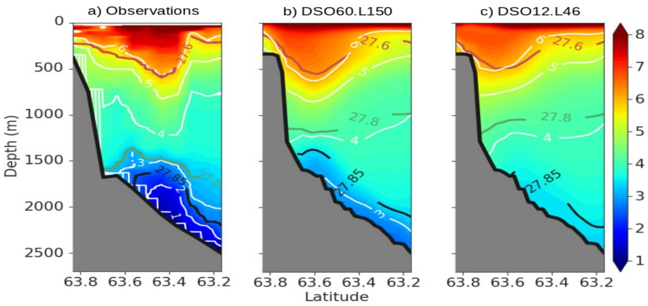

Figure 5: Potential Temperature (°C) at section 29 in (a) the observations (ASOF6-section, Quadfasel, 2004), (b) the 1/60°, 150 levels simulation, and (c) the 1/12°, 46 level simulation. Red/Green/Black full lines are isopycnals 27.6/27.8/27.85. White lines are isotherms by 1°C interval. For panel b), the section 29 is outside (~100 km downstream) the 1/60° AGRIF zoom, so the effective resolution is 1/12°. But the water masses acquired their properties upstream within the 1/60° resolution zoom. Observation data were downloaded at https://doi.pangaea.de/10.1594/PANGAEA.890362.

Modifications brought to the text (page 9, line 6 and following):

"Finally, in order to assess improvements in the sensitivity tests, the major flaws of the control simulation must be described. If similarities with observations are found at the sill, the evolution of the DSO plume in the Irminger basin is shown to be unrealistic in the present setup of the control simulation, and presents the same flaws as in the global run. This is demonstrated by the analysis of the temperature and potential density profiles at the most downstream cross-section (section 29) where the model solution is compared to observations (Fig. 5), and at the other cross-sections along the path of the DSO in the Control simulation (the plots on the left hand side of Fig. 6 and 7). The evolution of the DSO plume as it flows southward along the East Greenland shelf break is represented by a well-marked bottom boundary current (e.g. the bottom currents in Fig. 2) carrying waters of greater density than the ambient waters. Far downstream the sill (section 29) the observations show a well-defined plume of cold water confined below the 27.8 isopycnal under 1500 m depth (Fig. 5a). The bottom temperature is still below 1°C. In the Control simulation (Fig. 5c), one can clearly identify the core of the DSO plume with the 27.85 isopycnal below 1500 m, so it is clear that the plume has been sinking to greater depth as it moved southward. This evolution is only qualitatively consistent with the observations at this section because the modelled plume is significantly warmer, exhibiting a temperature of 3.5° (against 2°C or less in the observations). The temperature and salinity gradients separating the plume from the interior ocean are smaller than observed, indicating a greater dilution with ambient waters. The plume is barely distinguishable from the ambient fluid below 2000m when it is still well marked at that depth in the observations. The sinking and dilution of the plume as it flows

southward along the slope of the Greenland shelf are also well illustrated in Fig. 6 and 7 (left hand panels) which display the potential temperature at the other sections. If the overflow waters are still well-marked at section 16 (Fig. 6a), they are barely distinguishable from the ambient water at section 29."

Reviewer's comment 2.
Secondly the introduction of the manuscript is not satisfactory written, the style and organisation of paragraphs require clarifications and improvements. Please answer the following questions:
What is an overflow? How and where do overflows originate? How long do they propagate? Relative thickness, velocity, range of mass fluxes? Why it is so important in global simulations: e.g Impact on the Global Conveyer belt (MOC)? What are the main balance of forces in the overflows! Why is the fine resolution needed, what processes should be resolved in the ideal case? What is the problem in overflow simulation by z-coordinate models, show the numbers! say predicted temperature 3C higher, etc.

The information suggested by the reviewers' questions would likely be necessary in a review paper, or a study having for objective to reach the most realistic simulation of the overflows (i.e. accurately comparing with observations), as done in the studies of e.g. Magaldi et al. (2015), Koszalka et al. (2017), Almansi et al. (2017) or Spall et al. (2019). But the scope of our paper is different. The objective is to explore and document the limitations for the NEMO ocean circulation model to represent the overflow of the Denmark Strait, in a context that is relevant for global model simulations, i.e. with resolution and parameterisations now used in global model simulations. We consider that the introduction of the paper is broad enough to introduce the objective. It is already quite long (3 pages), and most questions raised by the reviewer were already addressed, but with less details than the reviewer suggested. Also, answers to some of the reviewer's questions were given in Section 2.3 when we assessed the solution of the control run and describe the major flaws of this simulation.

Nevertheless, the reviewer's comments indicate that the introduction can be improved. So we carefully went through it again and re-structured and modified several paragraphs in an attempt to account for the questions asked.

The introduction is now structured in eight paragraphs which address the following items:

- What is an overflow.
- Why overflows are important.
- Important processes and their representation in OGCMs.
- State of the art in direct simulations of overflows.
- Status of and issues relevant to global eddying models.
- Rationale of the study: what is needed to improve understanding.
- Objectives of the study.
- Outlines of the paper.

We indicate below the content of each paragraph, and we emphasize in magenta the text that directly answers the reviewer's questions.

(What is an overflow)

"Oceanic overflows are gravity currents flowing over topographic constraints like narrow straits, channels or sills, and down topographic slopes. Overflows carry dense waters formed in marginal seas or on continental shelves through intense air-sea exchanges (cooling, evaporation) from their source regions into the great ocean basins where they join the general ocean circulation (Legg et al., 2006, 2007). Overflows are often structured as plumes or boluses of dense fluid thick of a few hundred meters, accelerated toward great depths by gravity (Magaldi and Haine, 2015, Koszalka et al., 2017, Almansi et al., 2017, or Spall et al., 2019). As they cascade down over distances that may reach up to a few hundreds of kilometers with mean velocities varying between 0.25 to 1 ms^{-1}, they entrain ambient waters through advection and intense shear-driven mixing processes. After reaching a depth close to a neutral buoyancy level and a quasi-geostrophic equilibrium, the entrainment of ambient water is significantly reduced and the overflow becomes a neutrally buoyant bottom density current (Legg et al., 2009, Danabasoglu et al., 2010)."

(Why overflows are important)

“Overflows of importance because of their contribution to the general circulation are those associated with; the Denmark Strait and the Faroe Bank Channel where dense cold waters formed in the Arctic Ocean and the Nordic Seas flows into the North Atlantic (Girton and Standford, 2003, Hansen and Østerhus, 2007, Quadfasel and Käse, 2007, Brearley et al., 2012); the strait of Gibraltar where dense saline waters generated in the Mediterranean Sea overflow into the Atlantic Ocean (Baringer and Price, 1997); the strait of Bab-el-Manded where the highly saline Red Sea waters flow into the Gulf of Aden and the Indian ocean (Peters et al., 2005), and the continental shelves of the polar oceans (Killworth, 1977, Baines and Condie, 1998), in particular around Antarctica where the high salinity shelf waters formed in Polynyas ventilate the Antarctic Bottom waters (Mathiot et al., , Purkey et al., 2018). More reference papers can be found in Legg et al. (2009), Magaldi et al. (2015), Mastropole et al. (2017). Altogether, these overflows feed most of the world ocean deep waters and play an important role distributing heat and salt in the ocean. For the case of the Denmark Strait overflow (DSO hereafter), it feeds the Deep Western Boundary Current in the North Atlantic, and so contributes to the Atlantic Meridional Overturning Cell and the global thermohaline circulation (Dickson and Brown, 1994, Beismann and Barnier, 2004, Hansen and Østerhus, 2007, Dickson et al., 2008, Yashayaev and Dickson, 2008, Danabasoglu et al., 2010, Zhang et al., 2011, von Appen et al., 2014). This world-ocean wide importance of the overflows makes their representation a key aspect of ocean general circulation models (OGCMs).”

(Important processes and their representation in OGCMs)
“A variety of physical processes of different scales are involved in the control of overflows and their mixing with the ambient waters (Legg et al., 2007). Dynamical processes (e.g. hydraulic control/jump at sills/straits, mesoscale instability of the dense water plume, interactions of the plume with overlaying currents), have length scales of a few kilometers in the horizontal and a few tens of meters in the vertical. Such scales of motion are not resolved in present large-scale coarse resolution (non-eddying) ocean models used for climate studies but can be simulated in eddy-resolving models (Legg et al., 2007, 2008). Diapycnal mixing processes (e.g. entrainment of ambient waters into the cascading plume by shear-driven mixing, bottom friction, internal wave breaking) have even smaller scales (a few meters to a 1 mm) and cannot be resolved in present ocean models. Their effects are represented by a vertical turbulence closure scheme, the aim of which is to achieve a physically-based representation of this small-scale turbulence. However, models using fixed geopotential levels as vertical coordinate (i.e. z-level models) are known to generate spurious (i.e. excessive and non-physical) diapycnal mixing when moving dense overflow waters downslope. The link of this spurious mixing with the staircase-like representation of the bottom topography peculiar to these models is well established (Winton et al., 1998, Wang et al., 2008). The parameterisation of overflows in these models has been the topic of a number of studies (Beckmann and Döscher, 1997, Campin et al., 2012, Killworth and Edwards, 1999, Song and Chao, 2000, Danabasoglu et al., 2010, Wang et al., 2015). A large number of idealized model studies, many of them conducted in the DOME framework (Dynamics of Overflows Mixing and Entrainment, Legg et al., 2006, Legg et al., 2009), tested the ability of overflow parameterizations against very high-resolution simulations in a variety of OGCMs. When used in global simulations these parameterisations improve overflows, but still produce deep or bottom water properties that are not yet satisfactory if not inadequate (Condie et al., 1995, Griffies et al., 2000, Legg et al., 2009, Danabasoglu et al., 2010, Danabasoglu et al., 2014, Downes et al., 2011, Weijer, 2012, Heuzé et al., 2013, Wang et al., 2015, Snow et al., 2015). Past model studies performed with DOME-like idealized configurations also permitted to gain understanding on the dynamics of overflows and on the sensitivity of their representation in models to physical and numerical parameters (see Reckinger et al., 2015, for exhaustive references and a synthesis of the main findings). Significant differences between models due to the type of vertical coordinate system were pointed out (e.g. Ezer and Mellor, 2004, Legg et al., 2006, Wang et al., 2008, Laanaia et al., 2010, Wobus et al., 2011, Reckinger et al., 2015).”

(State of the art in direct simulations of overflows)
“Numerical modelling of dense water cascades with OGCMs designed to simulate the large scale circulation still represents a challenge, especially because the hydrostatic approximation on which these model rely remove the vertical acceleration from the momentum equation. This results in a misrepresentation of the diapycnal mixing processes (Özgökmen, 2004) and requires, to represent their effects, a turbulence closure scheme. Magaldi and Haine (2015), compared high-resolution (2 km) hydrostatic and non-hydrostatic simulations of dense water cascading in a realistic model configuration of the Irminger basin. They found that for such 2 km horizontal resolution, the parameterization of the non-resolved turbulence used in the

hydrostatic model was accurately representing the effects of the lateral stirring and vertical mixing associated with the cascading process.
Most recent high-resolution regional modelling studies of the Denmark Strait overflow (Magaldi et al., 2011, Koszalka et al., 2013, 2017, Almansi et al., 2017, Spall et al., 2019) or the Faroe Bank Chanel overflow (Riemenschneider and Legg, 2007, Seim et al., 2010) have been using hydrostatic model configurations of the MIT OGCM. These studies, as they provide modelled overflows in good agreement with observations, significantly improved the actual understanding of the overflows and their modelling. For the case of the DSO, the studies referred above especially pointed out the importance of the resolution of the cyclonic eddies linked to the dense overflow water boluses on the entrainment, and the importance of the dense water cascading from the East Greenland Shelf with the Spill Jet. On the modelling aspects, these studies provided some rationale regarding the grid-resolution that permit a representation of the overflows that agrees with observations (a resolution of 2 km in the horizontal and a few tens of meters near the bottom in the vertical). They also characterized the dependence on various model parameters regarding the mixing of the overflow waters with ambient waters. For the case of the Faroe Bank Channel overflow for example, Riemenschneider and Legg (2007) found the greatest sensitivity of the mixing in changes in horizontal resolution. However, the high resolution used in these regional studies cannot yet be used in eddying global model hindcast simulations of the last few decades or for eddying ensemble simulations."

(Status of and issues relevant to global eddying models)
"Indeed, global eddying OGCM are now commonly used at resolutions of 1/12°, which yields a grid-size of about 5 km in the region of the Nordic Seas overflows and may resolve with some accuracy the entrainment of ambient waters into the overflow plume by eddy-driven advection, but not the small-scale diapycnal mixing which still needs to be fully parameterized by the turbulence closure scheme. Chang et al. (2009) studied the influence of horizontal resolution on the relative magnitudes and pathways of the Denmark Strait and Iceland-Scotland overflows in a North Atlantic configuration of the HYCOM OGCM (Chassignet et al. (2003)). They found that at 1/12°, the highest resolution tested, the simulations show realistic overflow transports and pathways and reasonable North Atlantic three-dimensional temperature and salinity fields. The ability of HYCOM to represent the spreading of the overflow waters at 1/12° resolution was later confirmed by the studies of Xu et al. (2010), Xu et al. (2014). Marzocchi et al. (2015), provided an assessment of the ocean circulation in the subpolar North Atlantic in a 30-years long hindcast simulation performed with the ORCA12 configuration, a z-coordinate partial-step global implementation of the NEMO OGCM (Madec et al., 2016) at 1/12° resolution developed by the Drakkar Group (2014). They found that the model had some skills as the volume transport and variability of the overflows from the Nordic Seas were reasonably well represented. However, significant flaws were found in the overflow water mass properties that were too warm (by 2.5 to 3°C) and salty. This latter bias can be partly attributed to the excessive entrainment peculiar to the z-coordinate, but other sources of biases, like the warm and salty bias found in the entrained waters of the Irminger basin, a resisting bias in this type of model simulations (Treguier et al., 2005, Rattan et al., 2010), are likely to contribute."

(Rationale of the study: what is needed to improve understanding)
"Despite the progresses reported above, it is clear that overflow representation is still a resisting flaw in z-coordinate hydrostatic ocean models. NEMO (version 3.6) is now commonly used in eddying (1/4° to 1/12°) configurations for global or basin-scale, climate-oriented studies (e.g. Megan et al., 2014, Williams et al.,2015, Treguier et al., 2017, Sérazin et al., 2018), reanalyses and operational forecasts (Lellouche et al., 2013, Lellouche et al., 2018, Le Traon et al., 2017), or ensemble multi-decadal hindcast simulations (Bessières et al., 2017, Penduff et al., 2018). Even though their use by a growing community, model configurations like ORCA12 remain computationally expensive and sensitivity studies are limited. Therefore, there is a need to establish the sensitivity of the simulated overflows to the available parameterizations in a realistic framework relevant to the commonly used resolutions."

(Objectives of the study)
"The objective of this work is to provide a comprehensive assessment of the representation of overflows by NEMO in a realistic eddy-permitting to eddy-resolving configuration that is relevant for many present global simulations performed with this model, in particular with the standard 1/12° ORCA12 configuration setup similar to that presently used for operational forecasting by the CMEMS[1]. Therefore, we limit our investigation to the sensitivity of the overflow representation when standard parameters or resolution are varied, the objective being to identify the model parameters and resolutions of significant influence.

However, because NEMO is also used at much higher resolution (1/60°, e.g. Ducousso et al., 2017) and offers possibilities of local grid refinement (Debreu et al., 2007) already used with success (e.g. Chanut et al., 2008, Biastoch et al., 2009, Barnier et al., 2020), the use of a local grid refinement in overflow regions is also investigated. The approach is to set-up a regional model configuration that includes an overflow region that is similar, in terms of resolution and physical or numerical parameters, to the global ocean eddying configurations widely used in the NEMO community. The DSO is chosen as test case because of its importance and the relatively large amount of observations available. Considering that mesoscale eddies are not fully resolved at this resolution, the focus is on the overflow mean product and not on the details of the dynamics as it is done in the very-high resolution (2 km) studies of Magaldi et al. (2015) and Koszalka et al. (2017)."

(Outlines of the paper)

"This work is presented in three parts. The first part (Section 2) presents the method used to carry out the sensitivity tests. It describes the regional NEMO z-coordinate configuration developed to simulate the DSO, and the initial and forcing conditions common to all sensitivity simulations. It also describes the simulation strategy and the diagnostics developed for the assessment of the model sensitivity. The control simulation that represents a standard solution is run and diagnosed. The second part (Section 3) describes the sensitivity of the modelled overflow to a large number of parameters. Results from about 50 simulations are used, spanning vertical resolution (46, 75, 150, and 300 vertical levels), horizontal resolution (1/12°, 1/36° and 1/60°), lateral boundary condition (free slip and no-slip), bottom boundary layer parameterization, closure scheme, momentum advection scheme, etc. The third part (Section 4) describes in details the DSO produced by our best solution. We conclude the study with a summary of the main findings and some perspectives to this work."

We added the following references.

Almansi, M., T. W. N. Haine, R. S. Pickart, M. G. Magaldi, R. Gelderloos, and D. Mastropole, 2017: High-frequency variability in the circulation and hydrography of the Denmark Strait overflow from a high-resolution numerical model. J. Phys. Oceanogr., 47, 2999–3013, https://doi.org/10.1175/JPO-D-17-0129.1.

Barnier, B., Domina, A., Gulev, S., Molines, J.-M., Maitre, T., Penduff, T., Le Sommer, J., Brasseur, P., Brodeau, L., and P. Colombo, 2020: Modelling the impact of flow-driven turbine power plants on great wind-driven ocean currents and the assessment of their energy potential. Nat Energy ***5,*** *240–249. https://doi.org/10.1038/s41560-020-0580-2.*

Mathiot, P., Jourdain, N.C., Barnier, B., Gallée, H., Molines, J.-M., Le Sommer, J., and Penduff, T., 2012: Sensitivity of coastal polynyas and high-salinity shelf water production in the Ross Sea, Antarctica, to the atmospheric forcing. Ocean Dynamics 62, 701–723 (2012). https://doi.org/10.1007/s10236-012-0531-y.

Purkey S.G., Smethie W. M. Jr., Gebbie, G., Gordon, A. L., Sonnerup, R. E., Warner M. J., and Bullister, J. L., 2018: A Synoptic View of the Ventilation and Circulation of Antarctic Bottom Water from Chlorofluorocarbons and Natural Tracers. Annu. Rev. Mar. Sci., 10:8.1–8.25. https://doi.org/10.1146/annurev-marine-121916-063414.

Quadfasel, D., Käse, R., 2007. Present-day manifestation of the Nordic Seas overflows. In: Schmittner, A., Chiang, J.C.H., Hemmings, S.R. (Eds.), Ocean Circulation: Mechanisms and Impacts, Geophysical Monograph. American Geophysical Union, Washington. 10.1029/1 3GM07.

Spall, M.A., R.S. Pickart, P. Lin, W.v. Appen, D. Mastropole, H. Valdimarsson, T.W. Haine, and M. Almansi, 2019: Frontogenesis and Variability in Denmark Strait and Its Influence on Overflow Water. J. Phys. Oceanogr., 49, 1889–1904, https://doi.org/10.1175/JPO-D-19-0053.1

It would be great to have an illustration of spurious mixing due to advection+EVD.

In our "jargon", "spurious" means "excessive and unphysical". We make this clear in the texte (page 2 line 34).

“However, models using fixed geopotential levels as vertical coordinate (i.e. z-level models) are known to generate spurious (i.e. excessive and non-physical) diapycnal mixing when moving dense overflow waters downslope.”

Quantifying the “spurious” mixing due to numerical schemes has been done in dedicated idealized simulation (e;g. Illicak et al., Ocean Modelling 45–46 (2012) 37–58), but we do not know how to do this in a realistic and forced model simulation. Therefore, we acknowledge that we are not able to provide such an illustration.

If other coordinates are better, why are z-coordinates used?
There is no single coordinate that fulfils all the needs of global OGCM (e.g. we do not know about a global implementation of a σ-coordinate model), all coordinates (e.g. geopotential, terrain following, isopycnal) having advantages and disadvantages. The final choice is always pragmatic. NEMO is an OGCM used by a wide scientific and operational community and it is certainly important, if not necessary, to document the sensitivity of the representation of key processes (like DSO) to model parameters.

No change in the text.

What observations and criteria have been used to identify “improvement”?
Except for the observations of Mastropole et al. (2017) displayed in Fig. 4 and ASOF6-section of Quadfasel (2004) displayed in Fig. 5, and the bottom temperature at moorings in Fig. 17, we do not use directly observations for our assessment. However, we do use published observations to assess qualitatively the results of our simulations. Qualitative comparison are made for Fig. 15 with the microstructure measurements from Paka et al. (2013), for Fig. 6,7 with the hydrographic sections from the ASOF project (Quadfasel, 2004) at sections 16, 20, 24 and 29.

The most used criteria to identify improvements between twins simulations is a colder bottom temperature of the DSO waters, as we explained page14, lines 1).
“From the large set of diagnostics performed to assess the impact of model changes on the DSO, it was found that the”analysis of the bottom temperature in the Irminger Basin is quite a pertinent way to provide a first assessment of the changes in the properties of the overflow. This diagnostic is consequently used to first compare the different sensitivity simulations, an additional diagnostics are used later for more quantitative assessments of the DSO representation.”

Improvements are also identified if major flaws are reduced. These major flaws, identified on the time-mean properties of the overflow of the control simulation (section 2.3, 14-6 15-1,2), are: too warm bottom temperature, overflow depth not deep enough, weak temperature gradients between the plume and the ambient fluid (a not well-defined dense water plume).

We added a figure (Figure 5) comparing two experiments with observations at section 29 and provide more details on our assessment criteria in first paragraph of the Results section (Section 3, *Page 14 line 4):*
“Improvements between sensitivity tests are identified when one or several of the major flaws described in the previous section (section 2.3) are reduced. These flaws are; a too warm bottom temperature; an overflow not deep enough; and weak temperature gradients between the plume and the ambient fluid (a not well-defined dense water plume indicating too much dilution).”

*3. Please characterise the region: main parameters which are important for resolution of overflow: Rossby radius, Ekman depth and maximum/mean topography slopes, slope ratio for each resolution on the sill, as the authors have found this factor is most important. Ekman depth could be estimated from the bottom shear stresses: Hekm = Cdˆ0.5*U_bot/f (Thorpe, 1988) Soulsby (1983).*
This information is extensively described in the literature (see Quadfasel and Käse, 2007, for example). The first baroclinic radius of deformation is of the order of 20 km in the Irminger Sea. But this scale is not the one relevant to the instability of the dense water plume (a few kilometres, as we now mention in the introduction when mentioning the important processes).

Looking at the slope ratio for each resolution at and downstream the sill is difficult to use in a realistic setting since it varies greatly from a grid-point to another. This ratio is useful in the idealized experiment that we discuss in Fig. 10 and is chosen to be 5.

The comment on the Ekman depth led us to add a comment regarding its resolution with the vertical resolutions used. This is done in the appendix A in the discussion of Fig. A1 which compares the various vertical resolutions used in the study.

Text added in Appendix A (page 29, line 15):
*"**Vertical Resolutions used:** The variations of the cell thickness as a function of depth is presented in Fig. A1 for the four different vertical resolutions used. A rough estimate of the bottom Ekman layer is given by $h_E = \kappa U_*/f$ (Cushman-Roisin and Beckers, 2011) yields $h_E =$ ~45 m in our present model setting for an overflow speed of 0.5 m/s and U_* being calculated from the quadratic bottom friction of the model. Consequently, in the 600 m to 1500 m depth range that correspond to the initial depth range of the overflow, the bottom Ekman layer will only be partially resolved for model vertical resolution of ~10 to 15 m near the bottom, which according to Fig. A1 will happens only for a model resolution of 150 levels (2 to 3 points) and 300 levels (5 to 6 points)."*

We refer to this appendix in the description of the model configuration (Section 2.2, page 6 line 1):
"The cell-thickness as a function of depth is shown in Appendix A (Fig. A1) and the resolution of the bottom Ekman layer in the different vertical resolution settings is discussed."

Reference added:

Cushman Roisin B. and Beckers J. M., 2011: Introduction to Geophysical Fluid Dynamics , Physical and Numerical Aspects. Academic Press, Chap. 8, 219-246.

4. Winton 1998 experiment: "To show the effect of this concept, we simulate the descent of a continuous source of cold water down a shelf break in an idealized configuration of NEMO (with no rotation, comparable to that of Winton et al. (1998))." It is not the Winton, 1998 experiment. Winton compared with an EKMAN – type solution, so the dynamics was rotationally important, his solution was 2D on the f-plane. The solution, shown in fig 9 (Fig. 10 in revised version) is not relevant to the baseline study. You consider (fig 9) the propagation of dense boundary layer in a barotopic fluid with a very weak density difference in the plume and ambient waters (0.5C over 3000m depth). So, the balance is between gravity force and friction.

We agree that we do not reproduce the experiment of Winton et al. (W1988). We only illustrate the concept exposed by the schematic shown in the Fig. 7 of W1988 which does not imply rotation. We realize that our inappropriate reference to the paper of Winton et al. (1988) is the cause of a misunderstanding regarding the purpose of the idealized simulation used to produce our Fig. 10. Our idealized simulation only aims at illustrating how the hydrostatic model NEMO propagates dense water downward a slope, and how this process depends on the vertical resolution. This process is described in Section 2.1, page 6, lines 13-18.
In the idealized set-up of Fig. 10, the dynamics are dominated by advection (driven by horizontal pressure gradient) and diffusion. The model is hydrostatic, so there is no gravity force. Vertical motions are driven by vertical diffusion, and divergence of the horizontal flow that sets the vertical velocity (through non-divergence). Finally, we point out that the ambient fluid is not barotropic but homogeneous, and the density difference between the plume and the ambient fluid (5°C, not 0.5°C) is not weak.

The fact that the realistic model follows this paradigm is illustrated in Fig. R3.4 for the 1/60° resolution and Fig. R3.5 for the 1/12°, attached to our response to the review. It shows (at section 12 from the sill) that the front of the plume, defined by the 28.85 isopycnal is progressively sinking to great depth under the effect of a negative Richardson number (i.e. under the effect of the EVD parameterization).

The text is modified as follows, removing reference to W1988 where we think not appropriate and bring confusion:

Page 16 line 27:

"An explanation to this is searched for following the paradigm exposed in Fig. 7 of Winton et al. (1998) which states that the horizontal and vertical resolutions should not be chosen independently: the slope of the grid (Δz/Δx) has to equal the slope of the topography (α) to produce a proper descent of the dense fluid."

Page 16 line 32:

"To show how NEMO follows this concept, we simulate the descent of a continuous source of cold water down a shelf break in an idealized configuration (with no rotation)." ~~*comparable to that of Winton et al. (1998)).*~~

Page 18, lines 1-4:

"In that regime, the overflow simulated in the 300 vertical levels run (i.e. with 5 a local grid slope smaller than the topographic slope) presents warmer bottom waters (Fig. 9a) than in the 60 levels run, ~~*validating to a certain extent the rationale exposed in Winton et al. (1998)*~~ *and in agreement with the results obtained with the realistic DSO12 configuration."*

Also, you cannot claim that the second case (9b) is worse or better! Is this an effect of EVD or as twice as strong shear, seen in the panel 9b? It is not clear, that solution 9a are physically more consistent compared with 9b.

We agree. In both simulations, the plume propagates downward, essentially due to the high values of the vertical diffusivity (EVD) resulting from the static instability (due to advection of dense fluid over lighter fluid). The bottom water of the plume is colder in the 50 m resolution (60 levels) than in the 10 m resolution (300 levels). Therefore, we consider that the low-resolution case is better regarding the downslope propagation of the cold bottom temperature. We also consider that the upper part of the plume is more coherent in the 10 m resolution case due to a better resolution of the vertical shear (the *tke* scheme being sensitive to vertical resolution). This is explained in pages 17 and 18 in the paper (we removed the reference to Winton 1988 in this part as our idealized simulations do not address the same problem), a paragraph that we reproduce below emphasizing in magenta color the sentences that address these two points:

"In the absence of rotation, the pressure force pushes the blob over the shelf break and the EVD mixing scheme propagates the cold water down to the bottom as the blob moves toward deeper waters, generating an overflow plume. After about 5 days, the front of the plume has reached the end of the shelf break and entered the damping zone at the right side of the domain, reaching a quasi-stationary regime. In that regime, the overflow simulated in the 300 vertical levels run (i.e. with a local grid slope smaller than the topographic slope) presents warmer bottom waters (Fig. 10a) than in the 60 levels run in agreement with the results obtained with the realistic DSO12 configuration. Note that the vertical shear is more confined in the high-resolution case, which prevents the upward extent of the TKE induced mixing of the upper part of the overflow that is seen in the low-resolution case. Thus, the plume is more consistent in the high-resolution case but present warmer bottom waters. Note that when using a realistic bottom topography, the topographic slope will present large local variations and that it will be almost impossible to match the two slopes over the whole domain in a z-coordinate context. Therefore, increasing the number of vertical levels will not systematically degrade the overflow representation everywhere."

If you want comparisons with analytical solutions, I recommend reproducing Shapiro & Hill 1997 analytical solutions for cascading. This is not completely overflows (entrainment is weak), but it is a good test, as approved also by laboratory experiments, (Wobus et al, 2009 and Bruciaferri et al, 2018).

We retain the suggestions for future work testing new parameterization of non-hydrostatic effects.

My recommendation is to remove this paragraph from the paper, as it is not relevant to the study.

Having clarified the purpose and context of the idealized simulation and removed the inappropriate link to W1998, we retain this part because we consider it is a good illustration of our interpretation of the behaviour of the cascading in the realistic configuration.

5. I am not convinced that using EVD is a single source of increased simulated mixing when increasing the number of vertical levels. The authors state: What other processes that model start to resolve at finer vertical resolution could affect generation of strong shear and mixing, as inertial or internal waves, topographically

trapped Rossby waves? Please, look at high frequency variability at the water column, say, using a Hovmöller diagram. Fig 13a,c, shows the presence of small-scale (and probably high frequency) features. To my mind it shows presence of internal waves of high amplitude.

We do not pretend that EVD is the single cause of increased simulated mixing, and the properties of the overflow waters are certainly influenced by other mixing processes (*TKE* or numerically induced) than EVD. The *TKE* closure scheme is NEMO, like many other similar schemes, is consistent with an instability criterion based on a Richardson number (*Ri*). For this reason, the reviewer is right (in the next comment) when suggesting to look at *Ri*. For weak stratifications and significant shear, *TKE* provides large values of *Kz*, sometimes as large as the 10 m^2s^{-1} used in EVD. EVD is just a way to “boost” the TKE values in case of static instability ($N^2 > 0$).

In NEMO, the downslope cascading of dense waters from a bottom cell to a deeper bottom cell, which would be driven by vertical acceleration in a non-hydrostatic model, is made by the EVD vertical mixing. Therefore, the dense waters do not sink and accelerate downward but are mixed. Other processes have an impact on the simulated mixing, but by construction of the model, they are not dominant in the representation of the cascading.

The attribution of the high values of the vertical diffusivity coefficient (*Kz*) shown above the 27.85 in Fig.13a,c (1/60°) and not seen in Fig.13b,d (1/12°) is clearly a removal of static instability by EVD, as demonstrated in Figure R3.1 below, which shows hourly value of *Kz* and *Ri* at section 20 at two different times separated by 17 hours. The large *Kz* values between isopycnal 27.80 and 27.85 at hour 254 (Fig. R3.1a) are associated to negative *Ri*, indication removal of a static instability, thus mixing by EVD. At hour 271 (17 hours later, Fig R3.1b), the stratification is stable and *Kz* does not present anymore large values between those isopycnals.

We analysed this period in details (see Fig. R3.2 and Fig. 3.3 attached to this response), and we found that it correspond to the passage through the section of a bottom intensified cyclonic eddy (a bolus of overflow water). The core of the cyclonic eddy (Fig R3.2a), the tangential flow is off-shore and pushes dense water over lighted water, which generate static instability and turns on EVD. The dense water mixes with lighter water below. In the tail of the cyclonic eddy (Fig. R3.2b), the tangential flow is on-shore and does not generate static instability. This does not happens at 1/12° because the horizontal resolution is not enough to well resolve the boluses.

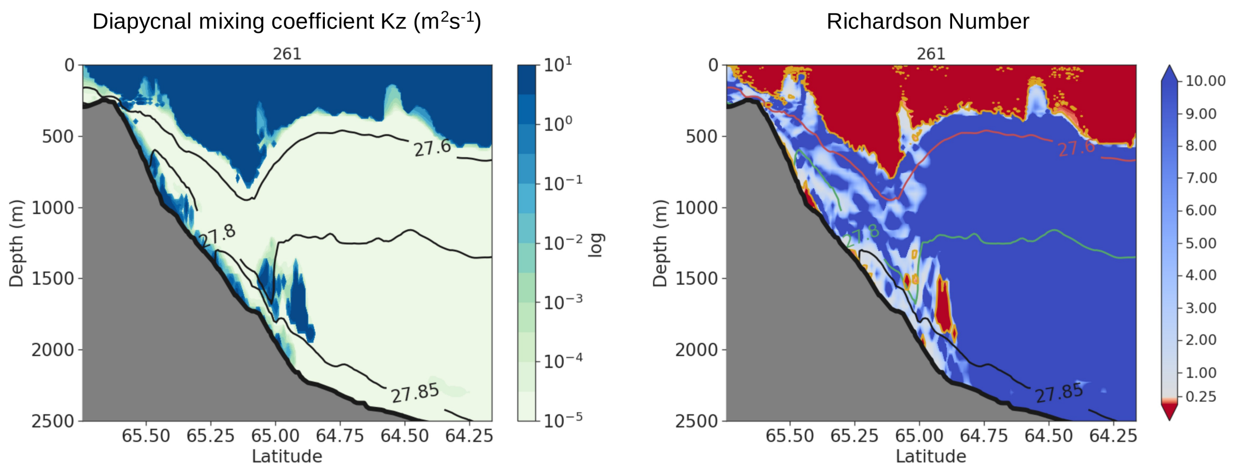

(a) Hour 254 of the 5th year of simulation

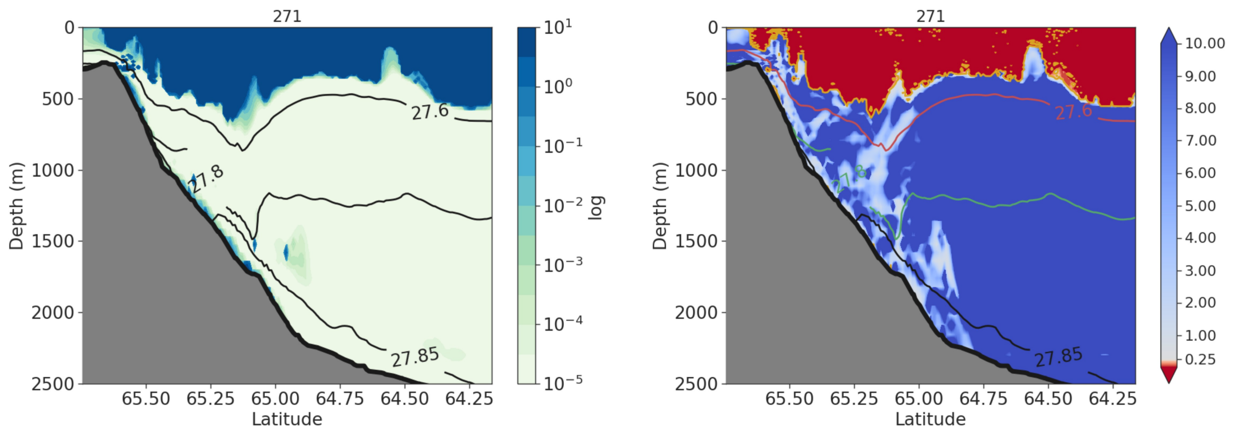

(b) Hour 271 of the 5th year of simulation

Figure R3.1: Hourly values of the vertical mixing coefficient Kz and of the Richardson number Ri across section 20 at two different times. Ri values of 0.25 are contoured in yellow. Negative Ri values are in dark red.

Therefore, our interpretation that this intermittent, but intense mixing event between those isopycnal is driven by EVD is correct.

Changes in the revised paper:
We modified Fig. 14a,c by picking two different times (those in the Figure above) when this mixing is present and when it is not, to illustrate its intermittency.
We do mention, without providing detailed explanations, that this feature is not seen in the 1/12° it is because it is driven by the cyclonic boluses not resolved at that resolution (section, page 21 line 16):
"In the case of DSO60.L150 (Fig. 14a,c) a small but noticeable mixing remains confined to a very thin bottom layer below the 27.85 isopycnal, and very little mixing occurs in the core of the overflow plume. Intermittent static instabilities occur between the 27.85 and the 27.8 isopycnals (shown by the large values of Kz in Fig. 14a). Our analysis (no figure shown) indicates that these instabilities are generated by advection toward the deep ocean of bolus of dense water by a cyclonic bottom intensified eddy. After the eddy passed through the section (Fig. 14c) the stratification is again stable. Such feature are not seen in the 1/12° simulation (Fig. 14b,d) because the horizontal resolution does not resolve properly the mesoscale eddies."

6. Another possible cause of an enhanced mixing in the fine vertical resolution is a parameterisation of diffusivity set in a weakly stratified condition. Indeed, in TKE vertical mixing scheme (and gls scheme in an strongly stratified conditions), the turbulent length scale is set as l= 0.1* TKEˆ(1/2)/N and vertical diffusivity AVT∼TKE/N, where TKE is a turbulent kinetic energy, defined by the tke equation but larger by some background value, N is a buoyancy frequency, which differs due to resolution. Subcritical Richardson numbers (Ri<Ricr∼1/4), responsible for generation of small –scale turbulent mixing are also vertical

resolution dependant. Let us consider a plume of dense water of constant density ro_plume propagating downslope in unstratified fluid (of density ro_0) with velocity U. Velocity shear is S=U/dz, the Richardson number at the edge of the plume is

Ri=N^2/S^2=g(Ro_plume –Ro_0)*dz/(U^2*roo)

will be smaller at the finer vertical resolution which results in more mixing entrainment on the top of the dense plume. This could be examined by comparison of statistics of occurrence the negative (EVD effects) and small positive Richardson numbers at the edge of plume simulations with different resolutions. The other possibility is to check this assumption, to evaluate the number of occurrence of AVT exactly fit to EVD parameterisations (10m^2/s, convection) and in the smaller range (~0.001-1m^2/s, Kelvin-Helmholtz instability). In the 1/12 resolution, (Fig 8, Fig 9 in the revised paper) I see combination of open-ocean convection (EVD) and shear instability turbulence. How do you explain a much larger area of open convection in the figure 8b, identified by 5-year mean very strong mixing from the surface to the bottom? May be at some point the water of other origin penetrates from the surface to the bottom and mixes with propagating plume?

We acknowledge that we did not count the occurrences of EVD. This must be done on-line during integration and this was not in the I/O part of the code, so we stored hourly mean values (i.e. averaged over 8 time steps) to have an estimate of the high frequency motions. One single EDV event will produce a *Kz* > 1.

We calculated the Richardson number *Ri* as suggested by the reviewer. As shown in Fig. R3.1 above, *Ri* and *Kz* are very consistent, which demonstrate that the *TKE* closure behaviour is very consistent with the stability criterion based on the Richardson number (which is expected). Note that since *Ri* and *Kz* provide almost the same information we do not show *Ri* in the paper.

We modified Fig. 9 and show the mean summer situation, so the winter mixed layer is not present, which allows to better focus on intermediate depths (see below).
It shows that the large *Kz* values between isopycnals 27.6 and 27.8 are not driven from the surface but are generated locally at mid depth. They are driven by the vertical shear existing between the northward surface current passing through the Denmark Strait (the NIIC) which is very variable in position and intensity, and the southward deep current carrying the overflow waters. We notice that the mixing is greater in the high resolution case. Several studies (e.g. Spall et al 2019) show that the NICC can occupy for short periods (few hours to day) the whole strait blocking the passage of the overflow. Our study does not focuses on this process although it is reproduced in our simulations, but of the descent of the dense waters. So our analysis first focuses on the *Kz* near the bottom (below isopycnal 27.85 or 27.8) and then we discuss the values of *Kz* at intermediate depths (Page 16 Line 19):
"The vertical diffusivity along the path of the overflow is shown in Fig. 9 for the 46 and the 300 level cases (the definition and method of calculation of the overflow path are given in Appendix B). Compared to the 46 level case, the 300 level case (Fig. 9b) exhibits greater values of the diffusion coefficient near and above the bottom along the path of the overflow. This enhanced mixing affects the overflow plume, which 200 km after the sill does not contains waters denser than 27.85, while such waters are still found 300 km down the sill in the 46 level case. The 300 level case also exhibits large values of diffusion coefficient at intermediate depth (between isopycnal 27.8 and 27.6). They are driven by the vertical shear existing between the northward surface current passing through the Denmark Strait (the NIIC) which is very variable in position and intensity, and the southward deep current carrying the overflow waters (e.g. Spall et al 2019). We notice that the mixing is significantly greater in the high resolution case, which indicate that this process could also contribute to the dilution of the overflow plume. However, it does not seem to affect the thickness of the 27.8 isopycnal."

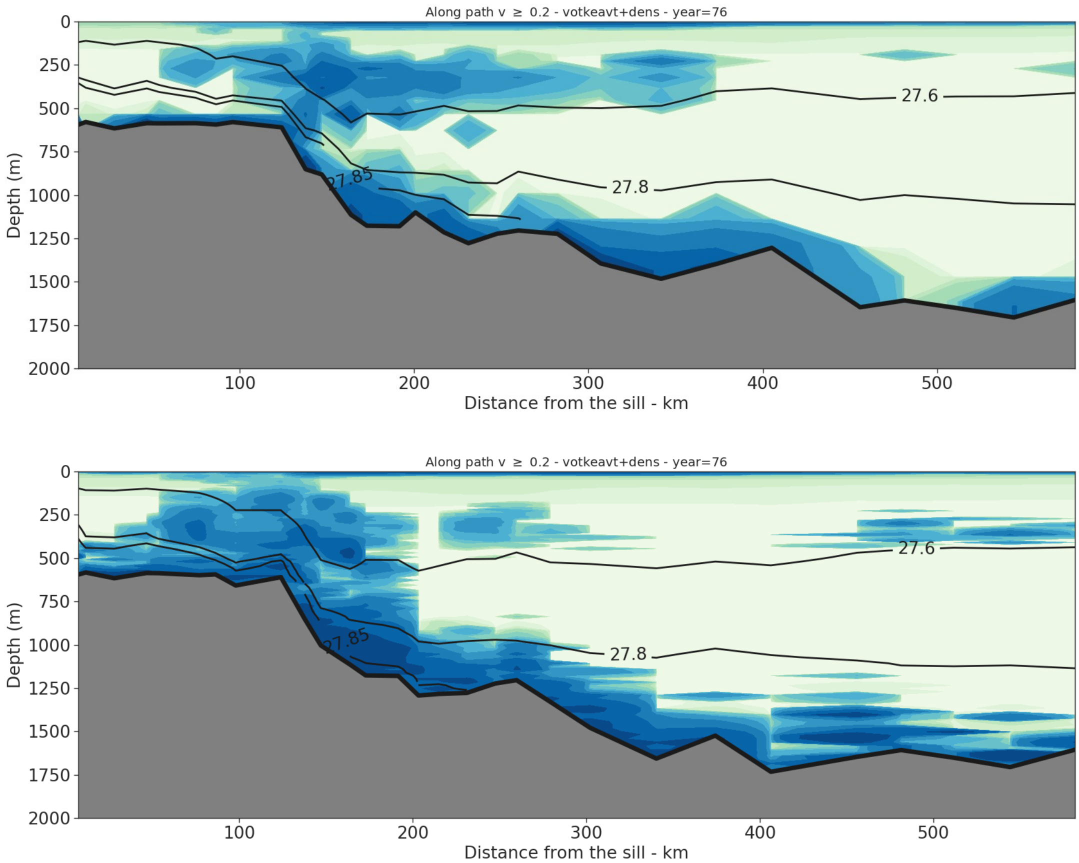

"Figure 9. Summer mean (5th year of simulation) of the vertical diffusivity coefficient along the path of the vein calculated for a) simulation DSO12.L46 and b) simulation DSO12.L300. Potential density values (_0) are shown by the contour lines colored in red (27.6), green (27.8) and black (27.85)."

7. Check consistency of bottom topography, specifically in the "worst case" L300. The authors state: "Bottom topography and coastlines are exactly those of the global 1/12 ORCA12 configuration and are not changed in sensitivity experiments, except when grid refinement is used. In this latter case the refined topography is a bi-linear interpolation of that at 1/12, so the topographic slopes remain unchanged". It is not seen from the figure 8, where bottom topography is different in simulations L46 and L300. Does adjective TVD scheme work similar in the different vertical resolutions?

Topographies are different because the path of the overflow in DSO12.L46 is different from the path in DSO12.L300 (Figure in appendix B).

The model uses a partial step bottom topography, which means that the thickness of the bottom level is adjusted to the real bottom depth. Therefore, the depth does not change when the vertical resolution changes, as it may be the case when a full cell representation of the bathymetry is used (is that latter case the bathymetry is changed to adapt to the thickness of the bottom cell). When horizontal resolution is increased, the topography is linearly interpolated, so the slope is not changed. The consistency of the topography of all simulations can be checked by looking at the bathymetric contours in figures 8, 11 and 12: they are all identical.

Minor comments:

Abstract: What observations and criteria have been used to identify "improvement"?

This is now better explained in the paper and does not need to be explicit in the abstract.

Contrary to expectations, in the given numerical set-up, the increase of the vertical resolution "It is found that when the local slope of the grid is weaker than the slope of the topography the result is a more diluted vein. Such a grid enhances the dilution of the plume in the ambient fluid and produces its thickening. Although the greater number of levels allows for a better resolution of the ageostrophic Ekman flow in the bottom layer, the final result also depends on how the local grid slope matches the topography" It is known

result from Winton et al. (1998), that the model should resolve slopes and Ekman layer, so if slopes are not resolved, vertical resolution cannot help.
We removed "contrary to expectation" as this could have been expected, although surprising that this still holds at 1/60° and 300 levels. This could be specific to the NEMO code.

1. From introduction it is not clear, what is overflow, how it is formed and what processes dominates in the dynamics. Even for pure numerical –oriented paper it is important to understand, what should be in the equations and why this resolution is chosen. "An oceanic overflow is a dense water mass" – is this a water mass (object) or process?
We accounted for these comments when revising the introduction of the paper to respond to the second major comments of the reviewer.

"Overflows of important magnitude are" – what do you mean under important magnitude?
We agree that the use of magnitude was not appropriate. We cite the overflow that are important for the general circulation. The text is now:
"Overflows of importance because of their contribution to the general circulation are …"

"is balanced by the intrusion of waters from regions different from where the overflow waters are formed" – please, rephrase it. "For example, the flux of cold waters formed in the Arctic Ocean and the Nordic Seas that enters the North Atlantic with the Denmark Strait and Faroe Bank Channel overflows is balanced by warm and salty Atlantic waters that flows over the Iceland-Scotland Ridge towards the Arctic Ocean via upper ocean currents" It sounds as Atlantic Warm currents are caused by compensation to overflow.
Many model studies have demonstrated that in the Atlantic Ocean, weak overflows result in a weak AMOC (e.g. Willebrand, 2001) which is turn reduced the meridional heat transport associated with the northward flowing warm Atlantic waters. In order to simplify the introduction already rich of information we just mention the contribution of the DSO to the deep circulation of the North Atlantic:
"For the case of the Denmark Strait overflow (DSO hereafter), it feeds the Deep Western Boundary Current in the North Atlantic, and so contributes to the Atlantic Meridional Overturning Cell and the global thermohaline circulation (Dickson and Brown, 1994, …"

"However, the dynamical processes that control overflows have rather small scales" – please, emphasise what small scales processes. What is the main balance in the overflows? Why spurious mixing is considered to be strong? It is not clear from the introduction. Refer to the paper, or just point out what is wrong due to spurious mixing (volume flux, salinity , temperature?)
We consider that the important changes made to the introduction respond to this comment, as processes, scales of motions are addressed, and spurious mixing is defined…

5. You mention the importance of non-hydrostatic physics and then mention Magaldi & Haine, 2015 paper (correct reference) showing different contrary results (see also Wobus et al, 2011).
"They also characterized the dependence on various model parameters regarding the mixing of the overflow waters with ambient waters." – I don't understand what do you mean here: mixing depends on parameters? Or something else, which parameters?
Our comments regarding the dependence on various model parameters concern the studies of Magaldi et al., 2011, … , which use the hydrostatic version of the MIR GCM, and in this version, the diapycnal mixing is "parameterized" by a turbulent closure scheme since there is not vertical acceleration (the vertical momentum equation being reduced to the hydrostatic pressure equation). These schemes have parameters to be tuned.
"Most recent high-resolution regional modelling studies of the Denmark Strait overflow (Magaldi et al., 2011, ~~2015,~~ Koszalka et al., 2013, 2017, Almnsi et al., 2017, Spall et al., 2019) or the Faroe Bank Chanel overflow (Riemenschneider and Legg, 2007, Seim et al., 2010) have been using hydrostatic model configurations of the MIT OGCM."
We remove the reference to Magaldi and Haine (2005) in this sentence, although relevant but confusing since this study is cited just above for the use of hydrostatic models.

"found a greater sensitivity of the mixing to horizontal resolution and, but to a lesser extent, to vertical resolution and vertical viscosity" is it resolved horizontal or vertical mixing? Or spurious? How mixing have been examined?

We modified this to emphasize only the sensitivity of resolution, most relevant for our study:
"For the case of the Faroe Bank Channel overflow for example, Riemenschneider and Legg (2007) found the greatest sensitivity of the mixing in changes in horizontal resolution. ~~The sensitivity to other parameters tested (bottom drag coefficient, strength of the inflow) were found to be minor.~~"

"but not the small-scale diapycnal mixing which still needs to be fully parameterized by the turbulent closure scheme." – please, rephrase it. It is true of course, as to resolve diapycnal mixing you need scales up to the dissipative one, which is of 1mm.
We rephrased it as we modified the introduction.
"Diapycnal mixing processes (e.g. entrainment of ambient waters into the cascading plume by shear-driven mixing, bottom friction, internal wave breaking) have even smaller scales (a few meters to a 1 mm) and cannot be resolved in present ocean models. Their effects are represented by a vertical turbulence closure scheme, the aim of which is to achieve a physically-based representation of this small-scale turbulence."

" a resisting bias in this type of model simulations are likely to contribute." – what is resisting bias?
A resisting bias is a bias that is not sensitive to the model parameters and cannot be corrected by parameter optimisation. Correcting the bias will require the development of new parameterisations. In the present case, it is more correct to use the word "persisting bias".

We now use "persisting bias" as bias that we haven't corrected.

Page 11: "The detailed list of theses experiments"
Corrected

Page 19: (15)
"In the case of DSO60.L150 (Fig. 13a,13c) the EVD driven mixing remains confined to a very thin bottom layer below the 15 27.85 isopycnal and very little mixing occurs in the core of the overflow plume" - If you look at the magnitude of near bottom mixing, it is too small to be EVD, probably is it shear-driven Ekman layer;
Yes. As we show in Fig. R3.3 added to this review, the EVD mixing is usually acting at the head of the plume and not inside. So within the plume, the mixing is due to the local shear (TKE), but it can be very large in the from of the plume during the phases when it is sinking.
In the paper, we use, to be consistent with the figure:
"… small but noticeable mixing …"

" Intermittent static instabilities occur between the 27.85 and the 27.8 isopycnals, the associated mixing being small since the temperature and salinity gradients are quite small there" - Figure shows very strong mixing>1m^2/s of high frequency and small scale. As T,S differences are small, Ri numbers to be small there, resulting in a strong intermittent mixing. What frequency and scales are? Is it small positive Ri (Kelvin-Helmholtz instability), or negative Ri (convection, EVD)?
We clarified this when discussing Fig. 14a,c.

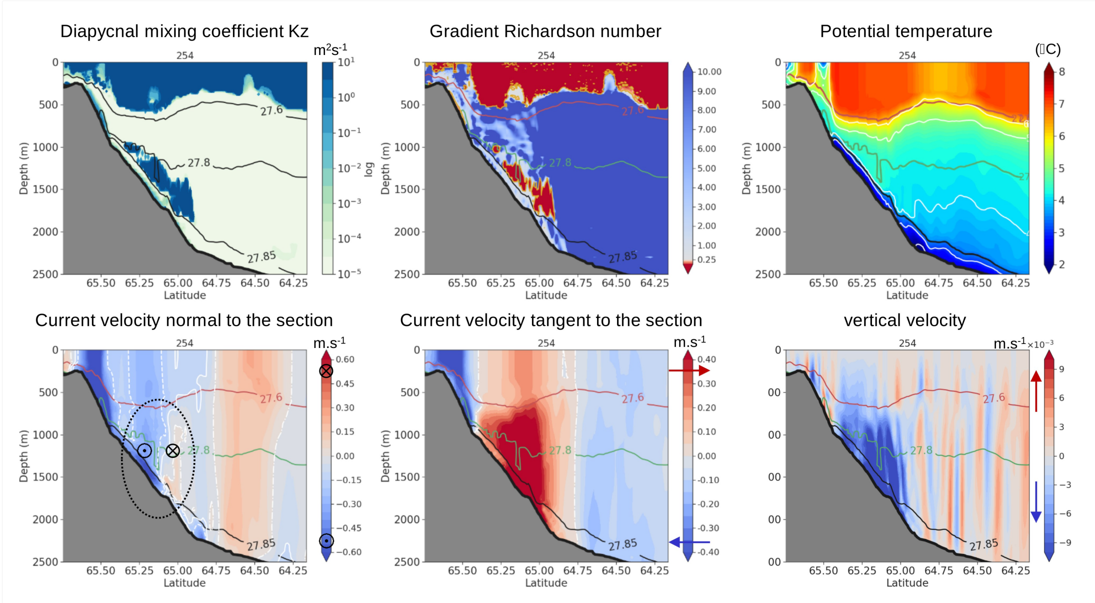

(a) Hour 254 of year 5

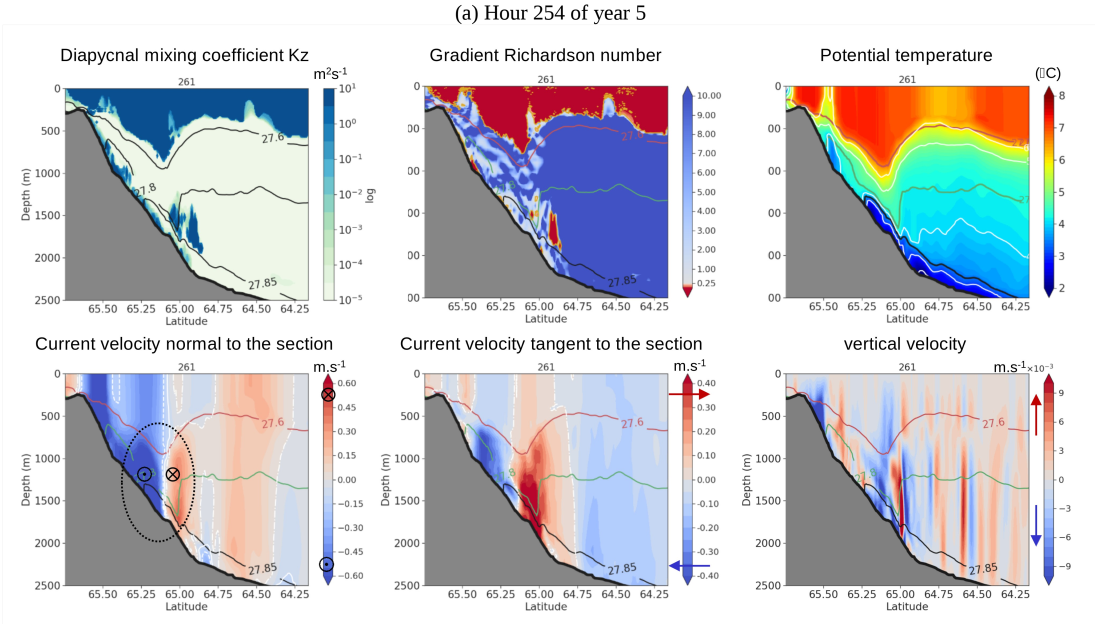

(b) Hour 261 of year 5

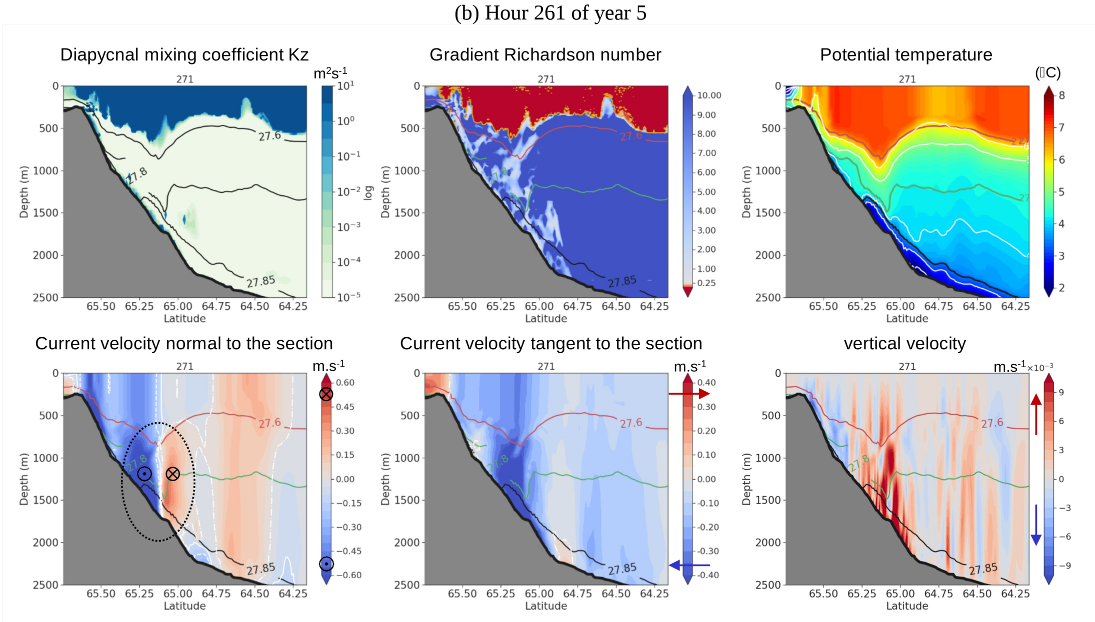

(c) Hour 271 of year 5

Fig. R3.2: Characteristics of the instantaneous (hourly mean) circulation at Section 12 after the sill in simulation DSO60.L150 (1/60°, 150 levels) at three different times. (a) Situation at hour 254 before the arrival of cyclonic eddy. (b) Situation at hour 261 when the bottom intensified cyclonic eddy is passing through the section. (c) Situation at hour 271 when the tail of the eddy is captured (see also Fig. R3.3). The cyclonic eddy is outlined by the dotted line circle in the panel showing the velocity normal to the section

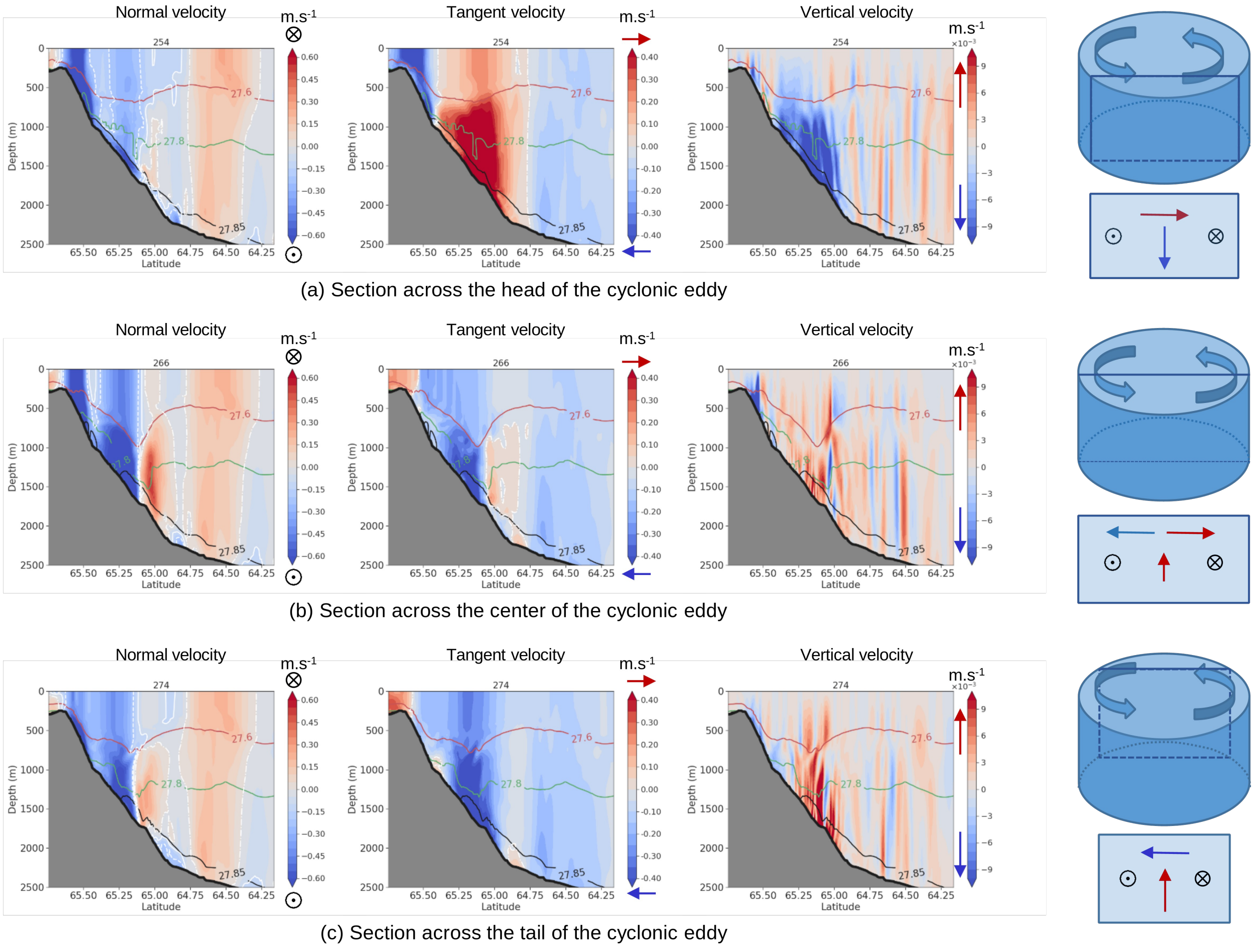

Fig. R3.3: Simulation DS060.L150. Components of the current velocity at Section 20 Schematic illustrating the passage of a cyclonic eddy. Schematics on the right summarise the organisation of the velocity field.

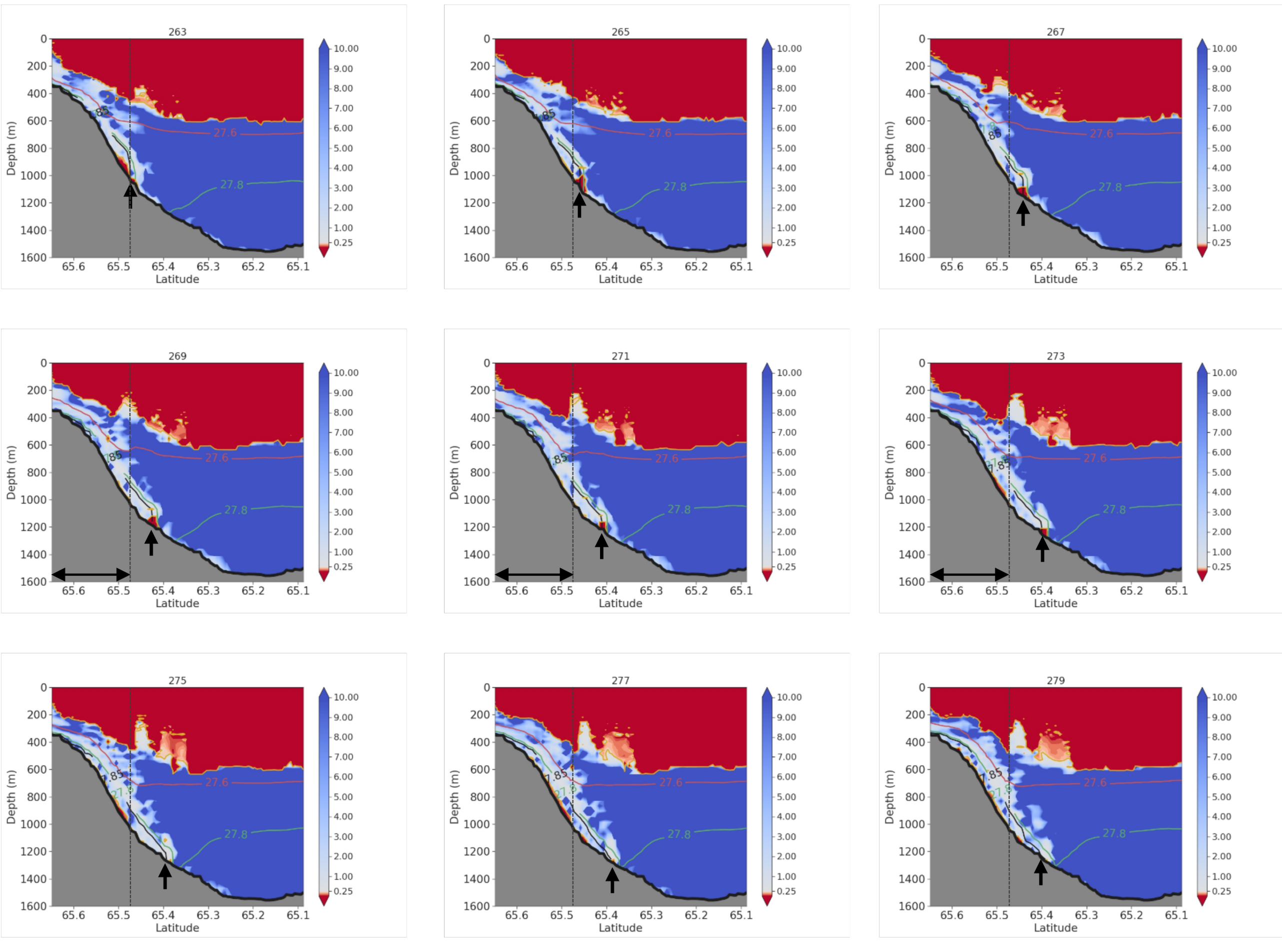

Fig. R3.4: Simulation DSO60.L150. Evolution of the hourly Richardson number, *Ri*, at section 12 over a 18 hours period (a plot every 2 hours). Negative values and values below 0.25 are colored in Red. The 0.25 contour is shown in yellow. Isopycnals 27.6, 27.8 and 27.85 are plotted in red, green and black respectively. The black arrows show the position of the front of the overflow plume defined as the deepest location of the 27.85 isopycnal, and the vertical dotted grey line indicate the initial position of the front at hour 263. As the front deepens with time, it is always associated with negative values of *Ri* which indicate that the EVD is turned on, illustrating the sinking of dense waters by the EVD parameterisation.

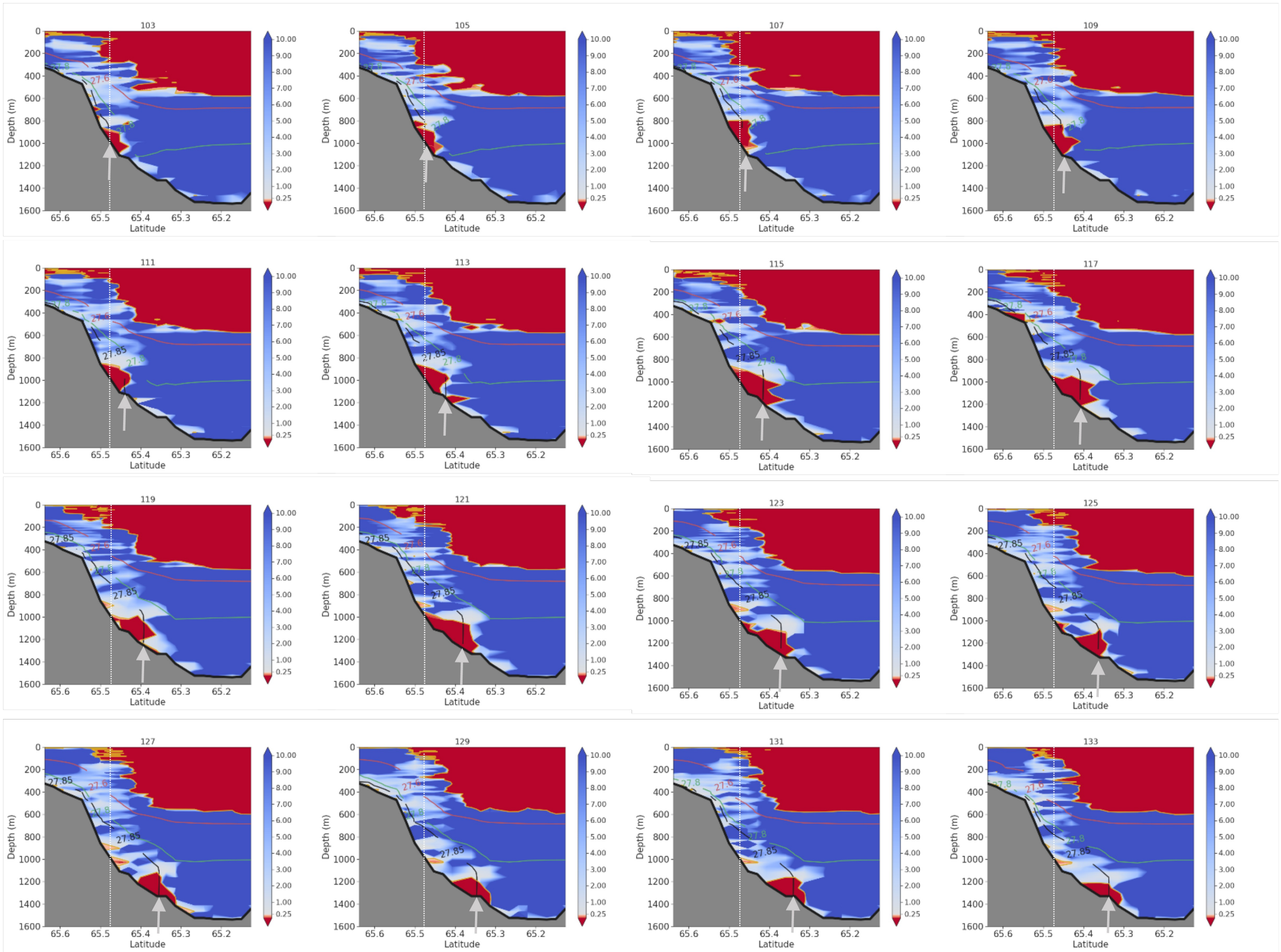

Fig. R3.5: Simulation DSO12.L150. Evolution of the hourly Richardson number, *Ri*, at Section 12 over a 32 hours period (a plot every 2 hours). Negative values and values below 0.25 are colored in Red. The 0.25 contour is shown in yellow. Isopycnals 27.6, 27.8 and 27.85 are plotted in red, green and black respectively. The grey arrow show the position of the front of the overflow plume defined as the deepest location of the 27.85 isopycnal, and the vertical dotted grey line indicate the initial position of the front at hour 103. As the front deepens with time, it is always associated with negative values of *Ri* which indicate that the EVD is turned on, illustrating the sinking of dense waters by the EVD parameterisation.

Representation of the Denmark Strait Overflow in a z-coordinate eddying configuration of the NEMO (v3.6) ocean model: Resolution and parameter impacts

Pedro Colombo[1], Bernard Barnier[1,4], Thierry Penduff[1], Jérôme Chanut[2], Julie Deshayes[3], Jean-Marc Molines[1], Julien Le Sommer[1], Polina Verezemskaya[4], Sergey Gulev[4], and Anne-Marie Treguier[5]

[1]Institut des Géosciences de l'Environnement, CNRS-UGA, Grenoble, 38050, France
[2]Mercator Ocean International, Ramonville Saint-Agne, France
[3]Sorbonne Universités (UPMC, Univ Paris 06)-CNRS-IRD-MNHN, LOCEAN Laboratory, Paris, France
[4]P. P. Shirshov Institute of Oceanology, Russian Academy of Sciences, Moscow, Russia
[5]Laboratoire d'Océanographie Physique et Spatiale, Brest, France

Correspondence: Pedro Colombo (pedro.colombo@univ-grenoble-alpes.fr)

Abstract. We investigate in this paper the sensitivity of the representation of the Denmark Strait overflow produced by a regional z-coordinate configuration of NEMO (version 3.6) to the horizontal and vertical grid resolutions and to various numerical and physical parameters. Three different horizontal resolutions, 1/12°, 1/36° and 1/60°, are used respectively with 46, 75, 150 and 300 vertical levels. In the given numerical set-up, the increase of the vertical resolution did not bring improvement at eddy-permitting resolution (1/12°). We find a greater dilution of the overflow as the number of vertical level increases, and the worse solution is the one with 300 vertical levels. It is found that when the local slope of the grid is weaker than the slope of the topography the result is a more diluted vein. Such a grid enhances the dilution of the plume in the ambient fluid and produces its thickening. Although the greater number of levels allows for a better resolution of the ageostrophic Ekman flow in the bottom layer, the final result also depends on how the local grid slope matches the topographic slope. We also find that for a fixed number of levels, the representation of the overflow is improved when horizontal resolution is increased to 1/36° and 1/60°, the most drastic improvements being obtained with 150 levels. With such number of vertical levels, the enhanced vertical mixing associated with the step-like representation of the topography remains limited to a thin bottom layer representing a minor portion of the overflow. Two major additional players contribute to the sinking of the overflow, the breaking of the overflow into boluses of dense water which contribute to spread the overflow waters along the Greenland shelf and within the Irminger Basin, and the resolved vertical shear that results from the resolution of the bottom Ekman boundary layer dynamics. This improves the accuracy of the calculation of the entrainment by the turbulent kinetic energy mixing scheme (as it depends on the local shear), and improves the properties of the overflow waters such that they more favorably compare with observations. At 300 vertical levels the dilution is again increased for all horizontal resolutions. The impact on the overflow representation of many other numerical parameters were tested (momentum advection scheme, lateral friction, bottom boundary layer parameterisation, closure parameterisation, etc.) but none had a significant impact on the overflow representation.

1 Introduction

Oceanic overflows are gravity currents flowing over topographic constraints like narrow straits, channels or sills, and down topographic slopes. Overflows carry dense waters formed in marginal seas or on continental shelves through intense air-sea exchanges (cooling, evaporation) from their source regions into the great ocean basins where they join the general ocean circulation (Legg et al. (2006), Legg et al. (2009)). Overflows are often structured as plumes or boluses of dense fluid thick of a few hundred meters, accelerated toward great depths by gravity (Magaldi and Haine (2015), Koszalka et al. (2017), Almansi et al. (2017), or Spall et al. (2019)). As they cascade down over distances that may reach up to a few hundreds of kilometers, they entrain ambient waters through advection and intense shear-driven mixing processes. After reaching a depth close to a neutral buoyancy level and a quasi-geostrophic equilibrium, the entrainment of ambient water is significantly reduced and the overflow becomes a neutrally buoyant bottom density current (Legg et al. (2009)).

Overflows of importance because of their contribution to the general circulation are those associated with; the Denmark Strait and the Faroe Bank Channel where dense cold waters formed in the Arctic Ocean and the Nordic Seas flows into the North Atlantic (Girton and Standford (2003), Brearley et al. (2012), Hansen and Østerhus (2007)); the strait of Gibraltar where dense saline waters generated in the Mediterranean Sea overflow into the Atlantic Ocean (Baringer and Price (1997)); the strait of Bab-el-Manded where the highly saline Red Sea waters flow into the Gulf of Aden and the Indian ocean (Peters et al. (2005)), and the continental shelves of the polar oceans (Killworth (1977), Baines and Condie (1998)), in particular around Antarctica where the high salinity shelf waters formed in Polynyas ventilate the Antarctic Bottom waters (Mathiot et al. (2012), Purkey et al. (2018)). More reference papers can be found in Legg et al. (2009), Magaldi and Haine (2015), Mastropole et al. (2017). Altogether, these overflows feed most of the world ocean deep waters and play an important role distributing heat and salt in the ocean. For the case of the Denmark Strait overflow (DSO hereafter), it feeds the Deep Western Boundary Current in the North Atlantic, and so contributes to the Atlantic Meridional Overturnin Cell and the global thermohaline circulation (Dickson and Brown (1994), Beismann and Barnier (2004), Hansen and Østerhus (2007), Dickson et al. (2008), Yashayaev and Dickson (2008), Danabasoglu et al. (2010), Zhang et al. (2011), von Appen et al. (2014)). This world-ocean wide importance of the overflows makes their representation a key aspect of ocean general circulation models (OGCMs).

A variety of physical processes of different scales are involved in the control of overflows and their mixing with the ambient waters (Legg et al. (2008)). Dynamical processes (e.g. hydraulic control/jump at sills/straits, mesoscale instability of the dense water plume, interactions of the plume with overlaying currents), have length scales of a few kilometers in the horizontal and a few tens of meters in the vertical. Such scales of motion are not resolved in present large-scale coarse resolution (non-eddying) ocean models used for climate studies but can be simulated in eddy-resolving models (Legg et al. (2008)). Diapycnal mixing processes (e.g. entrainment of ambient waters into the cascading plume by shear-driven mixing, bottom friction, internal wave breaking) have even smaller scales (from meters down to the milimetric scale) and cannot be resolved in present ocean models Girton and Standford (2003). Their effects are represented by a vertical turbulence closure scheme, the aim of which is to achieve a physically-based representation of this small-scale turbulence. However, models using fixed geopotential levels as vertical coordinate (i.e. z-level models) are known to generate spurious (i.e. excessive and non-physical) diapycnal mixing when moving dense water downslope. The link of this spurious mixing with the staircase-like representation of the bottom topography peculiar to these models is well established (Winton et al. (1998), Wang et al. (2008)). The parameterisation of overflows in these models has been the topic of a number of studies (Beckmann and Döscher (1997), Campin et al. (2012), Killworth (1977), Song and Chao (2000), Danabasoglu et al. (2010), Wang et al. (2015)). A large number of idealized model studies, many of them conducted in the DOME framework (Dynamics of Overflows Mixing and Entrainment, Legg et al. (2006), Legg et al. (2009)), tested the ability of overflow parameterizations against very high-resolution simulations in a variety of OGCMs. When used in global simulations these parameterisations improve overflows, but still produce deep or bottom water properties that are not yet satisfactory if not inadequate (Condie et al. (1995), Griffies et al. (2000), Legg et al. (2009), Danabasoglu et al. (2010), Danabasoglu et al. (2014), Downes et al. (2011), Weijer (2012), Heuzé et al. (2013), Wang et al. (2015), Snow et al. (2015)). Past model studies performed with DOME-like idealized configurations also permitted to gain understanding on the dynamics of overflows and on the sensitivity of their representation in models to physical and numerical parameters (see Reckinger et al. (2015), for exhaustive references and a synthesis of the main findings). Significant differences between models due to the type of vertical coordinate system were pointed out (e.g. Ezer and Mellor (2004), Legg et al. (2006), Wang et al. (2008), Laanaia et al. (2010), Wobus et al. (2011), Reckinger et al. (2015)).

Numerical modelling of dense water cascades with OGCMs designed to simulate the large scale circulation still represents a challenge, especially because the hydrostatic approximation on which these model rely remove the vertical acceleration from the momentum equation. This results in a misrepresentation of the diapycnal mixing processes (Özgökmen (2004)) and requires, to represent their effects, a turbulence closure scheme. Magaldi and Haine (2015), compared high-resolution ($2km$) hydrostatic and non-hydrostatic simulations of dense water cascading in a realistic model configuration of the Irminger basin. They found that for such $2km$ horizontal resolution, the parameterization of the non-resolved turbulence used in the hydrostatic model was accurately representing the effects of the lateral stirring and vertical mixing associated with the cascading process. Most recent high-resolution regional modelling studies of the Denmark Strait overflow (Magaldi et al. (2011), Magaldi and Haine (2015), Koszalka et al. (2013), Koszalka et al. (2017), Almansi et al. (2017), Spall et al. (2019)) or the Faroe Bank Chanel overflow (Riemenschneider and Legg (2007), Seim et al. (2010)) have been using hydrostatic model configurations of the MIT OGCM. These studies, as they provide modelled overflows in good agreement with observations, significantly improved the actual understanding of the overflows and their modelling. For the case of the DSO, the studies referred above especially pointed out the importance of the resolution of the cyclonic eddies linked to the dense overflow water boluses on the entrainment, and the importance of the dense water cascading from the East Greenland Shelf with the Spill Jet. On the modelling aspects, these studies provided some rationale regarding the grid-resolution that permit a representation of the overflows that agrees with observations (a resolution of $2km$ in the horizontal and a few tens of meters near the bottom in the vertical). They also characterized the dependence on various model parameters regarding the mixing of the overflow waters with ambient waters. For the case of the Faroe Bank Channel overflow for example, Riemenschneider and Legg (2007) found the greatest sensitivity of the mixing in changes in horizontal resolution. However, the high resolution used in these regional studies cannot yet be used in eddying global model hindcast simulations of the last few decades or for eddying ensemble simulations.

Indeed, global eddying OGCM are now commonly used at resolutions of 1/12°, which yields a grid-size of about $5km$ in the region of the Nordic Seas overflows and may resolve with some accuracy the entrainment of ambient waters into the overflow plume by eddy-driven advection, but not the small-scale diapycnal mixing which still needs to be fully parameterized by the turbulence closure scheme. **?** studied the influence of horizontal resolution on the relative magnitudes and pathways of the Denmark Strait and Iceland-Scotland overflows in a North Atlantic configuration of the HYCOM OGCM (Chassignet et al. (2003)). They found that at 1/12°, the highest resolution tested, the simulations show realistic overflow transports and pathways and reasonable North Atlantic three-dimensional temperature and salinity fields. The ability of HYCOM to represent the spreading of the overflow waters at 1/12° resolution was later confirmed by the studies of Xu et al. (2010) and Xu et al. (2014). Marzocchi et al. (2015) provided an assessment of the ocean circulation in the subpolar North Atlantic in a 30-years long hindcast simulation performed with the ORCA12 configuration, a z-coordinate partial-step global implementation of the NEMO OGCM (Madec et al. (2016)) at 1/12° resolution developed by the DRAKKAR Group (2014). They found that the model had some skills as the volume transport and variability of the overflows from the Nordic Seas were reasonably well represented. However, significant flaws were found in the overflow water mass properties that were too warm (by 2.5 to 3°C) and salty. This latter bias can be partly attributed to the excessive entrainment peculiar to the z-coordinate, but other sources of biases, like the warm and salty bias found in the entrained waters of the Irminger basin, a persisting bias in this type of model simulations (Treguier (2005), Rattan et al. (2010)), are likely to contribute.

Despite the progresses reported above, it is clear that overflow representation is still a persisting flaw in z-coordinate hydrostatic ocean models. NEMO (version 3.6) is now commonly used in eddying (1/4° to 1/12°) configurations for global or basin-scale, climate-oriented studies (e.g. Megan et al. (2014), Williams et al. (2015), Treguier et al. (2017), Sérazin et al. (2018)), reanalyses and operational forecasts (Lellouche et al. (2013), Lellouche et al. (2018), Le Traon et al. (2017)), or ensemble multi-decadal hindcast simulations (Bessières et al. (2017), Penduff et al. (2018)). Even though their use by a growing community, model configurations like ORCA12 remain computationally expensive and sensitivity studies are limited. Therefore, there is a need to establish the sensitivity of the simulated overflows to the available parameterizations in a realistic framework relevant to the commonly used resolutions.

The objective of this work is to provide a comprehensive assessment of the representation of overflows by NEMO in a realistic eddy-permitting to eddy-resolving configuration that is relevant for many present global simulations performed with this model, in particular with the standard 1/12° ORCA12 configuration setup similar to that presently used for operational forecasting by the CMEMS1. Therefore, we limit our investigation to the sensitivity of the overflow representation when standard parameters or resolution are varied, the objective being to identify the model parameters and resolutions of significant influence. However, because NEMO is also used at much higher resolution (1/60°, e.g. Ducousso et al. (2017.)) and offers possibilities of local grid refinement (Debreu et al. (2007)) already used with success (e.g. Chanut et al. (2008), Biastoch et al. (2009), Barnier et al. (2020)), the use of a local grid refinement in overflow regions is also investigated. The approach is to set-up a regional model configuration that includes an overflow region that is similar, in terms of resolution and physical or numerical parameters, to the global ocean eddying configurations widely used in the NEMO community. The DSO is chosen as test case because of its importance and the relatively large amount of observations available. Considering that mesoscale eddies are not fully resolved at this resolution, the focus is on the overflow mean product and not on the details of the dynamics as it is done in the very-high resolution ($2km$) studies of Magaldi and Haine (2015) and Koszalka et al. (2017).

This work is presented in three parts. The first part (Section 2) presents the method used to carry out the sensitivity tests. It describes the regional NEMO z-coordinate configuration developed to simulate the DSO, and the initial and forcing conditions common to all sensitivity simulations. It also describes the simulation strategy and the diagnostics developed for the assessment of the model sensitivity. The control simulation that represents a standard solution is run and diagnosed. The second part (Section 3) describes the sensitivity of the modelled overflow to a large number of parameters. Results from about 50 simulations are used, spanning vertical resolution (46, 75, 150, and 300 vertical levels), horizontal resolution (1/12°, 1/36° and 1/60°), lateral boundary condition (free slip and no-slip), bottom boundary layer parameterization, closure scheme, momentum advection scheme, etc. The third part (Section 4) describes in details the DSO produced by our best solution. We conclude the study with a summary of the main findings and some perspectives to this work.

2 Methods

2.1 Reference regional model configuration

We briefly describe the regional model configuration of reference used for the control run (changes being made afterwards in the different sensitivity tests). Version 3.6 of NEMO is used. The geographical domain is shown in Fig. 1. It includes part of the Greenland Sea, the Denmark Strait and a large part of the Irminger Sea. The reference NEMO setting has been designed to be representative of the solution that a global model would produce. Therefore, the configuration (geometry, numerical grid and schemes, physical parameterizations) has been extracted from an existing global ORCA12 configuration ($1/12°$ resolution, 46 z-levels) used in many simulations of the Drakkar Group (see Molines et al. (2014) for description and namelist). This configuration, referred to as DSO12.L46 (for 1/12° and 46 vertical levels) hereafter, is described with emphasis being given to parameters chosen for the control simulation from which sensitivity tests are performed. Changes that are made in the sensitivity tests are also indicated.

- Bottom topography and coastlines are exactly those of the global $1/12°$ ORCA12 configuration and are not changed in sensitivity experiments, except when grid refinement is used. In this latter case the refined topography is a bi-linear interpolation of that at $1/12°$, so the topographic slopes remain unchanged.
- The horizontal grid in the control run is a subset of the global tripolar grid at 1/12° (the so called ORCA12, $\sim 5km$ at the latitudes of the Irminger basin). The sensitivity to horizontal resolution is addressed by increasing the grid resolution to $1/36°$ ($\sim 2km$) and $1/60°$ ($\sim 1km$) over a small region that includes the Denmark Strait and a large part of the east Greenland shelf break (Fig. 1). The AGRIF 2-way grid refinement software (Debreu et al. (2007)) is used to connect the nested grids.
- Vertical resolution: The standard 46 fixed z-levels used in many Drakkar simulations are used in the Control simulation, with partial-steps to adjust the thickness of the bottom level to the true ocean depth (Barnier et al. (2006)). Sensitivity

experiments also use 75, 150 and 300 z-levels. The cell-thickness as a function of depth is shown in Appendix A (Fig. A1) and the resolution of the Ekman layer in the different vertical resolution settings discussed.

- Momentum advection scheme: A vector invariant form of the momentum advection scheme (the energy and enstrophy conserving EEN scheme, Sadourny et al. (1975), Barnier et al. (2006) with the correction proposed in Ducousso et al. (2017.)) is used in the control and sensitivity experiments with an explicit biharmonic viscosity. Sensitivity tests used the upstream-biased third order scheme (UBS scheme) available in NEMO. Since this scheme includes a built-in biharmonic-like viscosity term with an eddy coefficient proportional to the velocity, no explicit viscosity is therefore used in the momentum equation when used.

- Isopycnal diffusivity on tracers: The TVD (Total Variance Diminishing) scheme standard in NEMO is used with the Laplacian diffusive operator rotated along isopycnal surfaces. The slope of the isopycnal surfaces are calculated with the standard NEMO algorithm. The diffusion coefficient remains the same in all sensitivity experiments. A sensitivity experiment was made that calculates the slope of the isopycnal using the Griffies Triad Algorithm (Griffies (1998)).

- Vertical mixing: it is treated with the standard NEMO TKE scheme Madec et al. (2016) Reffray et al. (2015). Because the model uses a hydrostatic pressure, the case of unstable stratification is treated with an Enhanced Vertical Diffusivity (EVD) scheme that sets the value of the vertical diffusion coefficient to $10 m^2 s^{-1}$ in case of static instability of the water column. It is applied on tracers and momentum to represent the mixing induced by the sinking of the dense water. A few sensitivity experiments used the EVD scheme on tracers only. Other experiments used the $K-\epsilon$ closure scheme proposed in NEMO Reffray et al. (2015).

- Bottom boundary layer parameterization BBL: the control run does not use the BBL scheme that is available in NEMO, based on the parameterization of Beckmann and Döscher (1997). The scheme is tested in a sensitivity experiment.

- The free surface (linear filtered) scheme, the LIM2 sea-ice parameters, the scheme and data used at the lateral open boundaries, and the bulk formula and atmospheric forcing data that drive the model are identical in all experiments.

2.2 Initial conditions, surface and open boundary forcing

Data used to initialize the simulation and to drive the flow at the prescribed open boundaries are obtained from an ORCA12 simulation. This global simulation was initialized with temperature and salinity values from a climatology (Levitus, 1998) and started from rest. The atmospheric forcing that was used is the daily mean climatology of the 6-hourly DFS4.4 atmospheric forcing Brodeau et al. (2010). The forcing data of each day of the year is the climatological mean of that day calculated over the period 1958 to 2001 (see Penduff et al. (2018), for details). This global simulation was run for almost 9 decades with this climatological forcing being repeated every year. It has also been used in the studies of e.g. Sérazin et al. (2015), or Grégorio et al. (2015) to study the intrinsic inter-annual variability. Every DSO model simulation used in the present study (the control run and all sensitivity runs) is initialized with the state of the global run on January 1^{st} of year 72 and is run for a period of 5

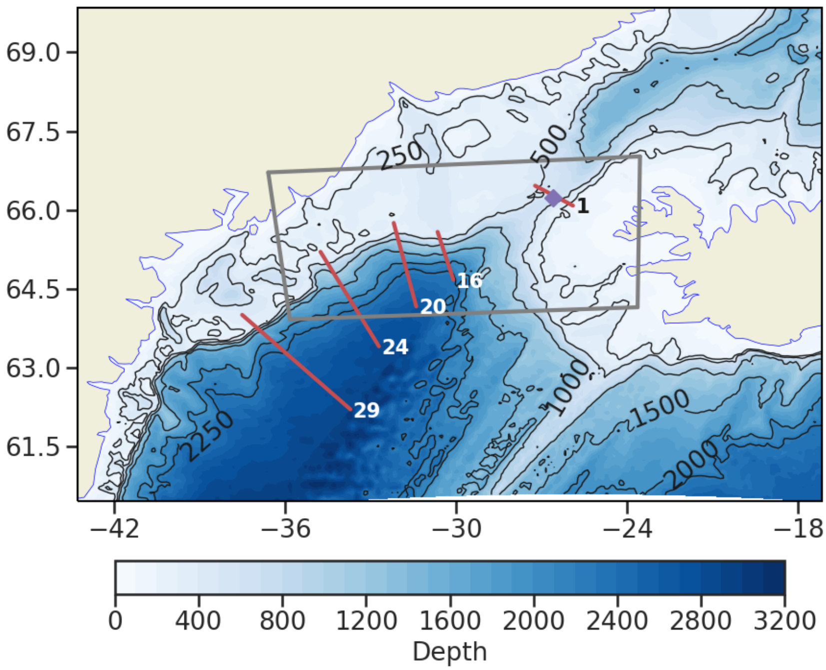

Figure 1. *Regional model domain. In colour the ocean depth. The 250, 500, 1000, 1500 and 2000 meter depth isobaths are contoured in black. The grey box indicates the region where the 2-way grid refinement* ($1/36^{\circ}$ *and* $1/60^{\circ}$) *is applied in some simulations. The location of the various sections used to monitor the model solution are shown by the red lines. Section 1 is the reference section chosen for the sill.*

years (until year 76). The atmospheric forcing is the same as in the global run and it is also repeated every year. The data used at the open boundaries of the DSO domain are extracted from years 72 to 76 of the global simulation (5 days mean outputs), so the open boundary forcing is fully consistent with the atmospheric forcing and the initial state.

We have chosen such a simulation scenario because several decades have passed from the initialization of the global run, and the model has reached a dynamical equilibrium and is close to thermodynamical equilibrium, which results in a negligible drift in the mass field. This allows to undoubtedly attribute the changes seen in the sensitivity experiments to the changes made in the model setting. During this period the transport at the sill of the Denmark Strait is very stable and close to observed values ($\sim 3Sv$, see Section 2.3).

In this scenario, the initial bottom stratification is expected to be particularly affected by biases introduced in the properties of the water masses by the unrealistic representation of the overflows in the z-coordinate framework, so any improvement achieved in the representation of the overflow should be rapidly identified. However, the presence of these model biases reduces the relevance of the comparison to observations.

2.3 Control simulation DSO12.L46

A control simulation (referred to as DSO12.L46), is performed with the characteristics described in Section 2.1 and the initial and forcing conditions described above. As expected from its design, the solution of the DSO12.L46 5-year long control run reproduces very faithfully the solution of years 72 to 76 of the global ORCA12 run. This was verified in different aspects of the circulation. The large-scale circulation patterns is found to be very similar in both simulations, as illustrated with the surface and bottom currents shown in Fig. 2. The predominant currents such as the East Greenland Current (EGC), the Irminger Current (IC) and the DSO itself are very similar between the global and the regional model. This circulation scheme also compares well with that described from observations in Daniault et al. (2016) and from an ORCA12 model circulation simulation in Marzocchi et al. (2015). The correspondence between Global and Control runs regarding the properties of abyssal waters was confirmed, especially at 29 different sections along the path of the overflow the sections location is outlined in Appendix B as well as the correspondence in transport and bottom mean temperature across these sections (not shown). The bottom temperature in the Irminger basin was found to be very similar in both simulations, with a diluted signature of the overflow waters as expected from a z-level model after a simulation of several decades. Therefore this regional model appears as a reliable simulator of what the global model produces in that region.

Most important for the present study are the properties of the overflow "source waters", i.e. the properties of the waters at the sill of the Denmark Strait. Fig. 3 shows the volume transport at the sill of waters flowing below the 27.8 isopycnal. Both the global and the control runs show very similar mean and variability and a transport that is very steady during the 5 years of simulation. The model mean ($\sim 3Sv.$) is comparable to but in the lower range of the values published in the work of Macrander et al. (2005) or Jochumsen et al. (2012). The standard deviation computed from 5-day outputs ($\sim 0.3Sv$ in the control run, increasing to $\sim 0.7Sv$ when calculated from daily values) is rather small when compared to the $1.6Sv$ of Macrander et al. (2005). The modelled flow of dense waters presents a marked seasonal cycle which is not present in observations (Jochumsen et al. (2012)). This signal is the signature of the large seasonality of the barotropic flow (Fig. 3) that constrains the whole water column.

Fig. 4 presents the characteristics of the mean flow across the sill. The model simulation is compared to the data of Mastropole et al. (2017) who processed over 110 shipboard hydrographic sections across Denmark Strait (representing over 1000 temperature and salinity profiles) to estimate the mean conditions of the flow at the sill. Compared with the compilation of observations of Mastropole et al. (2017) (Fig. 4a) the model simulation (Fig. 4c) shows a similar distribution of the isopycnals, specially the location of the 27.8 isopycnal. However, the observations exhibit waters denser than 28.0 in the deepest part of the sill which the model does not reproduce. Large flaws are noticed regarding the temperature of the deepest waters which are barely below 1°C when observations clearly show temperatures below 0°C (also seen in the observations presented in e.g. Jochumsen et al. (2012), Jochumsen et al. (2015), Zhurbas et al. (2016)). A bias toward greater salinity values (not shown) is also found in the control experiment which shows bottom salinity of 34.91 compared to 34.9 in the observations shown in Mastropole et al. (2017), but the resulting stratification in density shows patterns that are consistent with observations. The distribution of velocities (Fig. 4b) is also found realistic when compared with observations (i.e. the Fig. 2b of Jochumsen et al.

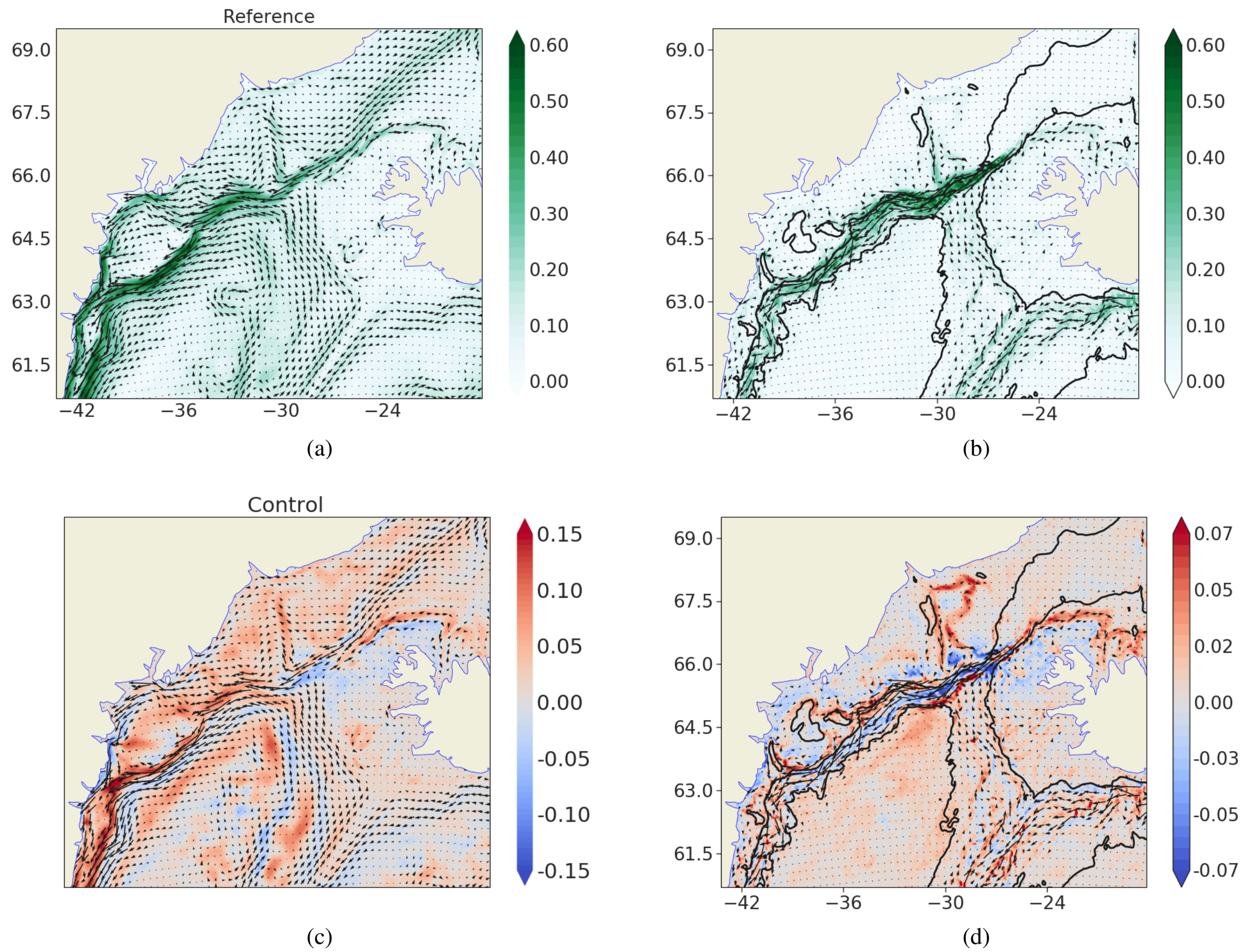

Figure 2. *Surface (a) and bottom (b) mean currents (year 76) in the global ORCA12 simulation. Vectors/Colors indicate current direction/speed in ms^{-1}. Surface (c) and bottom (d) mean currents (year 76) in the regional DSO12.L46 regional simulation. Vectors indicate direction of the current. Colors indicate the current speed difference between the global and the regional simulation (in ms^{-1}). Blue/red indicate that the current speed is greater/smaller in the global/regional simulation. Vectors at the bottom circulation are scaled by a factor of 7 compared to the surface for visibility reasons.*

(2012)) with a bottom intensified flow of dense waters (up to 0.4 ms^{-1}) in the deepest part of the sill. Although the present setup is designed to investigate model sensitivity in twin experiments and not for comparison with observations ends, the control run appears to provide a flow of dense waters at the sill that is stable over the 5 year period of integration and reproduces qualitatively the major patterns of the overflow "source waters" seen in the observations. Therefore, despite existing biases, the presence of a well identified dense overflow at the sill confirms the adequacy of the configuration for the sensitivity studies.

Finally, in order to assess improvements in the sensitivity tests, the major flaws of the control simulation must be described. If similarities with observations are found at the sill, the evolution of the DSO plume in the Irminger basin is shown to be

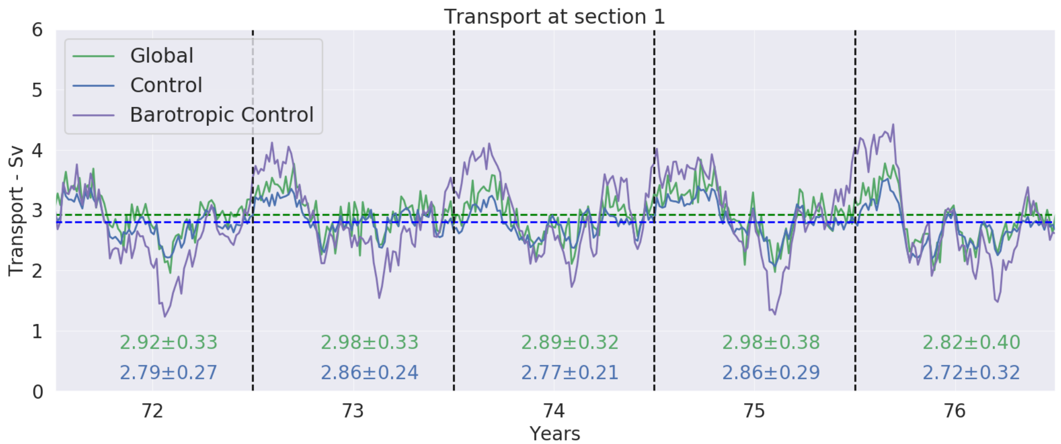

Figure 3. *Time evolution of the volume transport of waters of potential density greater than $\sigma_0 = 27.80kgm^{-3}$ at the sill section (Section 1 in Fig. 1) in the Control (blue line) and the Global (green line) simulations (the latter providing the open boundary conditions). Annual mean and std (in Sv) are indicated for every individual year of simulation. The depth-integrated (barotropic) transport is shown for the Control simulation (purple line). 5-day mean values are used to produce this figure.*

unrealistic in the present setup of the control simulation, and presents the same flaws as in the global run. This is demonstrated by the analysis of the temperature and potential density profiles at the most downstream cross-section (section 29) where the model solution is compared to observations (Fig. 5), and at the other cross-sections along the path of the DSO in the Control simulation (the plots on the left hand side of Fig. 6 and 7). The evolution of the DSO plume as it flows southward along the East Greenland shelf break is represented by a well-marked bottom boundary current (e.g. the bottom currents in Fig. 2) carrying waters of greater density than the ambient waters. Far downstream the sill (section 29) the observations show a well-defined plume of cold water confined below the 27.8 isopycnal under $1500m$ depth (Fig. 5a). The bottom temperature is still below 1°C. In the Control simulation (Fig. 5c), one can clearly identify the core of the DSO plume by the 27.85 isopycnal, so it is clear that the plume has been sinking to greater depth as it moved southward. This evolution is only qualitatively consistent with the observations at this section. The modelled plume is significantly warmer and exhibits a core temperature of 3.5° (against 2°C or less in the observations). The plume is also much wider than observed, exhibits much smaller temperature and salinity gradients separating the plume from the interior ocean, indicating a greater dilution with ambient waters. The plume is barely distinguishable from the ambient fluid below 2000m when it is still well marked at that depth in the observations. The sinking and dilution of the plume as it flows southward along the slope of the Greenland shelf is well illustrated in Fig. 6 and 7 (left hand panels) which display the potential temperature at the other sections. If the overflow waters are still well-marked at section 16 (Fig. 6a), it is barely distinguishable from the ambient water at section 29.

The bottom temperature shown in Fig. 8a illustrates this excessive dilution of the overflow waters. Indeed, the cold water tongue seen in the bottom of the Denmark strait at a temperature of about 2°C clearly sinks as it extends to the southwest and crosses the 1000 m and the 1500 m isobaths. But as it sinks, it is rapidly diluted and looses its “cold water” character, and is

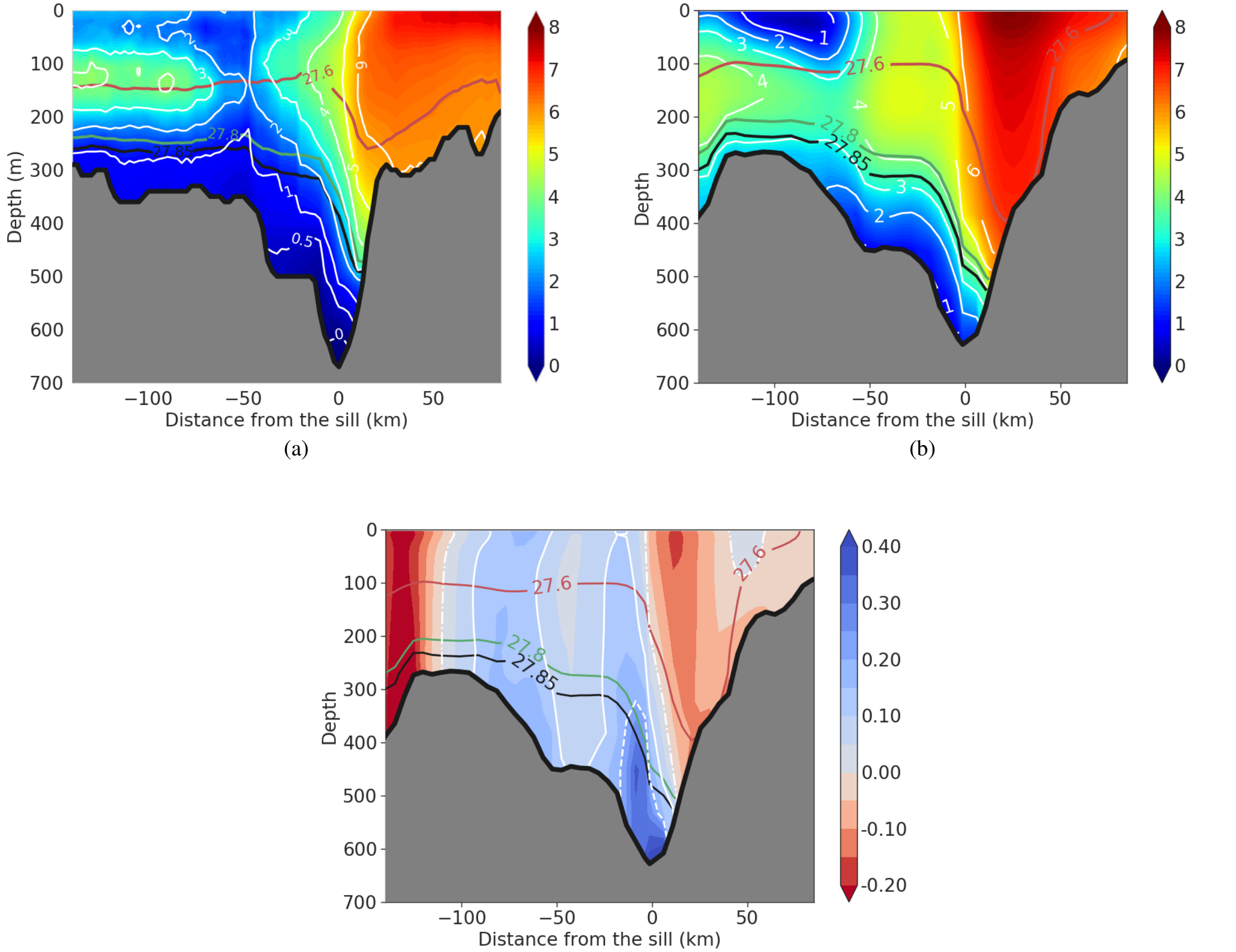

Figure 4. *Mean flow characteristics (annual mean of year 76) in the global simulation at the sill. Temperature (°C) in colours and white contours for (a) the observations (Mastropole et al. (2017)) and (b) the control simulation (1/12° and 46 vertical levels). Potential density values (σ_0) are shown by the contour lines coloured in red (27.6), green (27.8) and black (27.85). (c) The velocity normal to the section in the control simulation (southward velocity in blue colour being negative). White lines indicate the $0ms^{-1}$ contour (dashed-dotted line), the $-0.1ms^{-1}$ (full line) and the $-0.2ms^{-1}$ contour (dashed line). The model section being taken along the model coordinate, the topography is slightly different in the model.*

not distinguishable from the background waters beyond 64.5°N. Such plot of the bottom temperature summarizes rather well what we also learned in the analysis of the cross sections (e.g. Fig. 5). The same plot for the salinity (not shown) shows waters fresher than surrounding waters in the overflow path, with a salinity that increases from 34.91 at the sill to around 34.96 at

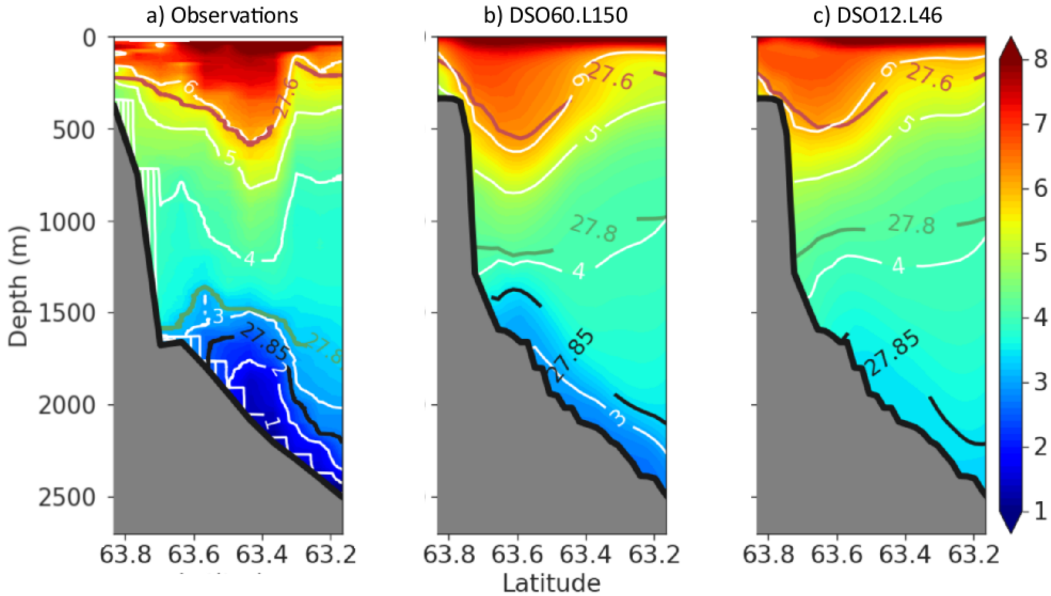

Figure 5. *Potential Temperature (°C) at section 29 in (a) the observations (ASOF6-section, Quadfasel (2004)), (b) the 1/60°, 150 levels simulation (annual mean), and (c) the 1/12°, 46 level simulation (annual mean). Red/Green/Black full lines are isopycnals 27.6/27.8/27.85. White lines are isotherms by 1°C interval. In panel b), the section 29 is outside (100 km downstream) the 1/60° AGRIF zoom, so the effective resolution is 1/12°. But the water masses acquired their properties upstream within the 1/60° resolution zoom. Observation data were downloaded at: https://doi.pangaea.de/10.1594/PANGAEA.890362*

1000 m and reaches the background value (~ 35.02) at 1500 m depth. This demonstrates the large dilution by entrainment with the waters of the Irminger current in the final solution.

3 Results from sensitivity experiments

We performed a large set of simulations (over 50) with different settings of the DSO model configuration in order to better understand the impact of the different parameters on the final representation of the DSO at a resolution of $1/12°$, including a few with local grid refinement. The detailed list of theses experiments is provided in Appendix A. Following the convention for DSO12.L46 , the simulations are referred as DSOxx.Lyy where xx informs on the horizontal grid resolution (e.g. 36 for 1/36°), and yy on the number of vertical levels (e.g. 150 for 150 levels). After testing different physical parameterizations, numerical schemes and grid resolutions, we concluded that the only parameters affecting the overall representation of the overflow in a significant way are the horizontal and vertical resolutions. No significant impact was found on the representation of the DSO for all the other parameters tested, the flaws described in the previous section resisting the changes. Therefore, we only present

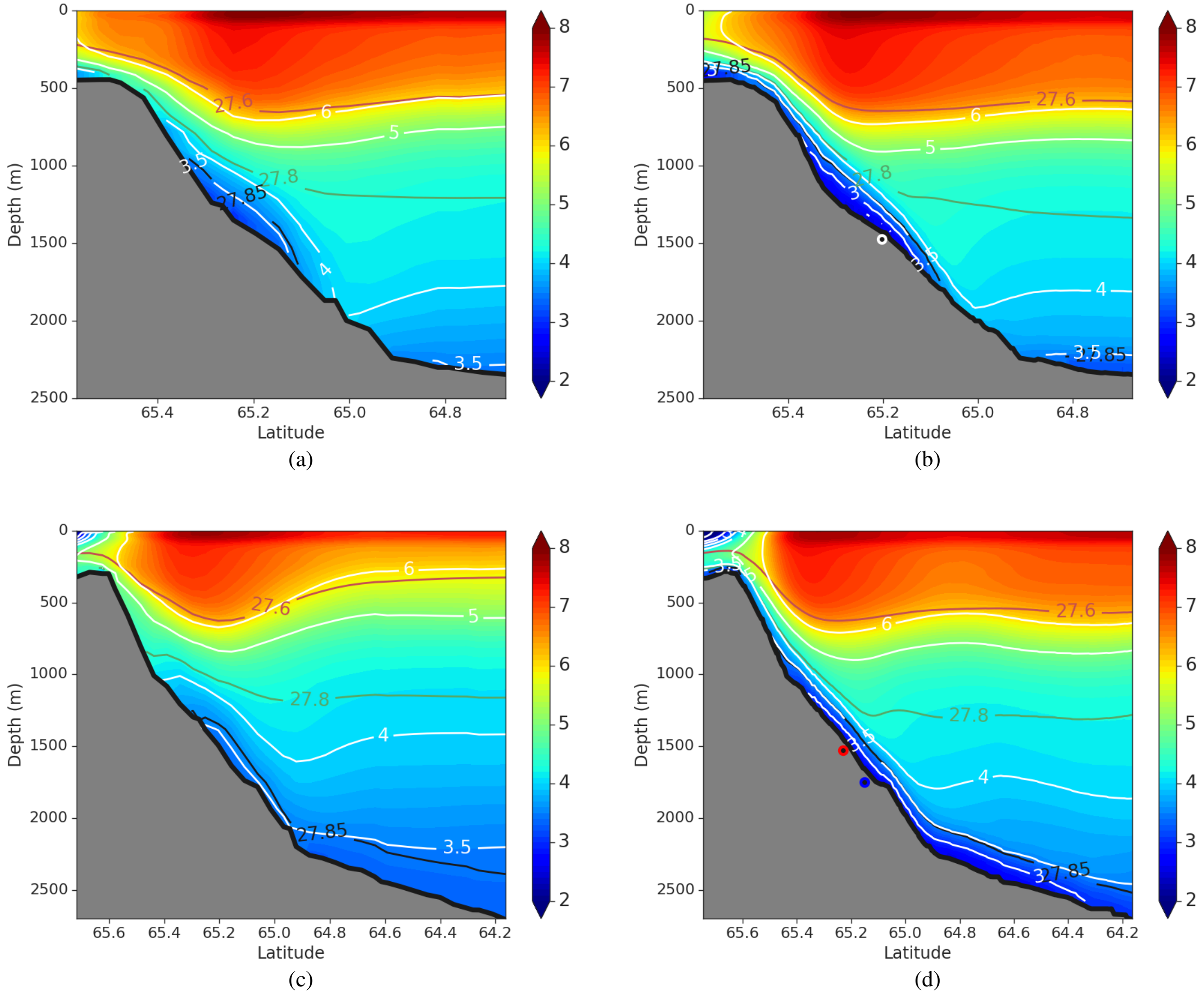

Figure 6. *Distribution with depth of the annual mean temperature (5th year of model run) at Section 16 (Dohrn Bank array) for a) simulation DSO12.L46, and b) simulation DSO60.L150 (in the refined grid), and at Section 20 (spill jet section) for c) simulation DSO12.L46, and d) simulation DSO60.L150 (in the refined grid). Temperature (°C) in colours with white contours. Potential density values (σ_0) are shown by the contour lines coloured in red (27.6), green (27.8) and black (27.85) The white-rimmed dot on figure (b) correspond to the location of the profiles displayed in Fig. 15 and the red-rimmed and blue-rimmed dots on figure (d) correspond to the locations of the profiles displayed in Fig. 13.*

the results obtained when the resolution (vertical or horizontal, or both) is changed. The other sets of sensitivity tests are very briefly discussed in Appendix A.

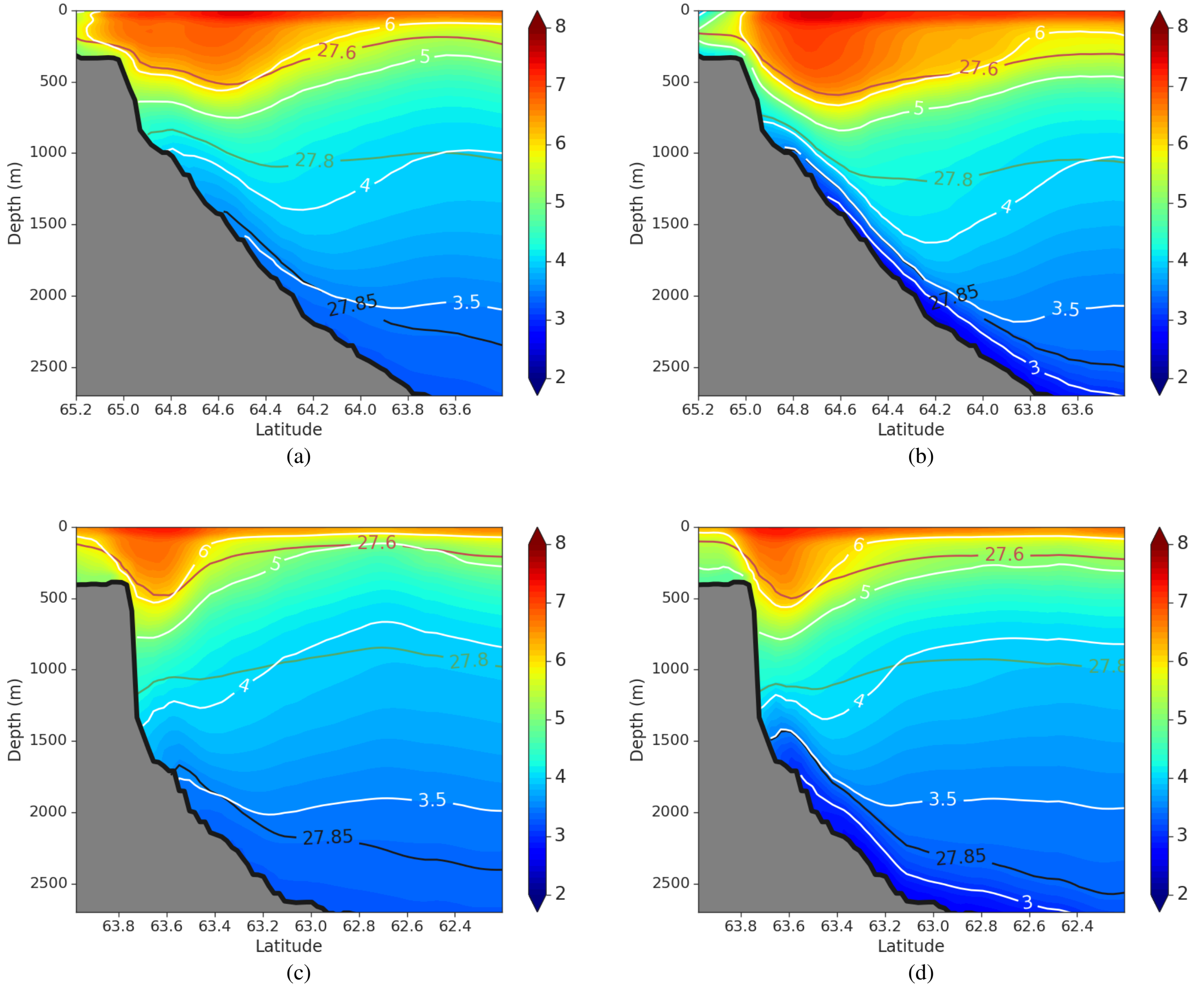

Figure 7. *As in Fig. 6 at Section 24 (TTO array) for a) simulation DSO12.L46 and b) simulation DSO60.L150, and at Section 29 (Angmagssalik array) for c) simulation DSO12.L46 and d) simulation DSO60.L150.*

From the large set of diagnostics performed to assess the impact of model changes on the DSO, it was found that the analysis of the bottom temperature in the Irminger Basin is quite a pertinent way to provide a first assessment of the changes in the properties of the overflow. This diagnostic is consequently used to first compare the different sensitivity simulations, and additional diagnostics are used later for more quantitative assessments of the DSO representation. Improvements between sensitivity tests are identified when one or several of the major flaws described in the previous (section 2.3) section are reduced. These major flaws, identified on the time-mean properties of the overflow of the control simulation (section 2.3) are; a too warm bottom temperature; an overflow not deep enough; and weak temperature gradients between the plume and the ambient fluid (a not well-defined dense water plume indicating too much dilution.)

3.1 Sensitivity to vertical resolution at $1/12°$

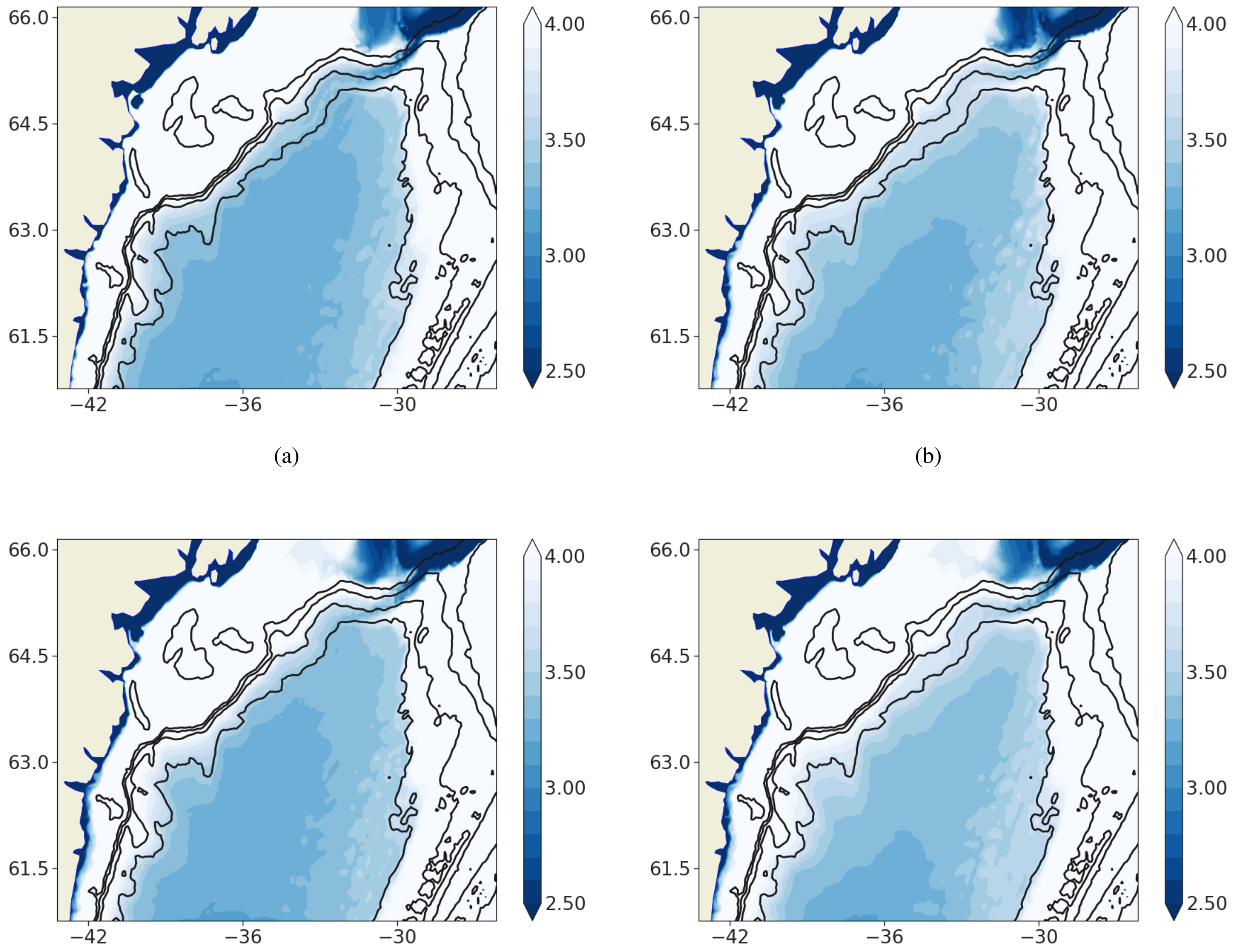

Figure 8. *Annual mean bottom temperature (5th year of simulation) in °C at $1/12°$ horizontal resolution in simulations differing the number of vertical levels. a) 46 levels (DSO12.L46) b) 75 levels (DSO12.L75), c) 150 levels (DSO12.L150) d) 300 levels (DSO12.L300). Isobaths 500m, 1000m, 1500m and 2000m are contoured in black.*

The first set of tests that we present is the sensitivity of the DSO representation to the vertical resolution at $1/12°$ horizontal grid resolution. The DSO12.L46 control run (46 levels) is compared with simulations with 75, 150 and 300 vertical levels, all other parameters being identical. The mean bottom temperature of the 5th year of these 4 simulations (Fig. 8) reveals that the increase in vertical resolution at $1/12°$ works to the detriment of the representation of the overflow. In the 75 levels case, the descent of the DSO plume stops at the 1500 m isobath blocked by a westward flow of warm Irminger waters that invades the 1500 m to 2000 m depth range. This yields a general warming of the bottom waters in the Irminger Basin and along the whole East Greenland shelf break. The overflow representation improves slightly in the 150 levels case as the DSO plume still reaches the 2000 m isobath, feeding the deep basin, but with less efficiency than in the 46 levels case. Finally, the representation of the DSO is even more degraded in the 300 level case, this resolution exhibiting the greatest dilution of the DSO waters among all resolutions. This deterioration of the overflow properties was verified in all the other diagnostics (hydrographic sections, T,S diagrams, etc.).

To understand that behavior, one recalls how the cascading of dense water is treated in the z-coordinate NEMO framework. In case of static instability (i.e. when the fluid at a given level has a greater potential density than the fluid at the next level below), the vertical mixing coefficient, usually calculated with the TKE closure scheme, is assigned a very large value (usually 10 m^2s^{-1}). This instantaneously (i.e. over one time step) mixes the properties (temperature, salinity, and optionally momentum) of the two cells, re-establishing the static stability of the stratification. This parameterisation, referred to as EVD (Enhanced Vertical Diffusion already described in Section 2.1), is at work to simulate the sinking (convection) and the cascading (overflow) of dense waters. Note that when the EVD was not used in our experiments, we noticed that the TKE mixing scheme often produced values of the diffusion coefficient larger than 1 m^2s^{-1} and in very particular cases exceeding 10 m^2s^{-1}.

The vertical diffusivity along the path of the overflow is shown in Fig. 9 for the 46 and the 300 level cases (the definition and method of calculation of the overflow path are given in Appendix B). Compared to the 46 level case (Fig. 9a), the 300 level case (Fig. 9b) exhibits greater values of the diffusion coefficient near and above the bottom along the path of the overflow. This enhanced mixing affects the overflow plume, which 200 km after the sill does not contains waters denser than 27.85, while such waters are still found 300 km down the sill in the 46 level case. The 300 level case also exhibits large values of diffusion coefficient at intermediate depth (between isopycnal 27.8 and 27.6). They are driven by the vertical shear existing between the northward surface current passing through the Denmark Strait (the NIIC) which is very variable in position and intensity, and the southward deep current carrying the overflow waters (e.g. Spall et al. (2019)). We notice that the mixing is significantly greater in the high resolution case, which indicate that this process could also contribute to the dilution of the overflow plume. However, it does not seem to affect the thickness of the 27.8 isopycnal. An explanation to this is searched for following the paradigm of Winton et al. (1998) which states that the horizontal and vertical resolutions should not be chosen independently: the slope of the grid ($\Delta z/\Delta x$) has to equal the slope of the topography (α) to produce a proper descent of the dense fluid (see their Fig. 7). If this is not the case, the vein of dense fluid thicken by mixing with the ambient fluid at a rate proportional to the ratio of the slopes $\alpha/(\Delta z/\Delta x)$.

To show how NEMO follows this concept, we simulate the descent of a continuous source of cold water down a shelf break in an idealized configuration (with no rotation). The configuration (Fig. 10) is as follows. A 20km wide shelf of depth 500m is located on the left side of the 2D domain. It is adjacent to a shelf break 250km wide reaching the depth of 3000m, and then the bottom is flat. Initial conditions are as follows: a blob of cold water is placed on the bottom of the shelf with a temperature of

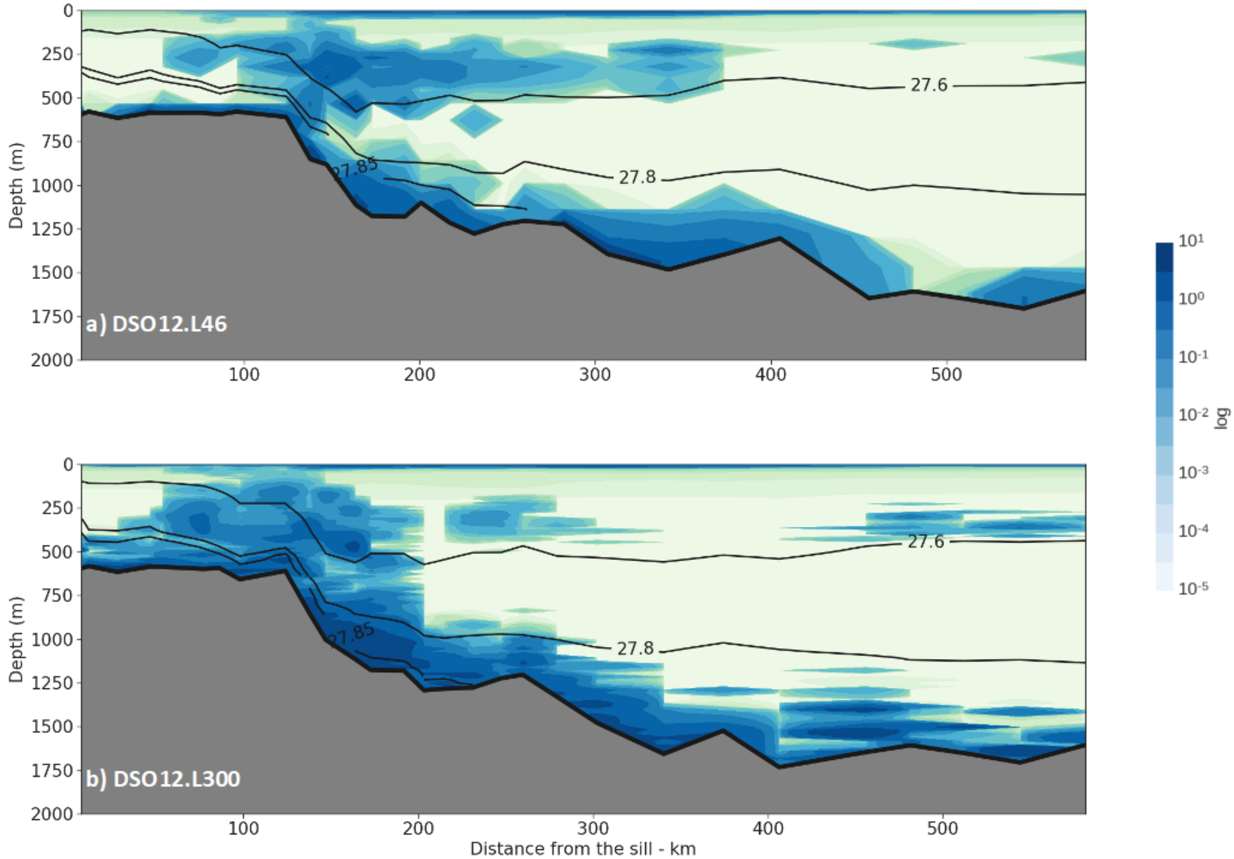

Figure 9. *Vertical diffusivity coefficient (summer mean in the 5th year of simulation) along the path of the vein calculated for a) simulation DSO12.L46 and b) simulation DSO12.L300. Potential density values (σ_0) are shown by the contour lines coloured in red (27.6), green (27.8) and black (27.85).*

10°C, the temperature of the ambient fluid in the rest of the domain being 15°C and the salinity being constant (35) in the whole domain. During the simulation, the temperature is restored on the shelf to its initial value to maintain the source of cold water. A relaxation to the ambient temperature is applied over the whole water column in the last 50km of the right side of the domain in order to evacuate the cold water. The horizontal grid resolution is 5km (comparable to the 1/12° resolution of our regional DSO configuration). Two simulations with different vertical resolutions are run. The first one uses 60 levels of equal thickness (50 m) such that the local grid slope always equals the slope of the bathymetry (Fig. 10a, $\Delta z = 50m$). In the second simulation, the vertical resolution is increase by a factor of 5 (300 vertical levels, Fig. 10b, $\Delta z = 10m$). In the absence of rotation, the pressure force pushes the blob over the shelf break and the EVD mixing scheme propagates the cold water down to the bottom as the blob moves toward deeper waters, generating an overflow plume. After about 5 days, the front of the plume has reached

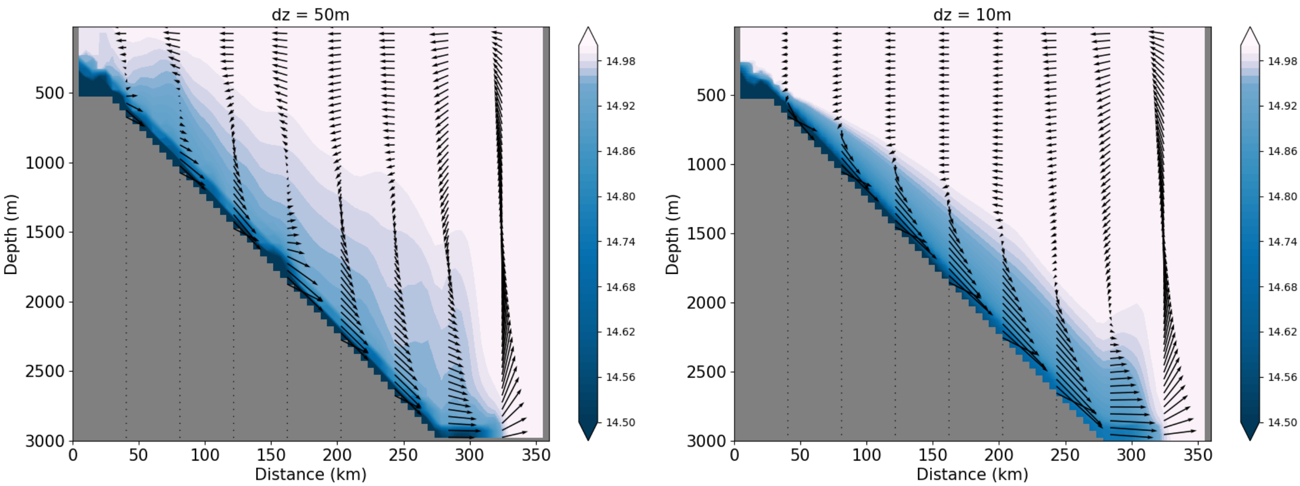

(a) (b)

Figure 10. *Idealized experiment simulating the rationale exposed in Fig. 7 of Winton et al. (1998). Cold water (10°C) descends a shelf break in a configuration with ambient water at 15°C after 9 days of simulation. Two vertical resolutions are used: a) $\Delta z = 50m$ b) $\Delta z = 10m$. Temperature (°C) in colors. Vectors represent the velocity, the vertical velocity being re-scaled according by the grid aspect ratio of case (a).*

the end of the shelf break and entered the damping zone at the right side of the domain, reaching a quasi-stationary regime. In that regime, the overflow simulated in the 300 vertical levels run (i.e. with a local grid slope smaller than the topographic slope) presents warmer bottom waters (Fig. 10a) than in the 60 levels run, in agreement with the results obtained with the realistic DSO12 configuration. Note that the vertical shear is more confined in the high-resolution case, which prevents the upward extent of the TKE induced mixing of the upper part of the overflow that is seen in the low resolution case. Note that when using a realistic bottom topography, the topographic slope will present large local variations and that it will be almost impossible to match the two slopes over the whole domain in a z-coordinate context. Therefore, increasing the number of vertical levels will not systematically degrade the overflow representation everywhere.

A set of simulations tested the effect of the different closure (i.e. vertical mixing) schemes available in NEMO (TKE with and without EVD, $k-\epsilon$ with and without EVD, constant diffusivity+EVD, Madec et al. (2016)). It was found that the choice of the vertical mixing scheme has a very small (insignificant) impact on the final representation of the overflow at $1/12°$.

3.2 Sensitivity to a local increase in horizontal resolution

3.2.1 The $1/36°$ case

The second set of tests that we present is the sensitivity of the DSO representation to the vertical resolution using a local horizontal refinement of $1/36°$ in the overflow region (see Fig. 1). The same range of vertical levels as for the $1/12°$ resolution case is investigated: 46 levels (DSO36.L46), 75 levels (DSO36.L75), 150 levels (DSO36.L150) and 300 levels (DSO36.L300).

The annual mean bottom temperature of the 5th year of simulation is shown in Fig. 11. Compared to the $1/12°$ cases the $1/36°$ cases present, at equivalent number of vertical levels, significantly colder bottom temperatures in the Irminger basin and along the East Greenland shelf break. This amelioration is rather small at 46 levels (Fig. 11a, the cooling is $\sim 0.4°C$), but is more significant for the other vertical resolutions. The greatest improvement is observed when the number of vertical levels is increased to 150 levels (Fig. 11c). In this case the signature of the DSO becomes evident. The bottom temperature of the overflow plume in its first 100 km cooled from a value of $\sim 3.6°C$ at $1/12°$ (Fig. 8a) to a value of $\sim 2.7°C$ (a remarkable cooling of $\sim 0.9°C$) while the temperature at the sill did not change.

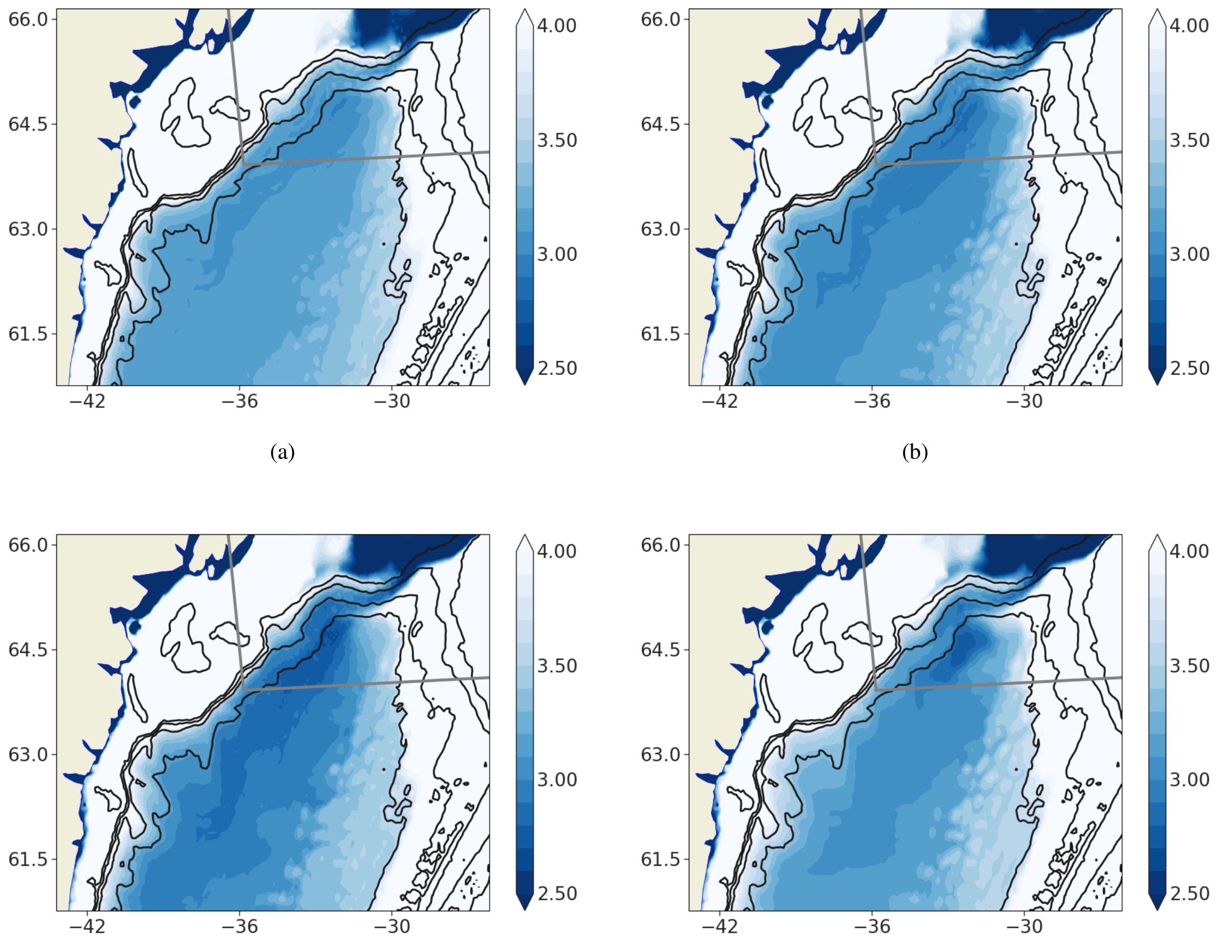

(a) (b) (c) (d)

Figure 11. *Annual mean of the bottom temperature of year 5 of simulations using grid refinement* $(1/36°)$ *a) DSO36.L46 b) DSO36.L75 c) DSO36.L150 d) DSO36.L300. Isobaths 500m, 1000m, 1500m and 2000m are contoured in black.*

The situation changes when increasing to 300 levels (Fig. 11d). The tendency for improvement noticed when increasing from 46 to 150 levels is reversing and the representation of the overflow is slightly degraded. This result is coherent with the explanation given for the $1/12°$ case. Once reached a vertical resolution that is adequate for a specific horizontal resolution for a given slope, increasing the vertical resolution will deteriorate the DSO representation by introducing excessive vertical mixing. A relevant remark here is that over-resolving the slope vertically worsens the overflow representation , which is consistent with the conclusions of Winton et al. (1998). In other words, there is an optimal number of vertical levels to be used for a given horizontal resolution for a given slope. Given the large variety of slopes present in the oceanic topography (and encountered by an overflow during its descent), modelling topographic constrained flows with z-coordinates appears as a quite difficult task.

3.2.2 The $1/60°$ case

We now evaluate the representation of the DSO at $1/60°$ (using a local refinement in the area shown in Fig. 1) with 46, 75, 150 and 300 vertical levels. At this resolution, the 46 levels and 75 levels cases shows solution very similar to that presented at the resolution of 1/36° (no significant additional improvement, no figure shown). A significant change is again observed for 150 levels (Fig. 12a). The signature of the overflow waters at the bottom is even stronger in this case, the cooling of the overflow plume being $\sim 1.1°C$ when compared to the $1/12°$ solution (Fig. 8a), and $\sim 0.2°C$ compared to the 1/36° case.

The solution of the 300 levels case at 1/60° (Fig. 12b) represents an improvement compared to the 1/36° case with the same vertical resolution. However, compared to the 1/60° and 150 levels solution (Fig. 12a) it shows a slightly greater dilution of the overflow and warmer temperatures at the bottom. Also the propagation of the dense water away from the refinement area is clearly better with 150 levels. This should be taken into consideration when choosing the refinement region if used in global implementations. Improvements brought to the representation of the overflow by the resolution increase to 1/60° and 150 levels can also be seen in Fig. 6 and 7 and is quantitatively assessed in the following section (Section 4). At every section, the DSO60.L150 overflow (right hand side plots) is clearly identified by a vein of cold waters well confined along the slope with temperatures below 3°C and always at least 0.5°C colder than in the reference simulation (DSO12.L46, left hand side plots). Temperature gradients between the core of the overflow and the interior ocean are also significantly increased, and the isopycnal 27.85 marks very well the limit of the vein of fluid. If a warm bias still exists compared to the observations of Quadfasel (2004) (bias for a part due to the unrealistic properties of the interior entrained waters), the agreement of the overflow pattern with the observations is nevertheless greatly improved.

4 Eddy-resolving solution ($1/60°$ grid and 150 levels)

The worsening of the DSO representation with increasing vertical resolution until a certain extent is observed with the three horizontal resolutions used in this study ($1/12°$, $1/36°$ and $1/60°$). The analysis of the high vertical diffusivity values due to the EVD demonstrated the dominant impact of this parameterization on the overflow at the resolution of 1/12° and emphasized the need for coherent vertical and horizontal grids. However, the improvements observed in both the DSO36.L150 and DSO60.L150 cases suggest that this impact is reduced and other drivers take control the evolution of the overflow plume when

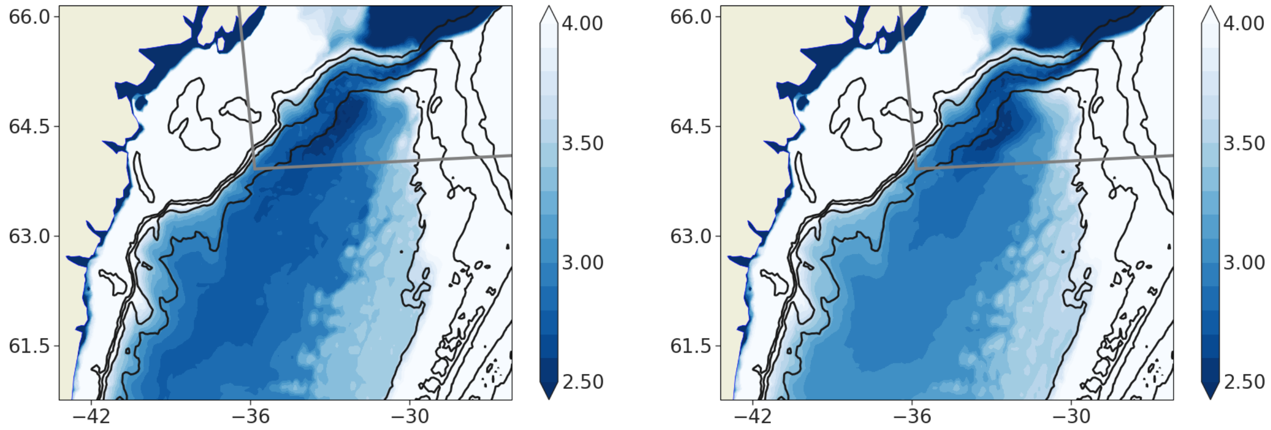

(a) (b)

Figure 12. *Annual mean of the bottom temperature in the 5th year of simulations using a grid refinement of* $1/60^{\circ}$ *for a) 150 vertical levels (DSO60.L150) and b) 300 vertical levels (DSO60.L300). Isobaths 500m, 1000m, 1500m and 2000m are contoured in black. The white box indicates the area of refinement.*

higher horizontal grid resolutions are used. To reach a better understanding of the reasons for improvement, we perform in this section an analysis of the overflow structure in the 1/60° and 150 level simulation (DSO60.L150).

Fig. 13 shows vertical profiles of the mean along slope velocity at two different locations on the shelf break at section 20 from four different simulations which use a large number of vertical levels (150 or 300). All profiles, except that of the 1/12° with 150 level case, show a bottom intensified boundary current confined in the first $200m$ above the bottom, and the presence of a sheared bottom Ekman layer better resolved with 300 levels but still well marked with 150 levels. This indicates the presence of a well defined overflow plume, as shown for the DSO60.L150 in Fig. 6d. This bottom signature has already been described in observations (Paka et al. (2013)). In the other $1/60^{\circ}$ cases with lower vertical resolution (DSO60.L46 and DSO60.L75, not shown) the Ekman driven vertical shear cannot be resolved and the whole dynamics of the current is dominated by the EVD mixing.

The absence of this bottom-confined intensified current in the DSO12.L150 simulation can be related to a similar cause, although the vertical resolution is sufficient to partially resolve the Ekman bottom layer. The analysis of the vertical mixing coefficient (Fig. 14b,14d) shows a very intense mixing in a rather thick layer all along the slope (between $500m$ and $2200m$) and, according to the previous rationale, the reason is the convective adjustment (EVD) governing the near bottom physics. This enhanced mixing seriously limits the development of a sheared flow in the bottom layer.

In the case of DSO60.L150 (Fig. 14a,14c) a small but noticeable mixing remains confined to a very thin bottom layer below the 27.85 isopycnal, and very little mixing occurs in the core of the overflow plume. Intermittent static instabilities occur between the 27.85 and the 27.8 isopycnals (shown by the large values of Kz in Fig. 14a). Our analysis (no figure shown)

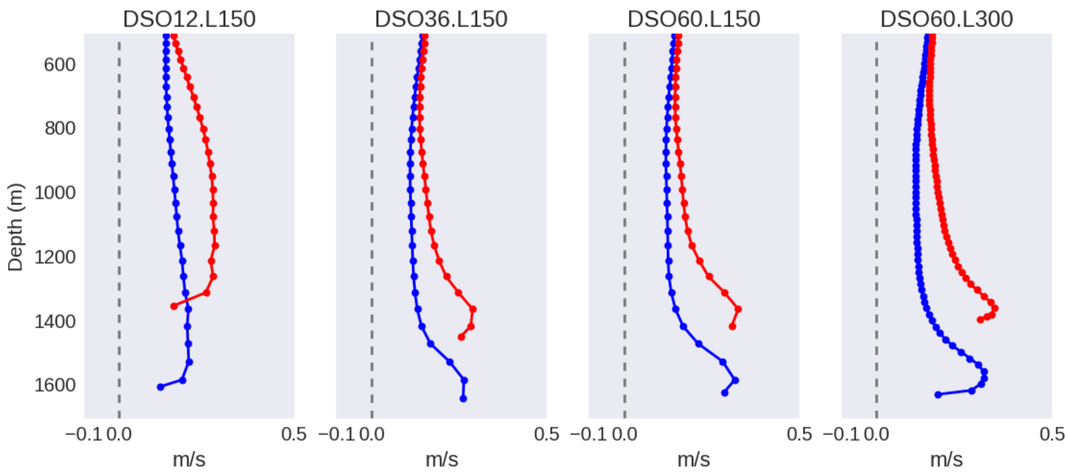

Figure 13. *Vertical profiles (annual mean) of the quasi along-slope velocity (ie. velocity normal to the section) at the two locations of section 20 indicated in figure 6d for simulations (a) DSO12.L150, (b)DSO36.L150, (c) DSO60.L150, and (d) DSO60.L300.*

indicates that these instabilities are generated by advection toward the deep ocean of bolus of dense water by a cyclonic bottom intensified eddy. After the eddy passed through the section (Fig. 14c) the stratification is again stable. Such feature are not seen in the 1/12° simulation (Fig. 14b,d) because the horizontal resolution does not resolve properly the mesoscale eddies. This behavior is consistent with the physical processes present in the DSO, the simultaneous action of the shear governing the entrainment in the overflow plume and the density gradient driving the overflow to the bottom. In this way, the use of coherent horizontal and vertical resolutions plays a key role since it allows the convective adjustment to occur in a limited portion of the plume without interfering with the other important processes driving the physics in the vein of dense fluid. We identify then three conditions for a proper representation of the DSO: coherent vertical and horizontal grids to avoid excessive convective adjustment (due to EVD or any other scheme); proper vertical resolution to resolve the shear induced by the Ekman layer dynamics; and enough horizontal resolution to resolve the boluses of the DSO (described afterwards). This agrees with what is stated in the idealized study of Laanaia et al. (2010), it is not the increase of vertical viscosity that enables the down-slope movement, but the resolution of the bottom Ekman layer dynamics.

Continuing with the description of the bottom flow, we show in Fig. 15 the vertical profiles of physical properties at a specific point at section 16, chosen close to where Paka et al. (2013) performed microstructure measurements (65.20°N 30.41°W) in order to allow for a direct comparison. Our DSO60.L150 simulation reproduces with a high degree of realism the main features of the observed plume (as shown in Fig. 4 of Paka et al. (2013)). As in the observations, the plume is nearly $200m$ thick and is located between $1200m$ and $1400m$ depth. Compared to the water above it, the modelled plume is characterized by a freshening of ~ 0.15 (~ 0.10 in the observations) and a cooling of $3.0°C$ ($\sim 3.5°C$ in the observations). The cross-slope and along-slope velocities show a speed-up of the flow in the plume of $\sim 0.2ms^{-1}$ and $\sim 0.6ms^{-1}$ respectively in observations, the corresponding values in the model being $0.3ms^{-1}$ and $0.7ms^{-1}$. Since this $200m$ thick plume is represented by 5 - 6 points

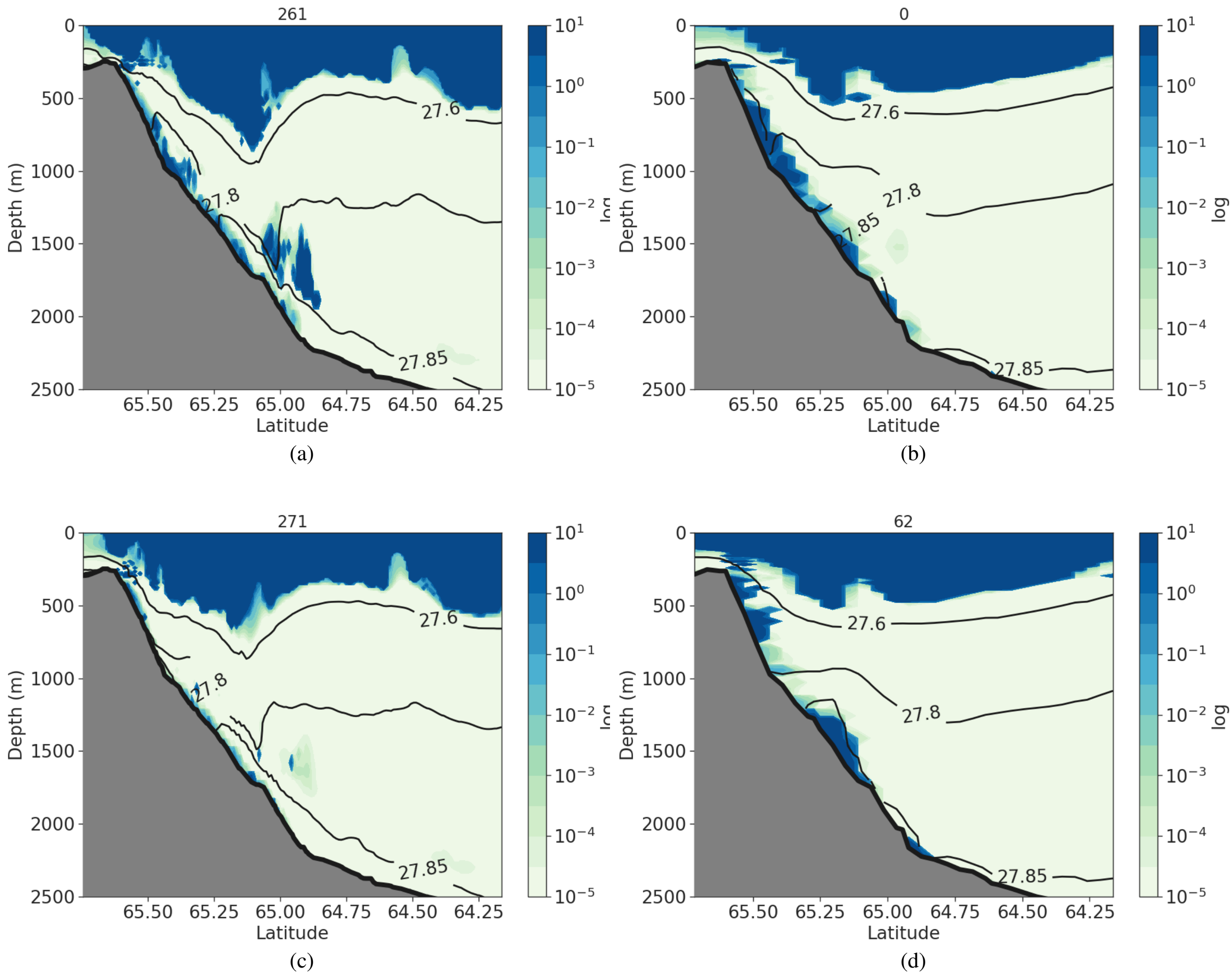

Figure 14. *Vertical diffusivity coefficient (hourly mean) at section 20 in simulations a,c) DSO60.L150 (in the refined grid), and b,d) DSO12.L150 in winter time (with 10 hours difference). In black: contours of isopycnals* 27.6*,* 27.80 *and* 27.85*.*

in the vertical, the use of 150L might be a lower bound for the number of vertical levels to use in order to properly represent the DSO.

The boluses of cold waters mentioned in different observational and modelling papers (see for example Girton and Standford (2003), Jochumsen et al. (2015), Magaldi and Haine (2015), Koszalka et al. (2017)) are also reproduced by the model. To illustrate this we show in Fig. 16 hourly outputs of the bottom temperature in a sequence that lasts only ~ 40 hours. First, in figure 16a the DSO appears as a cold water ($\sim 1°C$) plume that has already started its descent and is confined between the $500m$ and $1000m$ isobaths. Boluses of cold water ($\sim 2°C$) are also seen a few tens of km downstream in the depth range

$1500m$ to $2000m$ and in the deep Irminger Basin. Fifteen hours later (Fig. 16b), the DSO plume has sunk to $1500m$, seems to be adjusted to geostrophy and flows along isobaths. Another plume of cold water is moving through the sill. In the following 24 hours, the first plume moves along the shelf break (Fig. 16c) and breaks into a bolus which brings cold waters to the depth of $2000m$ (Fig. 16d). A significant entrainment of surrounding waters occurred during the breaking as the water in the bolus has gained about $0.5°C$. The bolus will continue its way to the Angmassalik array, i.e. section 29 in Fig. 1, and will contribute to cool the deep Irminger Basin. The second plume has crossed the sill and reached the $1000m$ isobath. It will later generate another bolus following the same process. The formation of the bolus happened in only 40 hours, showing the high frequency variability of the overflow and illustrating the difficulty of diagnosing its time-mean properties.

We attempted a quantitative comparison with the relatively long-term observations made at the mooring arrays reported in the study of Jochumsen et al. (2015). These arrays correspond to the Sill Array (section 1 in Fig. 1), the Dorhn Bank Array (section 16 in Fig. 1), and the Angmagssalik Array (section 29 in Fig. 1). Following Jochumsen et al. (2015) we reported in (Fig. 17) the minimum time-mean bottom temperature at these four sections for certain simulations. This figure somehow summarizes our main findings. In the $1/12°$ simulations, the temperature at the mooring arrays (i.e. the dilution of the overflow) increases with increasing vertical resolution, DSO12.L46 showing a lesser dilution for the first $200km$ of the overflow path than DSO12.L150. The best performing simulation at $1/36°$ is that with 150 levels (DSO36.L150). It shows a cooling of the bottom waters after the sill of about $0.5°C$ when compared to DSO12.L46. At $1/60°$ resolution, the best performing simulation is also that with 150 levels (DSO60.L150). When compared to the best 1/12° simulation (DSO12.L46) it shows an even greater cooling of the bottom waters after the sill ($0.7°C$). Increasing the vertical resolution to 300 levels produces a slightly greater dilution of the plume that could be considered as insignificant, but the computational cost is doubled. When comparing this set of best performing simulations with observations, it appears that the model always produces a much greater dilution of the physical properties of the overflow in the first $200km$ of its path. Improved initial and boundary conditions (i.e. correcting for the warm bias of $0.3C$ at the sill and for the warm and salty bias of the entrained waters of the Irminger Current) should reduce this difference but to a point which is difficult to estimate. Either way, the 1.5°C difference shown in Fig. 17 is a quite wide gap that such bias correction will likely not be sufficient to fill.

Finally, we would like to point out that the increase in resolution also improves the representation of topography. For example, the thin v-shaped channel over the sill (Fig. 4) is better represented as resolution increases. This leads to a more separated cold and fresh DSO current from the warm and relatively salty Irminger current, specially during the descent.

5 Summary and Conclusions

We evaluated the sensitivity of the representation of the Denmark Strait overflow in a regional z-coordinate configuration of NEMO to eddy-permitting to various eddy-resolving horizontal grid resolutions (1/12°, 1/36° and 1/60°), the number of vertical levels (46, 75, 150, 300), and to numerical and physical parameters. A first result is that the representation of the overflow showed very little sensitivity to any parameter except the horizontal and vertical resolutions. A second result is that, in the given numerical set-up, the increase of the vertical resolution did not bring any improvement when an eddy-permitting

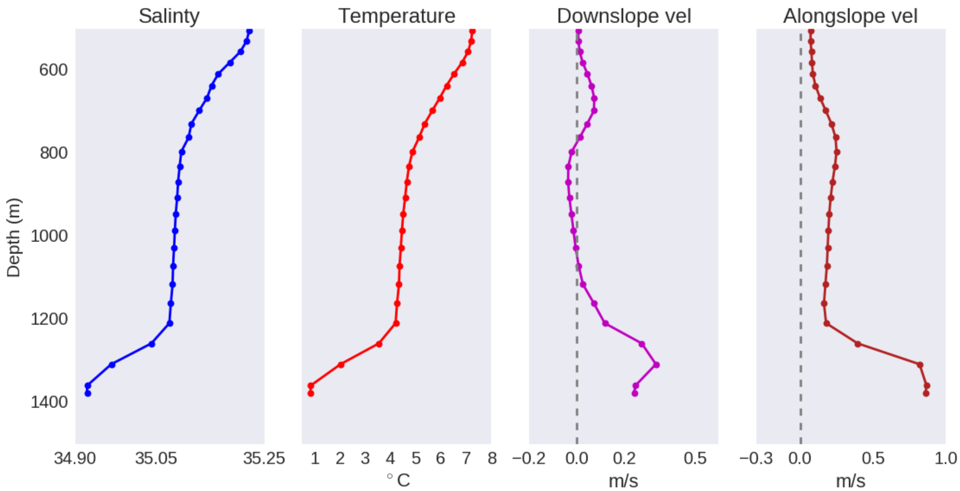

Figure 15. *Vertical profiles of the physical properties of the overflow plume in simulation DSO60.L150 (hour 10 on 01/February of year 5) at section 16 for the location indicated with a white-rimmed dot in Fig. 6b. a) Temperature, b) Salinity, c) cross-slope velocity, and d) Along-slope velocity.*

horizontal grid resolution of $1/12°$ (i.e. $\sim 5km$) is used. We found a greater dilution of the overflow as the number of vertical level was increased, the vein of current becoming warmer, saltier and shallower, the worse solution being the one with 300 vertical levels. Thanks to a point-wise definition of the center of the vein of current we were able to diagnose the vertical diffusivity along the path of the overflow. Our results show that, as expected in a z-coordinate hydrostatic model like NEMO, the sinking of the dense overflow waters is driven by the enhanced vertical diffusion scheme (EVD) that parametrizes the vertical mixing in case of a static instability in the water column. But our analysis showed that the smaller the local grid slope when compared to the topographic slope, the more diluted the vein. Since for a fixed horizontal resolution the grid-slope reduces as the number of vertical levels increases, the overflow is more diluted when a large number of levels is used. To limit this effect, an increase of the vertical resolution must be associated to an increase in the horizontal grid resolution.

We then tested the effect of increasing the number of vertical levels (46, 75, 150 and 300) as it was done at $1/12°$ but with an eddy-resolving horizontal grid resolution of $1/36°$ ($\sim 1.5km$). While only slight improvements were found for the 46 and 75 levels cases, the 150 levels case presented a drastic improvement. At such horizontal and vertical resolution the EVD convective adjustment associated with the step-like representation of the topography remained limited to a relatively thin bottom layer representing a minor portion of the vein. The increase to 300 levels caused a slight deterioration of the DSO representation, generating an increase of the EVD convective adjustment, and being therefore an excessive number of vertical levels for $1/36°$.

Finally, we performed the same series of sensitivity tests with a horizontal grid resolution of $1/60°$ ($\sim 1km$). With 46 and 75 levels, no appreciable differences where found with the correspondent cases at $1/36°$. The 150 levels solution showed an

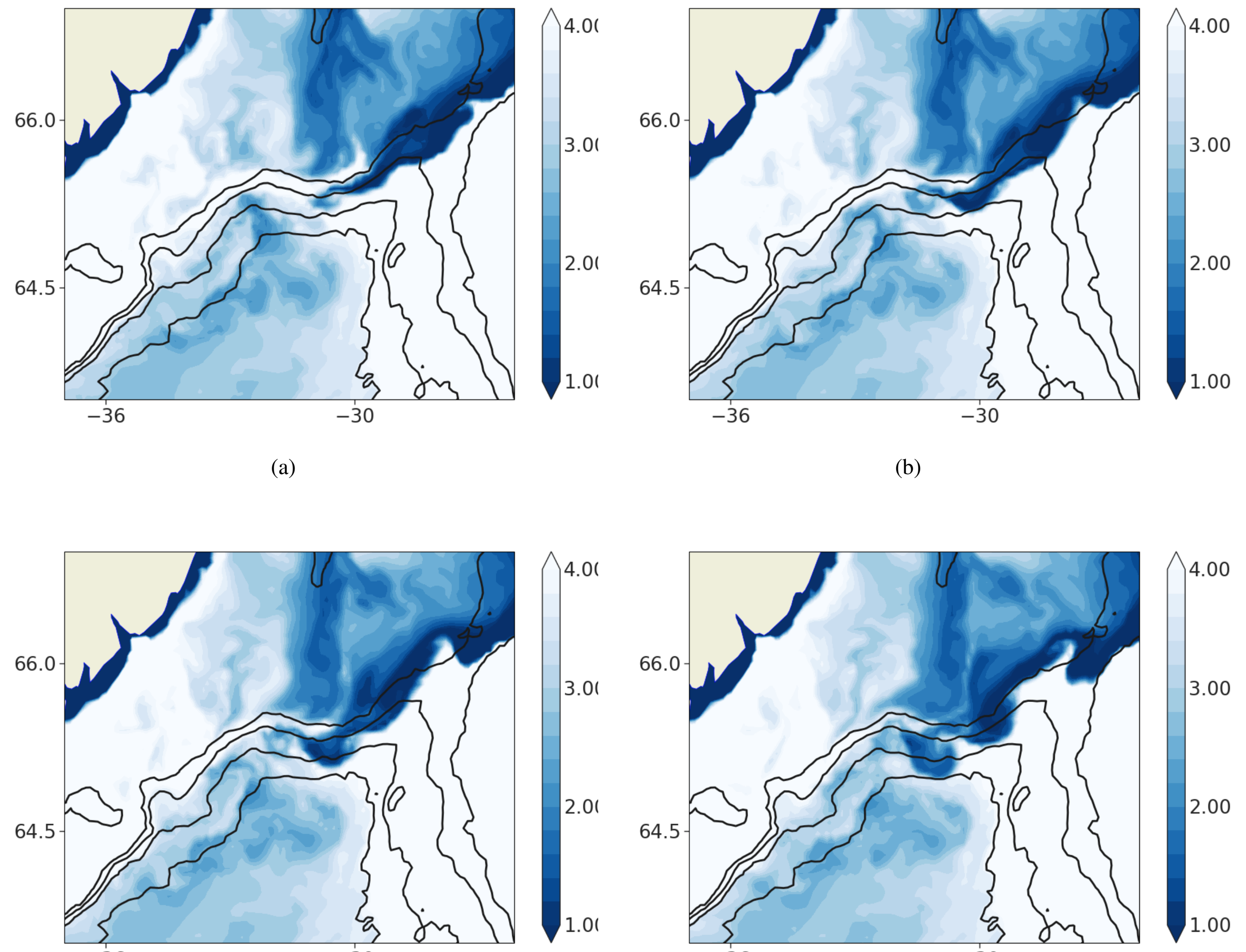

(a) (b) (c) (d)

Figure 16. *Hourly snapshots of bottom temperature in simulation DSO60.L150 for 4 January a) at 14h, b) 15h after, c) 26h after, d) 39h after. The 500m, 1000m, 1500m and 2000m isobaths are contoured.*

improvement even greater than at $1/36°$, being the most performing of all simulations presented in this work. The increase to 300 levels at $1/60°$ was again in detriment of the DSO representation for the same reasons a explained above. As for the 1/36° case, the EVD in the 1/60° and 150 levels case remained limited to a thin bottom layer representing a minor portion of the vein which limited the dilution of its properties. The major additional drivers of the sinking of the overflow at eddy-resolving resolutions are the generation of mesoscale boluses of overflow waters and the appearance of a resolved vertical shear that results from the resolution of the dynamics of the Ekman boundary layer. Combined to the isoneutral diffusion in

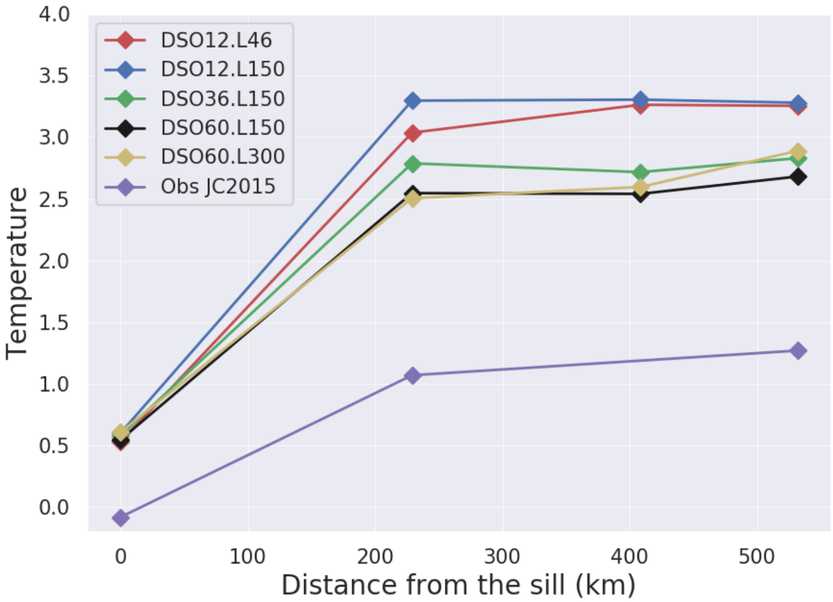

Figure 17. *Time mean minimum bottom temperature for five sensitivity simulations at the location of the observational arrays. The results of Jochumsen et al. (2015) are reported as Obs JC2015.*

the equation for tracers this allows a proper calculation of the entrainment by the TKE scheme and a significant improvement of the properties of the overflow waters.

One interesting conclusion of this work is that for most of the cases tested the EVD convective adjustment was the main parameter controlling the dynamics of the overflow and becoming the dominant player of the vertical mixing scheme. Indeed, the importance of many other numerical parameters were tested (momentum advection scheme, lateral friction, BBL parameterization, etc.) but none had a significant impact on the overflow representation. Moreover, our results show that the problematic of modelling the overflows is not only about resolving the driving ocean processes, but also about how the grid distribution copes with the phenomena to represent. The rationale that we proposed here is that the horizontal and vertical grid resolutions necessary to achieve a proper representation of the dynamical processes driving the overflows must be adjusted to be coherent with the slopes along which the overflow descends to limit the vertical extent of the vertical mixing that ends up deteriorating the final solution.

This conclusion draws attention to a limitation for future global simulations in z-coordinate since all flows that are topographically constrained do not flow along the same topographic slope. The model setting for which we obtained our best representation of the Denmark Strait overflow might not be suitable for an overflow in another location.

All in all, the best results were achieved with the local implementation in the overflow region of the two-way refinement software AGRIF at $1/60°$ with 150 vertical levels. With this drastic increase in horizontal and vertical resolution, among the highest to our knowledge in this type of study, we were able to at least partly resolve the bottom boundary layer dynamics and to simulate an overflow with properties comparable with those seen in the observations. However, significant discrepancies remained between the model and the observations, being possibly attributed to biases in the initial conditions, the overflow waters being too warm at the sill and the ambient waters entrained in the overflow being too warm and salty at the beginning of the simulations.

For a given vertical number of levels the cost of the implementation of AGRIF in this regional 1/60° configuration case was around 70 times the original cost at 1/12° resolution. Even if this implementation was effective and considering that smaller proportional costs are expected in configurations of larger domains, this appears as a computationally costly option. We therefore concluded that a more suitable solution should be searched for. In on going following studies we investigate the representation of the Denmark Strait overflow in a local implementation in NEMO of a terrain following s-coordinate.

Code and data availability. The code of the model corresponds to revision 6355 of NEMO v3.6 STABLE (see Madec et al. (2016) for more information), under the CeCILL licence. It can be downloaded from https://zenodo.org/record/3568221. The namelists and the post-processing scripts can also be downloaded from the same link. The data used to initialize and perform the simulations can be downloaded from https://zenodo.org/record/3568244 (1/12° and 1/36° horizontal resolution simulations) and https://zenodo.org/record/3568283 (1/60° horizontal resolution simulations). Model outputs and diagnostics are available upon request.

Appendix A: Summary of Experiments

We list here the experiments that we performed before arriving to the conclusions described on this paper. For each experiment we present the main findings in a very succinct way.

Experiment 1: Impact of BBL with vertical resolution, Full and partial steps at $1/12°$. Set of 12 simulations combining the possibilities of 46L, 75L and 300L with and without BBL, with partial steps or full steps. Additional tests with 150L and 990L in partial steps without BBL were performed. The variations with depths of the vertical levels is shown in Figure A1. The 46 levels vertical grid uses 29 levels in the first 2000 m and has a cell thickness of 210 m at that depth. The 75 level vertical grid uses 54 levels in the first 2000 m and has a cell thickness of 160 m at that depth. The 150 levels vertical grid uses 104 levels in the first 2000 m and has a cell thickness of 70 m from that depth. The 300 levels vertical grid uses 160 levels in the first 2000 m and has a cell thickness of 22m at that depth. The main findings are:

- Partial step is more performant than Full step no matter the vertical resolution or the use of BBL.
- More diluted waters when used BBL. Attributed to the grid direction of the sinking of waters (rather diagonal)
- More diluted waters with increasing vertical resolution

Experiment 2: Impact of vertical mixing scheme at $1/12°$ 300L. Five runs: TKE with and without EVD, background diffusivity only with EVD, $k-\epsilon$ with and without EVD. All solutions were extremely similar. After studying the whole set of diagnostics, we then concluded that the main driver of the descent of the DSO at $1/12°$ was the presence of high vertical diffusivity values due to density inversions.

Experiment 3: Impact of vertical resolution (46L, 75L and 300L) at $1/60°$ with UBS and EEN advection scheme. The use of the UBS scheme did not bring any significant different regarding the solution with the EEN scheme.

Experiment 4: Use of EVD on tracers only and on tracers and momentum using 46L, 75L and 300L with an horizontal resolution of $1/12°$ and $1/60°$. No significant changes observed.

Experiment 5: Free-slip and No-slip lateral boundary conditions using 46L, 75L and 300L with an horizontal resolution of $1/12°$ and $1/60°$. No-slip lateral boundary condition shown to improve to some extent the feeding of cold waters to the Irminger basin as expected (Hervieux (2007)). However, caution must be taken since it has already been shown that this lateral condition can deteriorate the overall global circulation (Penduff et al. (2007)). Only very local treatment approaches must be considered.

Experiment 6: Use of Non-Penetrative Convective adjustment instead of EVD at $1/12°$ with 46L and 75L. Almost no differences with EVD, this is believed to be due to the convective adjustment treatment included in the TKE scheme (as in Experiment 2 for 300L).

Vertical Resolutions used: The variations of the cell thickness as a function of depth is presented in Fig. A1 for the four different vertical resolutions used. A rough estimate of the bottom Ekman layer is given by $h_E = kU^*/f$ (Cushman Roisin and Becker (2011)) yields $h_E \sim 45m$ in our present model setting for an overflow speed of $0.5ms^{-1}$ and U^* being calculated from the quadratic bottom friction of the model. Consequently, in the $600m$ to $1500m$ depth range that correspond to the initial depth range of the overflow, the bottom Ekman layer will only be partially resolved for model vertical resolution of ~ 10 to $15m$ near the bottom, which according to Fig. A1 will happen only for a model resolution of 150 levels (2 to 3 points) and 300 levels (5 to 6 points).

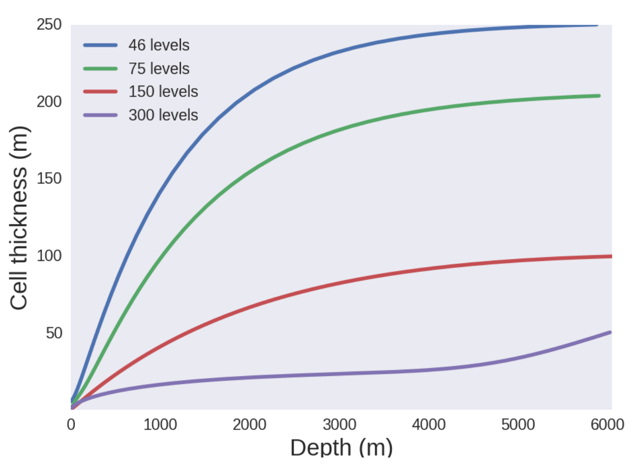

Figure A1. *Grid cell thickness as a function of depth for the 4 vertical grids used in the study.*

Appendix B: Path of the DSO - Calculation

Dickson and Brown (1994), used the density criteria $\sigma_\theta \geq 27.8$ to characterize the DSO considering that this value covers the range of water masses that forms the North Atlantic Deep Waters (NADW). In addition, for the Dohrn Bank, TTO and Angmassalik arrays Dickson and Brown (1994), used a southward velocity greater than zero as an additional criteria in order to guarantee that the water mass considered is effectively flowing in the southward direction. This criteria seems reasonable, since the observational arrays included a large part of the Irminger basin in which deep flows might have northward direction, and would therefore be wrongly considered as part of the DSOW. Brearley et al. (2012), used geographical and density criterias specific to each hydrographic section to define the vein of fluid in their hydrographic sections. Girton and Standford (2003), calculated the center and depth of the overflow by calculating the center of mass anomaly along a number of hydrographic sections. For each section, they limited the extent of the overflow to a width where 50% of the mass anomaly is contained. On the modeling side Koszalka et al. (2013), pointed out the problem represented by the use of the density alone to characterize the overflow, by affirming that the temperature and salinity transformation downstream of the Denmark Strait are not yet well quantified. To tackle this issue they proposed a complementary description of the overflow by using Lagrangian particles in an offline integration. While this method could be useful to answer some questions, its link with observations is not direct.

In this context we understand that a main characteristic that is not being taken into account for a vein of fluid that is characterized by a large transport is its velocity. However, finding a correct threshold for the southward velocity that works both for observations and model outputs is not an easy task. Of course this value has to be greater than zero. We might go a bit further and think that we probably should avoid including small velocities related to eddy processes in the Irminger Basin. On the work of Fan et al. (2013) observations were made of the mean peak azimuthal speeds for the anticyclones present in the Irminger basin, obtaining a value of $0.1ms^{-1}$.

From this point of view any discussion considering a lower threshold value for the overflow should start from at least $v \leq -0.1ms^{-1}$. We propose here a value of $v \leq -0.2ms^{-1}$ because we obtained very robust results. However intermediate values between $-0.1ms^{-1}$ and $-0.2ms^{-1}$ can be tested. We then propose a definition similar to the one given by Girton and Standford (2003) for horizontal and vertical positions of the DSO, doing so we define our understanding of the vein and its center.

$$X_{DSO} = \frac{\iint vxdzdx}{\iint vdzdx}; (\sigma_0 \geq 27.8, v \leq -0.2ms^{-1}) \tag{B1}$$

$$Z_{DSO} = \frac{\iint vzdzdx}{\iint vdzdx}; (\sigma_0 \geq 27.8, v \leq -0.2ms^{-1}) \tag{B2}$$

Compared to the definition used in Girton and Standford (2003), we use the local depth of the grid point as a weight instead of the local value of the total depth. As said before, the velocity was also added as a parameter to weight the position of each point. The value of X_{DSO} and Z_{DSO} give the horizontal and vertical position of the core of the vein for each section in particular.

The position of the center of the overflow has been calculated with equations B1 and B2 at each of the 29 sections shown in Figure B1, thus defining the mean path of the overflow in the simulations. This path is used to produce the results shown in Fig. 9 and in Fig. B1

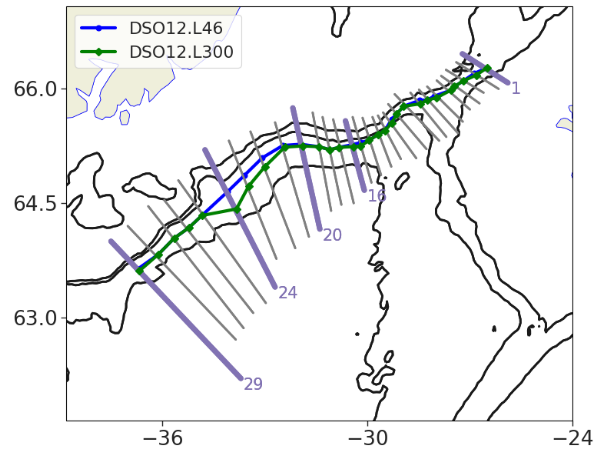

Figure B1. *Overflow path. Contours show the 500, 1000 and 2000 meter depth isobaths. The location of the various sections used to monitor the model solution are indicated by grey and purple lines. The blue/green dots indicate for each section the location of the center of the vein of the DSO in the Control simulation (blue, DSO12.L46) and in the 1/12° 300 levels simulation (green, DSO12.L300), the blue/green lines show the path of the overflow in these simulations.*

Author contributions. PC, BB, TP, JC, J-MM where part of the design of the experiments and diagnostics, as well as their evaluation. JD, JLS, PV, SG and A-MT where part as well of the diagnostic evaluation. PC and BB wrote the document. PC performed the experiments and performed the diagnostics with the support of JC and J-MM. All authors provided scientific input.

Competing interests. The authors declare that they have no conflict of interest.

Acknowledgements. PC was supported by UGA though an assistantship from Ministère de l'Enseignement supérieur, de la Recherche et de l'Innovation, and is now supported by CNRS through a grant from CMEMS. BB, J-MM, TP, JLS, and A-MT are supported by CNRS. JC is supported by Mercator Ocean International. Research leading to these results benefited from supports provided by the LEFE/GMMC program of INSU, the PHC Kolmogorov No 38102RF and the project 14.W03.31.0006 of the Russian Ministry of Science and Higher Education (BB, SG and PV). This work also benefited from many interactions with the DRAKKAR International Research Network (IRN) established between CNRS, NOCS, GEOMAR, and IFREMER. Most important, this research was granted access to important HPC resources under allocations A0030100727 and A0050100727 attributed by GENCI to DRAKKAR, simulations being carried out at the CINES supercomputer national facilities.

References

Almansi, M., Haine, T., Pickart, R. S., Magaldi, M., Gelderloos, R., and Mastropole, D.: High-Frequency Variability in the Circulation and Hydrography of the Denmark Strait Overflow from a High-Resolution Numerical Mode. Journal of Physical Oceanography, 47, 12, 2999-3013, doi: 10.1175/JPO-D-17-0129.1, 2017.

von Appen, W.-J., Koszalka, I.M., Pickart, R.S., Haine, T.W.N., Mastropole, D., and Magaldi, M.G.: East Greenland spill jet as important part of the AMOC. Deep Sea Res. I, 92, 75–84, 2014.

Baines, P. G., and Condie, S.A.: Observations and modelling of Antarctic downslope flows: A review, in Ocean, Ice and Atmosphere: Interactions at the Antarctic Continental Margin, S. Jacobs and R. Weiss, eds., Amer. Geophys. Union, 75, 29–49. 1998.

Baringer, M. O., and Price, J. F.: Mixing and Spreading of the Mediterranean Outflow. J. Phys. Oceanogr., 27, 1654–1677, 1997.

Barnier, B., Madec, G., Penduff, T., Molines, J., Treguier, A., Le Sommer, J., Beckmann, A., Biastoch, A., Böning, C. W., Dengg, J., Derval, C., Durand, E., Gulev, S., Remy, E., Talandier, C., Theetten, S., Maltrud, M., McClean, J., and De Cuevas, B.: Impact of partial steps and momentum advection schemes in a global ocean circulation model at eddy-permitting resolution. Ocean Dyn., 56, 543-567, 2006.

Barnier, B., Domina, A., Gulev, S., Molines, J.-M., Maitre, T., Penduff, T., Le Sommer, J., Brasseur, P., Brodeau, L., and P. Colombo: Modelling the impact of flow-driven turbine power plants on great wind-driven ocean currents and the assessment of their energy potential. Nat Energy 5, 240–249. https://doi.org/10.1038/s41560-020-0580-2, 2020.

Beismann, J.-O., and Barnier, B.: Variability of the meridional overturning circulation of the North Atlantic: sensitivity to overflows of dense water masses, Ocean Dyn., 54, 92–106, 2004.

Beckmann, A., and Döscher, R.; A method for improved representation of dense water spreading over topography in geopotential-coordinate models. J. Phys. Oceanogr., 27, 581–591, 1997.

Bessières, L; Leroux, S; Brankart, J.-M; Molines, J.-M; Moine, M.-P; Bouttier, P.-A; Penduff, T; Terray, L; Barnier, B; and Sérazin, G.: Development of a probabilistic ocean modelling system based on NEMO 3.5: application at eddying resolution. Geosci. Model Dev., 10, 1091-1106, https://doi.org/10.5194/gmd-10-1091-2017, 2017.

Biastoch, A., Böning, C. W., Schwarzkopf, F. U., and Lutjeharms, J. R. E.: Increase in Agulhas leakage due to poleward shift of the Southern Hemisphere westerlies, NATURE, Vol 462, 26 November 2009, doi:10.1038/nature08519, 2009.

Brearley, J. A., Pickart, R. S., Valdimarsson, H., Jonsson, S., Schmitt, R. W. and Haine, T. W. N.: The East Greenland boundary current system south of Denmark Strait. Deep-Sea Research I 63 1–19, doi:10.1016/j.dsr.2012.01.001, 2012.

Brodeau, L., Barnier, B., Treguier, A., Penduff, T., and Gulev, S.: An ERA40-based atmospheric forcing for global ocean circulation models. Ocean Modelling 31, 88-104, doi:10.1016/j.ocemod.2009.10.005, 2010.

Campin, J.M., and Goosse, H.: Parameterization of density-driven downsloping flow for a coarse-resolution ocean model in z-coordinates. Tellus 51A, 412–430, 1999.

Chang, Y. S., Garraffo, Z. D., Peters, H., and Özgökmen, T.: Pathways of Nordic Overflows from climate model scale and eddy resolving simulations, Ocean Modelling 29, 66–84, doi:10.1016/j.ocemod.2009.03.003, 2009.

Chanut, J., Barnier, B., Large, W., Debreu, L., Penduff, T., Molines, J., and Mathiot, P.: Mesoscale Eddies in the Labrador Sea and Their Contribution to Convection and Restratification. Journal of Physical Oceanography 38, 1617-1643, doi: 10.1175/2008JPO3485.1, 2008.

Chassignet, E.P., Smith, L.T., Halliwell, G.R., and Bleck, R.: North Atlantic simulation with the HYbrid Coordinate Ocean Model (HYCOM): impact of the vertical coordinate choice, reference density, and thermobaricity. J. Phys. Oceanogr. 33, 2504–2526, 2003.

Condie, S.A.: Descent of dense water masses along continental slopes, J. Mar. Res. 53, 897–928, doi: 10.1357/0022240953212936, 1995.

Cushman Roisin, B., and Beckers, J. M.: Introduction to Geophysical Fluid Dynamics , Physical and Numerical Aspects. Academic Press, Chap. 8, 219-246, 2011.

Danabasoglu, G., Large, W. G., and Briegle, B. P.: Climate impacts of parameterized Nordic Sea overflows, J. Geophys. Res., 115, C11005, doi:10.1029/2010JC006243, 2010.

Danabasoglu, G., and Co-authors: North Atlantic simulations in coordinated ocean-ice reference experiments phase II (CORE-II). Part I: mean states, Ocean Modelling, 73, 76–107. 2014.

Daniault, N., Mercier, H., Lherminier, P., Sarafanov, A., Falina, A., Zunino, P., Pérez, F.F., Ríos, A.F., Ferron, B., Huck, T., Thierry, V., and Gladyshev, S.: The northern North Atlantic Ocean mean circulation in the early 21st century, Progress in Oceanography 146, 142–158. doi:10.1016/j.pocean.2016.06.007, 2016.

Debreu, L., Vouland, C., Blayo, E.: AGRIF: Adaptive grid refinement in Fortran. Computers & Geosciences 34, 8-13, doi:10.1016/j.cageo.2007.01.009, 2008.

Dickson, R.R., and Brown, J.: The production of North Atlantic Deep Water: Sources, rates and pathways, J. Geophys. Res., 99, 12319–12341, 1994.

Dickson, B., Dye, S., Jonsson, S., Köhl, A., Macrander, A., Marnela, M., Meincke, J., Olsen, S., Rudels, B., Valdimarsson, H., and Voet, G.: The overflow flux west of Iceland: variability, origins and forcing. In: Dickson, R.R., Meincke, J., Rhines, P. (Eds.), Arctic–Subarctic Ocean Fluxes. Defining the Role of the Northern Seas in Climate. Springer Science + Business Media, Washington, DC, chapter 19, pp. 443–474, 2008.

DRAKKAR Group (Tréguier, A.-M., Barnier, B., Blaker, A.T., Biastoch, A., Böning, C.W., Coward, A., Deshayes, J., Duchez, A., Hirschi, J., Le Sommer, J., Madec, G., Maze, G., Molines, J.-M., New, A., Penduff, T., Scheinert, M., Talandier, C.): DRAKKAR: Developing high resolution ocean components for European Earth system models. CLIVAR Exchanges Newsletter, No.64 (Vol 19, No.1), 2014.

Downes, S.M., Gnanadesikan, A., Griffies, S.M., Sarmiento, J.L.: Water mass exchange in the Southern Ocean in coupling climate models. J. Phys. Oceanogr. 41, 1756–1771, doi:10.1175/2011JPO4586.1, 2011.

Ducousso, N., Le Sommer, J., Molines, J., and Bell, M.: Impact of the "Symmetric Instability of the Computational Kind" at mesoscale- and submesoscale-permitting resolutions. Ocean Modelling 120, 18-26, doi: 10.1016/j.ocemod.2017.10.006, 2017.

Ezer, T., and Mellor, G.L.: A generalized coordinate ocean model and a comparison of the bottom boundary layer dynamics in terrain-following and in z-level grids. Ocean Modelling. 6, 379–403, 2004.

Fan, X., Send, U., Testor, P., Karstensen, J., and Lherminier, P : Observations of Irminger Sea Anticyclonic Eddies. J. Phys. Oceanogr., 43, 805–823, doi: 10.1175/JPO-D-11-0155.1, 2013

Grégorio, S.,Penduff, T., Sérazin, G., Molines, J., Barnier, B., and Hirschi, J.: Intrinsic variability of the Atlantic meridional overturning circulation at interannual-to-multidecadal time scales. Journal of Physical Oceanography 45 (7), 1929-1946, 2015.

Girton, J.B., and Sandford, T. B.: Descent and Modification of the Overflow Plume in the Denmark Strait. Journal of Physical Oceanography 33, 1351-1364, 2003

Griffies, S.: The gent-mcwilliams skew-flux, J. Phys. Oceanogr., 28, 831–841,1998

Griffies, S. M., Pakanowski, R. C., and Hallberg, R. W.: Spurious Diapycnal Mixing Associated with Advection in a z-Coordinate Ocean Model. Monthly Weather Review 128, 2935–2946, 2003.

Hansen, B., and Østerhus, S.: Faroe Bank channel overflow 1995-2005, Progress in Oceanography, 75, 817-856, doi:10.1016/j.pocean2007.09.004, 2007.

Hansen, B., Østerhus, S., Turrell, W.R., Jónsson, S., Valdimarsson, H., Hátún, H., and Malskær Olsen, S.: The Inflow of Atlantic Water, Heat, and Salt to the Nordic Seas Across the Greenland–Scotland Ridge, . In: Dickson, R.R., Meincke, J., Rhines, P. (Eds.), Arctic–Subarctic Ocean Fluxes. Defining the Role of the Northern Seas in Climate. Springer Science + Business Media, Washington, DC, chapter 1, pp. 1–13, 2008.

Hervieux, G.: Numerical study of current-topography interactions: subpolar gyre, Gibraltar and Nordic Sea straits. Université Joseph-Fourier - Grenoble I <tel-00730205>, 2007

Heuzé, C., Heywood, K. J., Stevens, D. P., and Ridley, J. K.: Southern Ocean bottom water characteristics in CMIP5 models. Geophys. Res. Lett., 40, 1409–1414, doi:10.1002/grl.50287, 2013.

Jochumsen, K., Quadfasel, D., Valdimarsson, H., and Jónsson, S.: Variability of the Denmark Strait overflow: Moored time series from 1996–2011. Journal of Geophysical Research 117, doi:10.1029/2012JC008244, 2012.

Jochumsen, K., M. Köllner, D. Quadfasel, S. Dye, B. Rudels, and H. Valdimarsson (2015), On the origin and propagation of Denmark Strait overflow water anomalies in the Irminger Basin, J. Geophys. Res. Oceans, 120, 1841–1855, doi:10.1002/2014JC010397, 2015.

Koszalka, I., Haine, T., and Magaldi, M.: Fates and Travel Times of Denmark Strait Overflow Water in the Irminger Basin. J. Phys. Oceanogr. 43 (12), 2611–2628, doi:10.1175/JPO-D-13- 023.1, 2013.

Koszalka, I., Haine, T., and Magaldi, M.: Mesoscale mixing of the Denmark Strait Overflow in the Irminger Basin. Ocean Modelling 112, 90-98, doi:10.1016/j.ocemod.2017.03.001, 2017.

Killworth, P. D.: Mixing of the Weddell Sea continental slope. Deep-Sea Res., 24, 427–448, 1977.

Killworth, P., and Edwards, N.: A turbulent bottom boundary layer code for use a numerical ocean models, Journal of Physical Oceanography, pp. 1221–1238, 1999.

Laanaia, N., Wirth, A., Molines, J. M., Barnier, B., and Verron, J.: On the numerical resolution of the bottom layer in simulations of oceanic gravity currents. Ocean Sci., 6, 563-572, 2010.

Legg, S., Hallberg, R. W., and Girton, J. B.: Comparison of entrainment in overflows simulated by z-coordinate, isopycnal and non-hydrostatic models. Ocean Modelling, 11, 69-97, 2006.

Legg, S., Jackson, L., and Hallberg, R. W.: Eddy-Resolving Modeling of Overflows. Ocean Modeling in an Eddying Regime, 63-81, doi.org/10.1029/177GM06, 2008.

Legg, S., Briegleb, B., Chang, Y., Chassignet, E., P., Danabasoglu, G., Ezer, T., Gordon, A., L., Griffies, S., Hallberg, R., Jackson, L., Large, W., Özgökmen, T. M., Peters, H., Price, J., Riemenschneider, U., Wu, W., Xu, X., and Yang, J.: Improving oceanic overflow representation in climate models. BAMS, Vol. 90, 5, 657-670, 2009.

Lellouche J.-M., O. Le Galloudec, M. Drévillon, C. Régnier, E. Greiner, G. Garric, N. Ferry, C. Desportes, C.-E. Testut, C. Bricaud, R. Bourdallé-Badie, B. Tranchant, M. Benkiran, Y. Drillet, A. Daudin, and De Nicola, C.: Evaluation of global monitoring and forecasting systems at Mercator Ocean, Ocean Sci., 9, 57–81, doi:10.5194/os-9-57-2013, 2013.

Lellouche, J.-M.., and co-authors: The Mercator Ocean global high-resolution monitoring and forecasting system. In New Frontiers in Operational Oceanography, E. Chassignet, A. Pascual, J. Tintoré, and J. Verron, Eds., GODAE OceanView, 563-592, doi:10.17125/gov2018.ch20, 2018.

Le Traon, P. Y., and co-authors: The Copernicus Marine Environmental Monitoring Service: Main scientifict achievements and future prospects. Mercator Ocean Journal, 56, September, 101 pp., 2017.

Macrander, A., Send, U., Valdimarsson, H., Jónsson, S., and Käse, R. H.: Interannual changes in the overflow from the Nordic Seas into the Atlantic Ocean through Denmark Strait. Geophysical Research Letters 32, doi:10.1029/2004GL021463, 2005.

Macrander, A., Käse, R. H., Send, U., Valdimarsson, H., and Jónsson, S.: Spatial and temporal structure of the Denmark Strait Overflow revealed by acoustic observations. Ocean Dynamics 57, 75-89, doi:10.1007/s10236-007-0101-x, 2007.

Madec, G., and the NEMO Team, 2016: NEMO ocean engine. Note du Pôle de modélisation, Institut Pierre-Simon Laplace (IPSL), France, No 27 ISSN No 1288-1619.

Magaldi, M., Haine, T., and Pickart, R. S.: On the Nature and Variability of the East Greenland Spill Jet: A Case Study in Summer 2003. Journal of Physical Oceanography 41, 2307-2327, doi:10.1175/JPO-D-10-05004.1, 2011.

Magaldi, M., and Haine, T.: Hydrostatic and non-hydrostatic simulations of dense waters cascading off a shelf: The East Greenland case. Deep-Sea Research I 96, 89-104, doi:10.1016/j.dsr.2014.10.008, 2015.

Marzocchi, A., Hirschi, J. J.-M., Holliday, P. N., Cunningham, S. A., Blaker A. T., Coward A. C.,: The North Atlantic subpolar circulation in an eddy-resolving global ocean model, Journal of Marine Systems 142, 126–143, doi:10.1016/j.jmarsys.2014.10.007, 2015.

Mastropole, D., R. S. Pickart, H. Valdimarsson, K. Våge, K. Jochumsen, and J. Girton (2017), On the hydrography of Denmark Strait, J. Geophys. Res. Oceans, 122, 306–321, doi:10.1002/2016JC012007, 2017.

Mathiot, P., Jourdain, N.C., Barnier, B., Gallée, H., Molines, J.-M., Le Sommer, J., and Penduff, T., 2012: Sensitivity of coastal polynyas and high-salinity shelf water production in the Ross Sea, Antarctica, to the atmospheric forcing. Ocean Dynamics 62, 701–723 (2012). https://doi.org/10.1007/s10236-012-0531-y.

Megann, A., Storkey, D., Aksenov, Y., Alderson1 S., Calvert, D., Graham, T., Hyder, P., Siddorn, J., and Sinha, B.: GO5.0: the joint NERC–Met Office NEMO global ocean model for use in coupled and forced applications. Geosci. Model Dev., 7, 1069–1092, doi:10.5194/gmd-7-1069-2014, 2014.

Molines, J.-M., B. Barnier, T. Penduff, A. M. Treguier, and J. Le Sommer, 2014: ORCA12.L46 climatological and interannual simulations forced with DFS4.4: GJM02 and MJM88. Drakkar Group Experiment Rep. GDRI-DRAKKAR-2014-03-19, 50 pp.

Özgökmen, T. M., Fischer, P. F., Duan, J., and Iliescu, T.: Entrainment in bottom gravity currents over complex topography from three-dimensional nonhydrostatic simulations, Geophy. Research Letters, 31, L13212, doi:10.1029/2004GL020186, 2004.

Paka, V., Zhurbas, V., Rudels, B., Quadfasel, D., Korzh, A., and Delisi, D.: Microstructure measurements and estimates of entrainment in the Denmark Strait overflow plume, Ocean Sci., 9, 1003–1014, doi:10.5194/os-9-1003-2013, 2013.

Purkey, S.G., Smethie, W. M. Jr., Gebbie, G., Gordon, A. L., Sonnerup, R. E., Warner, M. J., and Bullister, J. L.: A Synoptic View of the Ventilation and Circulation of Antarctic Bottom Water from Chlorofluorocarbons and Natural Tracers. Annu. Rev. Mar. Sci., 10:8.1–8.25. https://doi.org/10.1146/annurev-marine-121916- 063414, 2018.

Penduff, T., Juza, M., Barnier, B., Zika, J, Dewar, W., Treguier, A., Molines, J., and Audiffren, N.: Sea Level Expression of Intrinsic and Forced Ocean Variabilities at Interannual Time Scales. Journal of Climate 24, 5652-5670, doi:10.1175/JCLI-D-11-00077.1, 2011.

Penduff, T., Sérazin, G., Leroux, S., Close, S., Molines, J.-M., Barnier, B., Bessières, L., Terray, L., and Maze, G.: Stochastic variability of ocean heat content: Climate-relevant features and observational implications, Oceanography 31(2), doi:10.5670/oceanog.2018.210, 2018.

Peters, H., Johns, W.E., Bower, A. M., and Fratantoni, D. M.: Mixing and Entrainment in the Red Sea Outflow Plume. Part I: Plume Structure, Journal of Physical oceanography, 35, 569-583, 2005.

Quadfasel, D., (2004) - Cruise Report FS Alexander von Humboldt 44-04-12.Techincal report 1-04.Institut für Meereskunde Zentrum für Marine und Atmosphärische Wissenschaften, Universität Hamburg. Unpublished manuscript.

Rattan S., Myers, P., Treguier, A.-M., Theetten, S., Biastoch, A., and Böning, C.: Towards an understanding of Labrador Sea salinity drift in eddy-permitting simulations, Ocean Modelling 35, 77–88, doi:10.1016/j.ocemod.2010.06.007, 2010.

Reckinger, S., Petersen, M. R., and Reckinger, S. J.: A study of overflows simulations using MPAS-Ocean: Vertical grids, resolution, and viscosity. Ocean Modelling, 96, 291-313, doi 10.1016/j.ocemod.2015.09.006, 2015.

Reffray, G., Bourdalle-Badie, R., and Calone, C.: Modelling turbulent vertical mixing sensitivity using a 1-D version of NEMO, Geosci. Model Dev., 8, 69–86, doi:10.5194/gmd-8-69-2015, 2015.

Riemenschneider, U., Legg, S.: Regional simulations of the Faroe Bank Channel overflow in a level model. Ocean Modelling 17, 93–122, 2007.

Sadourny, R.: The dynamics of finite-difference models of the shallow-water equations. J. Atmos. Sci. 32(4), 680–689, 1975.

Seim, K., S., Fer, I., and Berntsen, J.: Regional simulations of the Faroe Bank Channel overflow using a sigma-coordinate ocean model. Ocean Modelling, doi:10.1016/j.ocemod.2010.06.002, 2010.

Sérazin, G., Penduff, T., Grégorio, S., Barnier, B., Molines, J., and Terray, L.: Intrinsic variability of sea level from global ocean simulations: Spatiotemporal scales. Journal of Climate 28 (10), 4279-4292, 2015.

Sérazin, G., Penduff, T., Barnier, B., Molines, J., Arbic, B., Müller, M., and Terray, L.: Inverse Cascades of Kinetic Energy as a Source of Intrinsic Variability: A Global OGCM Study. Journal of Physical Oceanography 48 (6), 1385-1408, 2018.

Snow, K., Hogg, A. McC., Downes, S. M., Sloyan B. M., Griffes, S. M., and Bates, M. L.: Sensitivity of abyssal water masses to overflow parameterisations, Ocean Modelling, 89, 84-103. 2015.

Song, T., Y., and Chao, Y.: An Embedded Bottom Boundary Layer Formulation for Z-Coordinate Ocean Models, Journal of Atmospheric and Oceanic Technology, 17, 546-560, 2010.

Spall, M. A., Pickart, R. S., Lin, P., von Appen, W.-J., Mastropole, D., Valdimarsson, H.: Frontogenesis and variability inDenmark Strait and its influence on overflow water.Journal of Physical Oceanography,49(7), 1889–1904, 2019.

Treguier, A.M., Theeten, S., Chassignet, E.P., Penduff, T., Smith, R., Beismann, L.T.J.O., Boning, C.: The North Atlantic subpolar gyre in four high-resolution models. Journal of Physical Oceanography 35, 757–774, 2005.

Treguier, A.-M., Lique, C., Deshayes, J., and Molines, J.-M.: The North Atlantic Eddy Heat Transport and Its Relation with the Vertical Tilting of the Gulf Stream Axis, Journal of Physical Oceanography, 47 (6),1281-1289, 2017.

Voet, G., and Quadfasel, D.:Entrainment in the Denmark Strait overflow plume by meso-scale eddies. Ocean Sci., 6, 301–310, 2010.

Wang, Q., Danilov, S., and Schröter, J.: Comparison of overflow simulations on different vertical grids using the Finite Element Ocean circulation Model. Ocean Modelling, 20, 313-335, 2008.

Wang, H., Legg, S.A., and Hallberg, R.W.: Representation of the Nordic Seas overflows and their large scale climate impact in coupled models. Ocean Modelling, 86, 76-92, doi 10.1016/j.ocemod.2014.12.005, 2015.

Weijer, W., Sloyan, B.M., Maltrud, M.E., Jeffery, N., Hecht, M.W., Hartin, C.A., Sebille, E.V., Wainer, I., and Landrum, L.: The Southern Ocean and its climate in CCSM4, J. Clim. 25, 2652–2675, doi: 10.1175/JCLI-D-11-00302.1, 2012.

Williams, K. D., Harris, C. M., Bodas-Salcedo, A., Camp, J., Comer, R. E., Copsey, D., Fereday, D., Graham, T., Hill, R., Hinton, T., Hyder, P., Ineson, S., Masato, G., Milton, S. F., Roberts, M. J., Rowell, D. P., Sanchez, C., Shelly, A., Sinha, B., Walters, D. N., West, A., Woollings, T., and Xavier, P. K.: The Met Office Global Coupled model 2.0 (GC2) configuration, Geosci. Model Dev., 88, 1509–1524, doi:10.5194/gmd-88-1509-2015, 2015.

Winton, M., Hallberg, R., and Gnanadesikan, A.: Simulation of density-driven frictional downslope flow in z-coordinate ocean models. J. Phys. Oceanogr., 68, 2163–2174, 1998.

Wobus, F., Shapiro, G. I., Maqueda, M.A.M, and Huthnance, J.M: Numerical simulations of dense water cascading on a steep slope. Journal of marine Research, 69, 391-415, 2011.

Xu, X., Schmitz Jr., W. J., Hurlburt, H. E., Hogan, P. J., Chassignet, E. P.: Transport of Nordic Seas overflow water into and within the Irminger Sea: An eddy-resolving simulation and observations. J. Geophys. Res. 115, doi:10.1029/2010JC006351, 2010.

Xu, X., Rhines, P. B., Chassignet, E. P., Schmitz Jr., W. J.: Spreading of Denmark Strait Overflow Water in the Western Subpolar North Atlantic: Insights from Eddy-Resolving Simulations with a Passive Tracer. Journal of Physical Oceanography 45 (12), 2913-2932, 2014.

Yashayaev, I., and Dickson, B.: Transformation and fate of overflows in the northern North Atlantic. Arctic–Subarctic Ocean Fluxes. Defining the Role of the Northern Seas in Climate, R. R. Dickson, J. Meincke, and P. Rhines, Eds., Springer Science and Business Media, 505–526, 2008.

Zhang, R., Delworth, T.L., Rosati, A., Anderson, W.G., Dixon, K.W., Lee, H.-C., and Zeng, F.: Sensitivity of the North Atlantic ocean circulation to an abrupt change in the Nordic Sea overflow in a high resolution global coupled climate model. J. Geophys. Res. 116, C12024, 2011.

Zhurbas, V. M., Paka, V. T., Rudels, B., and Quadfasel, D.: Estimates of Entrainment in the Denmark Strait Overflow Plume from CTD/LADCP Data. Marine Physics 56, 205–213, 2016.